Studies on the regulation of the activity potential of Matrix Metalloproteinase 2

By

Hassan Sarker

A thesis submitted in partial fulfillment of the requirements for the degree of

Doctor of Philosophy

Department of Biochemistry

University of Alberta

Abstract

Matrix metalloproteinase 2 (MMP2), also known as gelatinase A or 72 kDa type IV collagenase, is a member of a family of 25 different Zn^{2+}-dependent endopeptidases that cleave a broad range of proteins including extracellular matrix proteins (such as collagens, laminin, fibrillin and aggrecan), cell surface receptors (e.g., the insulin receptor), growth factors as well as cytokines and chemokines (such as monocyte chemoattractant protein-3). Excessive and deficient MMP2 activity can contribute to pathogenesis of osteoarthritis, cancer, and cardiovascular diseases. Our understanding of the cellular biology of MMPs in the vascular endothelium, vascular smooth muscle, and myocardium has undergone major advances in recent decades. However, the roles of MMPs in the circulatory system have not been clarified. The molecular interactome of MMPs in the blood has not been elucidated. It is unclear whether all MMPs circulate free or bound to endogenous inhibitors or to other proteins found in the blood whose large abundance makes them putative interactors that may influence the activity potential of MMPs in the blood. Clarifying the transport and regulation of MMP2 in the blood circulation was one of the objectives of this research. This research extends the phenotypic characterization of MMP2 deficiency to include circulating levels of cytokines and chemokines, soluble cytokine receptors, angiogenesis factors, bone development factors, apolipoproteins and hormones. Investigations into the interactome of MMP2 in the plasma led to the identification of fibrinogen – an acute phase reactant – as a natural inhibitor of MMP2 exhibiting a mixed-type (combination of competitive and non-competitive) inhibition mechanism. Furthermore, we found that apolipoprotein A1 – the major protein component of high-density lipoprotein (HDL) - allosterically increases the proteolytic activity of MMP2. This finding revealed MMP2 to be an allosteric enzyme. Together, the findings presented in this thesis indicate that a network of blood-borne proteins, including

fibrinogen and ApoA1/HDL, may regulate the activity potential of MMP2 in the circulation. We postulate a novel hypothesis: blood-borne proteins, including fibrinogen and ApoA1/HDL, bind MMP2 effectively acting as “transporter and regulator of the activity potential (TRAP)” complexes of MMP2 and may cause MMP2 activity to increase, decrease or remain unchanged—without immediate biological effects—while simultaneously enabling secreted MMP2 in the blood to reach distal target organs and participate in inter-organ communication.

Preface

This thesis is an original work by Hassan Sarker (HS) under the guidance of Dr. Carlos Fernandez-Patron (CFP). Some of the research conducted for this thesis forms part of an international research collaboration, directed by Dr. Fernandez-Patron at the University of Alberta, which led to peer-reviewed publications with me as the first author. Specific contributions by co-authors in publications and a manuscript (submitted for publication) used in this thesis are mentioned in the preface in the beginning chapters 2, 3 and 4. Jack Moore (Alberta Proteomics and Mass Spectrometry Facility, University of Alberta) performed the mass spectrometry analyses in chapter 3 and provided the written method in 3.5.6. Audric Moses at the University of Alberta Faculty of Medicine & Dentistry Lipidomics Core (RRID: SCR_019176) performed the FPLC analyses in chapter 4 and provided the written method in 4.5.3.

The research projects, of which this thesis is a part, received research ethics approval from the University of Alberta Research Ethics Board, project names: "MMP2 deficiency syndrome" (study ID: Pro00068611 (human ethics)) and "Metalloproteinases in disease" (study ID AUP00000253 (animal use)); study investigator: Carlos Fernandez-Patron.

The work presented in this thesis was adapted from our following published papers: "Sarker, H., Hardy, E., Haimour, A., Karim, M. A., Scholl-Bürgi, S., Martignetti, J. A., Botto, L., Fernandez-Patron, C. Comparative Serum Analyses Identify Cytokines and Hormones Commonly Dysregulated as Well as Implicated in Promoting Osteolysis in MMP2-Deficient Mice and Children. *Frontiers in Physiology*, 11:568718 (2020)" and "Sarker, H., Hardy, E., Haimour, A., Botto, L., Maksymowych, W., Fernandez-Patron, C. Identification of fibrinogen as a natural inhibitor of MMP2. *Scientific Reports* 9, 4340, (2019)". The research presented in chapter 4 has been adapted from our work currently deposited as a preprint manuscript in Research Square (https://doi.org/10.21203/rs.3.rs-3897886/v1), under a CC BY 4.0 license. The manuscript is currently being peer reviewed for publication. The literature review on MMP biology presented in the introduction (chapter 1) contains excerpts adapted from our review article that was published as "Sarker, H., Haimour, A., Toor, R., Fernandez-Patron, C. The emerging role of epigenetic mechanisms in the causation of aberrant MMP activity during human pathologies and the use of medicinal drugs. *Biomolecules*, 11(4):578 (2021)".

Acknowledgements

I wish to acknowledge the constant guidance and mentorship I have received from my supervisor Dr. Carlos Fernandez-Patron and my supervisory committee members Dr. Zamaneh Kassiri and Dr. Richard Fahlman. Since joining the Fernandez-Patron lab in 2017, I have had the opportunity to work on multiple projects which have allowed me to grow as a researcher and increase my critical thinking skills. I received the support and guidance I needed from my supervisor and committee to lead my projects to completion which have resulted in five first-author and four co-author publications.

I want to acknowledge all our collaborators who have made our research projects possible. I want to thank Dr. Walter P. Maksymowych, Dr. Lorenzo D. Botto, Dr. John A. Martignetti and Dr. Sabine Scholl-Bürgi for providing us with valuable biological specimens for our research. Special thanks to Dr. Eugenio Hardy for his tremendous input towards experiment design and his critical reviews of our manuscripts which greatly improved their quality. I also want to thank Dr. Rashmi Panigrahi and Ms. Ana Lopez-Campistrous for their contributions in the structural studies and experiments.

Finally, I also wish to acknowledge the funding support I have received from the Department of Biochemistry and the Faculty of Graduate Studies and Research at the University of Alberta. Also, the funding support from Natural Sciences and Engineering Council of Canada and the University of Alberta Hospital Foundation to the Fernandez-Patron lab have made it possible to complete the projects.

Table of Contents

List of Tables

List of Figures

List of Abbreviations

A2MG – Alpha-2-macroglobulin

ACTH – Adrenocorticotropic hormone

ApoA1 – Apolipoprotein A1

ApoA2 – Apolipoprotein A2

ApoE – Apolipoprotein E

BMP-9 – Bone morphogenic protein-9

BN-PAGE – Blue native polyacrylamide gel electrophoresis

CTGF – Connective tissue growth factor

DKK-1 – Dickkopf-1

EGF – Epidermal growth factor

ELISA – Enzyme-linked immunosorbent assay

FBG – Fibrinogen

FGF – Fibroblast growth factor

Flt-3 ligand – fms-like tyrosine kinase-3 ligand

G-CSF – Granulocyte colony-stimulating factor

GM-CSF – Granulocyte-macrophage colony-stimulating factor

GROα/CXCL1 – chemokine ligand 1

HB-EGF – Heparin-binding EGF-like growth factor

HDL – High-density lipoprotein

HGF – Hepatocyte growth factor

HAT – histone acetylase

HDAC – histone deacetylase

HDM – histone demethylase

ICAM-1 – Intercellular Adhesion Molecule 1

IFN – Interferon alpha-2

IGFBP-3 – insulin-like growth factor-binding protein-3

IL – Interleukin

IP-10/CXCL10 – Interferon gamma-induced protein-10 / chemokine ligand-10

KC/CXCL1 – Keratinocyte-derived cytokine

LDL – Low density lipoprotein

LIF – Leukemia inhibitory factor

LIX – Lipopolysaccharide-induced CXC chemokine

MCP – Monocyte chemoattractant protein

M-CSF – Macrophage colony-stimulating factor

MDC (CCL22) – Macrophage-derived chemokine

MIG (cxcl9) – Monokine induced by interferon gamma

MIP – Macrophage inflammatory proteins

MMP – Matrix metalloproteinase

OA - Osteoarthritis

OC – Osteocalcin

OPG – Osteoprotegrin

OPN - Osteopontin

PDGF – Platelet-derived growth factor

PLGF - Placental growth factor

PTH – Parathyroid hormone

RA – Rheumatoid arthritis

RANTES / CCL5 – Regulated on activation, normal T cell expressed and secreted

sCD30 – soluble CD30

sCD40L – soluble CD40 ligand

SDS-PAGE – Sodium dodecyl-sulfate polyacrylamide gel electrophoresis

sEGFR – Soluble epidermal growth factor receptors

sIL-1R – soluble interleukin-1 receptor

SOST – Sclerostin

sRAGE – soluble receptor for advanced glycosylation endproducts

sTNFR – Soluble tumor necrosis factor receptors

sVEGF – Soluble vascular endothelial growth factor

TGF – Transforming growth factor

TIMP – Tissue inhibitor of metalloproteinases

TNF – Tumor necrosis factor

VEGF – Vascular endothelial growth factor

VLDL – Very low-density lipoprotein

Amino acid abbreviations

Ala, A alanine

Arg, R arginine

Asn, N asparagine

Asp, D aspartate

Cys, C cysteine

Gln, Q glutamine

Glu, E glutamate

Gly, G glycine

His, H histidine

Ile, I isoleucine

Leu, L leucine

Lys, K lysine

Met, M methionine

Phe, F phenylalanine

Pro, P proline

Ser, S serine

Thr, T threonine

Trp, W tryptophan

Tyr, Y tyrosine

Val, V valine

1 Chapter 1: Introduction

1.1 Structure of Matrix Metalloproteinases (MMPs)

1.1.1 General structural features of MMPs

Matrix metalloproteinases (MMPs) are a family of 25 highly homologous, multi-domain endopeptidases that depend on an active site Zn^{2+} to catalyze the hydrolysis of peptide bonds(*1, 2*). MMPs are expressed as zymogens and generally consist of an N-terminal signal peptide sequence, a pro-peptide domain, a catalytic domain, and a C-terminal hemopexin-like domain linked to the catalytic domain via a hinge region with a few exceptions(*1, 3*). Small secreted MMPs such as MMP-7, MMP23 and MMP26 lack the hemopexin-like domain and the hinge region, and therefore have reduced ability to bind and cleave large collagen molecules(*1, 3, 4*). The gelatinases, MMP2 and MMP9, uniquely contain three fibronectin type II-like repeats (also called the collagen binding domain) inserted into the catalytic domain which enhances collagen binding and cleavage(*1-3*) . MMP23 contains unique domains such as the cysteine array, IgG-like domain and interleukin-1 type II receptor-like domains and does not contain the hemopexin domain(*1, 3, 4*). MMP-14 (also known as MT1-MMP), -15, -16, and -24 contain a transmembrane domain which allows them to anchor to the cell surface membrane(*3, 4*). The N-terminal signal peptide is required for the secretion of pro-MMPs and is removed after translation. The pro-peptide of MMPs is highly conserved and has a crucial cysteine residue in a conserved region (PRCGXPD) that interacts with the active site Zn^{2+} to block the active site from binding substrates in a mechanism termed “cysteine switch”(*4, 5*). The catalytic Zn^{2+} is coordinated by three conserved histidine residues (HEXXHXXGXXH) in the catalytic domain. A hinge region confers structural flexibility and facilitates MMPs’ interactions with substrates, cell-surface proteins, and tissue inhibitors(*4, 6, 7*) while a hemopexin-like domain facilitates substrate

recognition and determines substrate specificity. The hemopexin-like domain is also involved in the interaction of MMPs with cell-surface receptors, inhibitors, and activators as well as in cellular internalization of MMPs, which may result in their degradation as well as intracellular actions(*4, 8-10*).

1.1.2 Structural features of MMP2

The research presented in this thesis is focused on MMP2, also known as gelatinase A or 72 kDa type IV collagenase, which is the most abundant MMP in the blood. The *MMP2* gene, located on chromosome 16, produces a proMMP-2 protein which is comprised of 660 amino acids (Mw = 73,882), and consists of a signal peptide (Met1-Ala29), a pro-peptide domain (Ala30-Asn109), a catalytic domain (Tyr110-Thr465), three fibronectin type II -like repeats inserted into the catalytic domain (Ala228-Asp392), a flexible hinge region (Pro466-Asp471) and a hemopexin-like domain (Asp472-Cys660)(*11*). Prior to their release from the synthesizing cells, the signal peptide is removed and MMP2 is generally secreted as a zymogen (proMMP2) containing the pro-peptide which is subsequently cleaved by other proteases (including other MMPs) to produce the mature proteolytically active form of MMP2 with a molecular weight of 62 kDa. There are two Zn^{2+} ions and three Ca^{2+} ions that are coordinated by amino acids in the catalytic domain and the hemopexin-like domain with the exception a Cysteine residue in the pro-peptide that coordinates the catalytic Zn^{2+} ion to confer the "cysteine switch" mechanism to inhibit catalytic activity in proMMP2(*4, 5*). Upon activation, the interaction of Cys–Zn^{2+} is disrupted, which allows the Zn^{2+} ion to act as a nucleophile and bind a water molecule to initiate a proteolysis reaction.

1.2 Functions of Matrix Metalloproteinases

Historically, the predominant understanding of the function of MMPs was degradation of structural components of the extracellular matrix. However, we have since come to know that MMPs are proteases that cleave a broad range of proteins besides extracellular matrix proteins (e.g., collagens, laminin, fibrillin, and aggrecan) such as cell surface receptors (e.g., the insulin receptor), growth factors (such as IGFBP-3, Heparin-binding EGF, precursor of TGFβ and CTGF) as well as cytokines and chemokines (such as monocyte chemoattractant protein-3, interleukin-1β, interleukin-2Rα, Pro-TNFα)(*1, 4, 9*). Through their proteolytic activity, MMPs influence a wide range of biological processes including but not limited to cell migration and proliferation, osteoclast activation, bone remodeling, cardiac remodeling, adipocyte differentiation, platelet aggregation, growth factor activation and release, angiogenesis, vasoconstriction, and modulation of inflammation(*1, 3, 4, 9, 12, 13*). MMP targets include the organs where MMPs are synthesized and distal organs which MMPs can reach through the blood circulation.

1.3 Regulation of MMP activity and expression

1.3.1 Zymogen activation

MMPs are expressed as inactive zymogens containing a pro-domain which confers the first level of regulation of MMP activity after translation. The pro-domain blocks the active site via the cysteine-switch mechanism and is cleaved by endopeptidases (such as activated MMPs, membrane-anchored MMP-14, plasmin and furin) to convert the zymogen into their proteolytically active form(*4, 5, 9*). Alternatively, the blockage of the active site by the cysteine-switch can also be disrupted by post-translational modifications (phosphorylation), reactive oxygen species, as well as alkylating compounds (such as organomercurial 4-

aminophenylmercuric acetate) to activate the zymogen without needing to cleave the pro-domain(*14*). The pro-domain can also be cleaved through autolysis mediated by allosteric perturbation of the zymogen(*5, 14, 15*).

MMP2 zymogen activation happens at the cell surface through a unique multi-step pathway that involves MMP-14 (MT1-MMP) and the TIMP2(*16*). The inhibitory N-terminal domain of tissue inhibitor of metalloproteinase 2 (TIMP2) binds cell surface-anchored MMP14 and the non-inhibitory C-terminal domain binds the hemopexin-like domain of proMMP-2, allowing an adjacent, non-inhibited MMP14 to cleave the bound proMMP-2 at a cleavage site in the pro-peptide domain. ProMMP2 may also be activated by other MMPs such as MMP15 by a different mechanism that does not require TIMP2(*17*).

1.3.2 Endogenous inhibitors

Once activated, the proteolytic activity of MMPs is regulated by multiple endogenous inhibitors, such as tissue inhibitors of metalloproteinases (TIMPs), α-2-macroglobulin, and fibrinogen(*14, 18*).

1.3.2.1 TIMPs

There are four TIMPs (TIMP-1, -2, -3 and -4) that bind and reversibly inhibit all MMPs in a 1:1 stoichiometry with varying degrees of efficacy(*19*). TIMPs are low molecular weight proteins consisting of 184-194 amino acids comprising an inhibitory N-terminal and a non-inhibitory C-terminal domain(*4*). Each domain contains three conserved disulphide bonds that contribute to generate a tertiary structure consisting of loops. The N-terminal loop slots into the active site of MMPs and a N-terminal cysteine residue (conserved across all TIMPs) bidentately chelates the catalytic Zn^{2+} ion and expels the water molecule bound to the Zn^{2+} ion, thus inhibiting MMP proteolytic activity(*4*).

Although the TIMPs are highly similar in terms of structure and their mechanism of MMP inhibition, they have different expression patterns in different organs. Like MMPs, the expression of TIMPs depends on various physiological stimuli in diverse cell types(*20*). While TIMP1, TIMP2 and TIMP3 are ubiquitously expressed in various mammalian tissues, TIMP4 is expression is restricted to specific tissues such as the heart, kidneys, ovaries, pancreas, colon, testes, brain, and adipose tissue (*21*).

1.3.2.2 Other endogenous inhibitors of MMP2

Apart from TIMPs, the acute phase protein alpha-2-macroglobulin (A2MG) is a well characterized inhibitor of MMPs including MMP2(*22, 23*). Human A2MG is a plasma glycoprotein with a molecular weight of 725 kDa and consists of four identical subunits (~180 kDa each). It is a broad-spectrum inhibitor of proteases and functions by entrapping the target proteases within itself(*24*). In a physiological context, the resultant protease-inhibitor complex is subsequently removed by receptor-(low density lipoprotein receptor-related protein-1) mediated endocytosis(*25, 26*).

Other reported physiological inhibitors of MMP2 include the secreted form of β-amyloid precursor protein(*27*), a C-terminal fragment of procollagen C-proteinase enhancer protein(*28*), and RECK (a GPI-anchored glycoprotein)(*29*). The inhibitory mechanisms of these inhibitors are not known.

Adding to the list, we have identified fibrinogen to be a physiological inhibitor of MMP2 (chapter 3). Fibrinogen is a 340 kDa dimeric glycoprotein comprised of two sets of three polypeptide chains (Aα, Bβ and γ) that are interconnected by 29 disulfide bridges(*30*). Like A2MG, fibrinogen is a positive acute-phase protein in the circulation, where its physiological concentration (1.8-4 mg/mL (5.29-11.8 μM))(*31*)) can increase by up to 10-folds in response to

inflammatory stimuli(*32*).We found that at physiological concentrations, fibrinogen concentration-dependently inhibited (40-70% inhibition) the proteolytic activity of MMP2 towards its substrate gelatin (denatured collagen) and exhibited specificity towards MMP2 as it did not inhibit MMP9(*18*).

1.3.3 Epigenetic control of *MMP* gene transcription

Transcriptional regulation of MMP activity involves transcription factors, DNA polymorphisms and promoter/enhancer elements, and epigenetic mechanisms. The concept of "epigenesis" finds its origin in the scientific debate regarding processes that drive development in cells. It proposed that chemical reactions involving soluble cellular components can influence cell development(*33*). With increased understanding of chromosomes and DNA, the concept of epigenesis has evolved. Epigenetics builds on the notion that all somatic cells in an organism contain the same DNA, with different cell types exhibiting different patterns of gene expression that can be clonally inherited(*33*). Quantifiable epigenetic mechanisms of gene regulation involve chemical modifications on DNA (such as methylation) and DNA-bound histone proteins (such as methylation or acetylation of histone tails)(*33*). Chemical modifications of DNA and histones regulate gene expression through impacting the extent of DNA compaction and therefore the accessibility of transcriptional machinery to genes(*34, 35*). These modifications include but are not limited to methylation, acetylation and phosphorylation. Histone modifications in addition to DNA methylation are heritable changes that alter gene expression but not the DNA sequence of genes(*36*). Such epigenetic modifications are mediated by DNA methyltransferases, histone acetylases (HATs), histone deacetylases (HDACs) and histone demethylases (HDMs)(*36-40*) and through the interaction of small non-coding RNA, such as microRNAs and small-interfering RNAs, with their corresponding target mRNA, which result in

gene silencing effects by way of mRNA degradation or transcriptional repression(*36, 41*). Multiple miRNAs with potential regulatory effects on MMPs have been identified(*42*), some of which have been confirmed experimentally.

Varied gene expression patterns of MMP family members across different cell types may be caused by cell-type specific expression of transcription factors and polymorphisms in the promoters of MMP genes in addition to DNA methylation and histone modifications(*43*).

The promoter regions of at least fourteen *MMP* genes (*MMP*-1, -2, -9, -11, -14, -15, -16, -17, -21, -23, -24, -25, -26 and -28) and all four tissue inhibitors of metalloproteinases (TIMP-1, -2, -3 and -4) contain CpG islands that are prone to DNA methylation by DNA methyltransferases (*44, 45*). DNA methylation generally induces gene repression by preventing transcription factor binding or by attracting methyl-CpG binding proteins that are transcriptional repressive(*36, 37*). 5-aza-2'-deoxycytidine, a DNA methyltransferases inhibitor, reversed hypermethylation at the *MMP9* promoter (hypermethylation of a promoter represses gene transcription) and concomitantly induced *MMP9* gene expression in lymphoma cell lines(*46*). *MMP1* expression is silenced by methylation of a single CpG site that can be rescued by 5-aza-2'-deoxycytidine(*45*). In the colon cancer cell line HCT 116, the deletion of DNA methyltransferases *Dmt-1* and *Dmt3b* as well as treatment with demethylating agents induced *MMP3* gene expression without affecting *MMP1* or *MMP2(47)*. Treatment of human non-Hodgkins Raji B lymphoma cells with the demethylating agent 5-aza-2'-deoxycytidine did not induce *MMP3* expression, but instead concentration-dependently increased *MMP10* transcription(*47*). These studies suggest that methylation of CpG sites is a mechanism of MMP gene regulation at the level of transcription and DNA methylation/demethylation alters MMP gene transcription in a cell-specific fashion.

Histone-modifying enzymes that introduce chemical modifications on histone tails, particularly H3/H4 acetylation, methylation or phosphorylation, work alongside chromatin-remodelling complexes to impose control on gene expression by modulating chromatin structures and accessibility of gene promoters (*48, 49*). Histone deacetylase 2 and chromatin-remodeling enzyme Mi-2, when recruited to the *MMP9* promoter, reduce H3/H4 acetylation levels and DNA accessibility, consequently repressing *MMP9* gene expression(*50*). Similar transcriptional control via histone modifications and chromatin remodeling has been observed for *MMP*-1, -10 and -13(*51, 52*). Further research is needed to better understand the roles of DNA methylation and histone modifications in regulating the network of MMPs that maintain extracellular matrix homeostasis.

1.4 MMP dysregulation in pathophysiology via epigenetic mechanisms

Dysregulation of MMP refers to either an aberrant increase in MMP expression and activity or a downregulation of MMP2 activity due to a genetic deficiency in MMP expression or excessive inhibition by endogenous inhibitors. Dysregulation of MMP activity is implicated in a wide range of pathologies including but not limited to bone/cartilage disease, cancer, and cardiovascular disease (e.g., atherosclerosis)(*3, 53-58*). The possible involvement of epigenetic mechanisms in the causation of aberrant MMP activity in the settings of acute and chronic diseases is important for predicting disease development and progression as well as for designing more efficacious therapeutic interventions.

1.4.1 Cancer

MMPs promote cancer progression through distinct mechanisms, including i) activation of growth factors(*59*), ii) interference with apoptosis pathways(*60*), iii) promoting growth of tumor

vasculature(*61*), and iv) promoting tissue invasion and metastasis(*62*). There is mounting evidence of epigenetic dysregulation of *MMP* gene expression contributing to cancer progression.

Strongin *et al*. demonstrated that the pro-invasive MT1-MMP/MMP-2/TIMP-2 axis is epigenetically regulated in cancer cells(*63*). Low migratory breast carcinoma MCF-7 cells exhibited epigenetic transcriptional silencing of MT1-MMP and MMP-2 via hypermethylation of CpG sites in their respective gene promoters and histone H3 lysine-27-trimethylation. In contrast, highly migratory glioblastoma cells exhibited hypomethylation of CpG sites and low levels of H3 lysine-27-trimethylation(*63*). Corroborating these results, DNA methyltransferases inhibition with 5-aza-2'-deoxycytidine increased transcription of *MT1-MMP* and *MMP2* in pancreatic cancer cells, thereby increasing their invasiveness(*64*). In breast cancer cell lines MCF-7 and MDA-MB-436, 5-aza-2'-deoxycytidine induced demethylation of CpG sites in the *MMP9* promoter and histone H3 lysine-4-trimethylation (epigenetic marker of open chromatin allowing gene transcription)(*39*), resulting in increased *MMP9* expression(*65*). Further, treatment of urothelial cancer cell lines with 5-aza-2'-deoxycytidine or trichostatin A (histone deacetylase inhibitor) induced transcription of 22 MMPs and promoted cancer cell proliferation, migration and invasion(*66*). In glioblastoma cell lines, expression of microRNAs targeting DNA methyltransferases induced *MMP2* and *MMP9* expression(*67*). MMP gene expression can be dysregulated in cancer cells indirectly via epigenetic control of *GRK6*. This gene encodes G protein-coupled receptor kinase 6 (GRK6), an enzyme involved in repressing angiogenesis, tumor growth and metastasis(*68*). GRK6 decreases expression of cancer promoting genes, *MMP2* and *MMP7*(*69*). In lung adenocarcinoma cells, the *GRK6* promoter is hypermethylated and GRK6 expression is repressed, which promotes cell migration and invasion(*69*). Thus,

ablation of the GRK6-mediated repression of MMP-2 and MMP-7 may increase the invasiveness of lung adenocarcinoma cells.

Cock-Rada *et al.* 2012 showed that H3K4 methyltransferase SMYD3 epigenetically regulates the transcription of *MMP9* gene in a fibrosarcoma cell line (HT1080) and B-cell lymphosarcoma cell line (TBL3) infected with *T. annulata*(*70*). Increased *MMP9* mRNA levels in TBL3 cells were associated with greater H3K4me2 and H3K4me3 marks in the regulatory region of the *MMP9* promoter. The elevated histone marks were determined to be the result of SMYD3 as it was the only methyltransferase significantly induced in TBL3 cells. SMYD3 induces transcriptional activation by binding to 5′-CCCTCC-3′ or 5′-GGAGGG-3′ DNA sequences in the promoter region of genes including *MMP9*. Further, HT1080 cells transfected with siRNAs against SMYD3 resulted in decreased cell migration and proliferation accompanied by decreased levels of *MMP9* mRNA and protein. Similar results were achieved by knocking down only *MMP-9*. Therefore, SMYD3 acts as an epigenetic regulator of *MMP9* and consequently affects cancer invasion.

MMP9 has also been reported to be the target of miR-211(*71*). In grade IV glioblastoma multiformed specimens miR-211 expression is suppressed as a result of abnormal methylation of its promoter(*71*). An inverse relationship between the expression of miR-211 and MMP-9 protein levels was observed. Asuthkar *et al.* (2012) also showed that miR-211 overexpression and shRNA specific for *MMP9* (pM) treatments was associated with anti-proliferative and apoptotic signaling in 4910 cancer stem cells and U87 glioma cells. Following the treatments, an increase in the cleaved 35 kDa fragment of Caspase-9 is observed which is indicative of Caspase-9 activation. This then triggers pro-apoptotic pathways following effector caspase cleavage and activation. The overexpression of miR-211 also inhibits glioma cell invasion and migration via

suppressing *MMP9* expression. Other known targets of miRNAs in cancers include *MMP2*, *MMP9*, *MMP13*, *MMP14*, and *MMP16* and their substrates such as type I, II and IV collagens(*44, 45*).

1.4.2 Cardiovascular diseases

Aberrant activity of MMPs contributes to the development and progression of atherosclerosis by influencing the local inflammatory response at the site atherosclerosis plaque formation and by catalyzing plaque rupture – an event that ultimately culminates in myocardial infarction and heart failure(*72*). Recent evidence implicate epigenetic control of MMP expression in atherosclerosis. Induced hypomethylation of *MMP2* and *MMP9* via microRNA-29b upregulation is a mechanism by which oxidized low density lipoprotein (oxLDL) contributes to atherosclerosis(*73*). The oxLDL promotes atherosclerotic plaque formation by inducing smooth muscle cell migration and proliferation. In human aortic SMC, oxLDL induced cell migration via upregulated expression and activation of MMP-2 and MMP-9 due to the fact that both MMPs promote smooth muscle cell migration(*74*). Analysis of DNA methylation status of *MMP2* and *MMP9* following oxLDL treatment revealed significant demethylation in the two genes(*73*). DNMT3b mRNA and protein levels in human aortic SMCs significantly decreased after oxLDL treatment(*73*). DNMT3b knockdown in oxLDL-treated human aortic SMCs significantly increased *MMP2* and *MMP9* mRNA levels indicating that *MMP2* and *MMP9* were repressed by DNA methylation. These results show that up-regulated *MMP2* and *MMP9* expression resulted from decreased DNA methylation due to DNMT3b down-regulation. Further, Chen *et al.* (2011) also determined that microRNA-29b was up-regulated in a dose- and time-dependent manner in oxLDL treated SMCs(*73*). These results suggest that microRNA-29b indirectly modulates DNA methylation of *MMP2* and *MMP9* and thus their expression by regulating the expression of

DNMT3b.Thus, DNA methylation leading to aberrant expression of MMPs can significantly influence the progression and development of atherosclerosis.

Similarly, hypomethylation of the *MMP9* gene and aberrant upregulation of *MMP9* expression is observed in Kawasaki disease – a pediatric vascular disease characterized by inflammation of coronary arteries(*75*). Methylation status of the CpG sites of *MMP9* shows strong negative correlation with mRNA expression levels, indicating that *MMP9* is repressed by DNA methylation(*75*). Further, differential methylation status in all MMP genes was induced by intravenous immunoglobulin treatment in Kawasaki disease patients(*75*).

1.4.3 Bone / cartilage diseases

MMPs modulate bone growth, development and repair processes through their actions on extracellular matrix components and as such, dysregulated MMP expression and activity is implicated in bone diseases such as osteoarthritis (OA) and rheumatoid arthritis(*14*). Genome-wide analysis of DNA methylation status involving osteoarthritis patients found *MMP3*, *MMP9* and *MMP13* genes to be hypomethylated (with increased gene expression) in osteoarthritis *versus* non- osteoarthritis chondrocytes(*76, 77*). Percentage of methylated CpG sites of these MMP genes in clonal chondrocytes from osteoarthritis patients versus controls were: 80% versus 96% for *MMP13*, 19% versus 53% for *MMP9*, 43% versus 70% for *MMP3*(*77*). The study concluded that the altered expression of cartilage degrading MMPs resulted from clonally heritable epigenetic changes that may exacerbate osteoarthritis.

MicroRNA-222 and microRNA-27b regulate *MMP13* expression in osteoarthritis chondrocytes(*78*). Song *et al.* (2015) found that miR-222 expression is downregulated and its target HDAC-4 consequently is up-regulated in OA chondrocytes(*78*). Elevated HDAC-4 expression thereby increased *MMP13* expression via histone de-acetylation. The study also

showed that inhibition of HDACs by Trichostatin A (TSA) lowered HDAC-4 and MMP-13 protein expression in OA chondrocytes, thereby confirming the role of HDAC-4 in regulating MMP-13. MMP-13 when overexpressed can exacerbate OA(*79*). Akhtar *et al.* (2010) found a direct inhibitory effect of miR-27b on the expression of *MMP13* gene in OA chondrocytes(*79*). MicroRNA miR-27b interacts with the 3′-untranslated region of *MMP13* mRNA which contains a complementary sequence to the miR-27b seed sequence and downregulates *MMP13* expression at the post-transcriptional level(*79*). MiR-27b expression was found to be significantly reduced in OA cartilage when compared to normal cartilage. OA chondrocytes exhibiting higher levels of miR-27b produced significantly less MMP-13 protein upon IL-1*β* stimulation compared to chondrocytes that were not transfected with a miR-27b mimic and inhibition of miR-27b increased MMP-13 protein expression in IL-1*β*–stimulated chondrocytes when compared with control OA chondrocytes. These findings indicate that miR-27b acts as regulator of MMP-13 protein expression in human OA chondrocytes(*79*).

In rheumatoid arthritis (RA), abnormal histone modifications and DNA methylation both lead to aberrant upregulation of MMP gene transcription(*80*). Genome-wide DNA hypomethylation is observed in rheumatoid arthritis synovial fibroblasts (RASF), resulting in upregulated expression of 186 genes including *MMP1* and *MMP14*(*81*). In RASF, histone H3 lysine-4-trimethylation (histone marker for active transcription) is increased, while transcription-repressive H3 lysine-27-trimethylation is decreased in the promoters of *MMP1*, *MMP3*, *MMP9* and *MMP13*(*82*). Interestingly, despite increased active histone markers in its promoter, *MMP9* expression was not upregulated by interleukin-6 (IL-6) induction, while *MMP1*, *MMP3* and *MMP13* were upregulated. This occurs as a result of the IL-6-inducible transcription factor STAT3 being recruited to the promoters of *MMP1*, *MMP3* and *MMP13* but not to the *MMP9* promoter(*82*).

The differential expression of MMP genes with similar histone methylation states suggests that epigenetic mechanisms work in concert with canonical mechanisms of MMP transcription control.

Furthermore, recent evidence suggests that *MMP9* expression in RA may also be epigenetically regulated by miRNAs. Wang *et al.* (2019) reported that fibroblast-like synoviocytes from patients with RA exhibited elevated miR-145-5p expression and increased *MMP9* mRNA and proteins levels(*83*). Overexpression of miR-145-5p induced the nuclear translocation of p65, an thereby activating NF-κB which induces the expression of *MMP9,* by binding the *MMP9* promoter region(*83*). These demonstrate that miR-145-5p can indirectly modulate the expression of *MMP9* in patients with RA(*83*).

1.5 The interactome of MMPs in the blood circulation

Circulating MMPs, including MMP2, may interact with one or more of the four endogenous TIMPs to form enzyme-inhibitor complexes(*4, 9, 19*). MMPs are also inhibited by the broad-spectrum protease inhibitor α-2-macroglobulin which consists of four protease binding domains(*23*). Under normal physiological conditions, MMP2 can enter the blood circulation. In many pathological conditions, the disease foci (e.g., bones and cartilage in arthritis, tumors in cancer, ischemic site in the infarcted heart) release large quantities of MMPs into the systemic circulation. Whether MMPs in the circulation are transported in complexes with their inhibitors and/or other proteins is unknown. Potential MMP-containing protein complexes in the circulation could serve as transporters and regulators of the activity potential of MMPs, keeping activated MMPs inert and/or preventing the zymogens from being activated, while they are transported from the sites of expression (synthesis foci) to distally located target tissues where MMPs digest extracellular matrix (ECM) and non-ECM substrates. The research presented in

this thesis (chapters 3 and 4) describes the identification of two interactors of MMP2 in the blood with opposing effects on its activity – fibrinogen and apolipoprotein A1 (ApoA1).

1.6 Objectives of this work

Among MMPs, MMP2 (gelatinase A) is constitutively expressed by most cell types(*2, 3, 84, 85*). In disease conditions, such as hypertensive disorders or myocardial infarction, MMP2 synthesis and secretion into the blood circulation are increased, due to the activation of vascular endothelium and myocardium as well as because of immune cells infiltration(*86-88*). Affected organs (such as arteries and heart) become foci of MMP2 synthesis. In other diseases such as arthritis, the affected joints and bone tissue become synthesis foci of MMPs including MMP2. How MMP2 is transported or regulated in the blood circulation is poorly understood. The impact of increased MMP2 secretion on inter-organ communication is unclear. The potential contribution of increased levels of circulating MMP2 to proteolytic damage to target organs positioned distal to MMP2 synthesis sites has not been explored. Plausibly, proteolytic damage of distal target organs by increased circulating MMP2 levels can promote (or exacerbate) preexisting comorbidities or cause distal organ dysfunction. However, how MMP2 reaches distal target organs or how the activity of MMP2 is regulated in the blood is unclear. Clarifying the transport and regulation of MMP2 in the blood circulation was the focus of this research. In this research, we investigated the hypothesis that specific proteins and complexes transport MMP2 and regulate its activity in the blood.

1.7 Organization of the thesis

The thesis is organized into five chapters. Following relevant background information on MMPs in this current chapter, in chapter 2 we present our new findings and published data on the

characteristics of MMP2 deficiency in humans and mice. Next, chapter 3 presents our discovery of a novel endogenous inhibitor of MMP2. In chapter 4, we describe a novel role of apoproteins and high-density lipoprotein particles in allosterically increasing MMP2 activity – a previously unknown characteristic of MMP2 being allosteric enzymes. Finally, chapter 5 draws conclusions from each chapter and presents avenues for future research.

2 Chapter 2: Comparative serum analyses identify cytokines and hormones commonly dysregulated as well as implicated in promoting osteolysis in MMP2-deficient mice and children

Hassan Sarker, Eugenio Hardy, Ayman Haimour, Mahmoud A. Karim, Sabine Scholl-Bürgi, John A. Martignetti, Lorenzo D. Botto, Carlos Fernandez-Patron

Preface

This chapter represents the work accepted for publication in *Frontiers in Physiology* in 2020 as "Sarker, H., Hardy, E., Haimour, A., Karim, M. A., Scholl-Bürgi, S., Martignetti, J. A., Botto, L., Fernandez-Patron, C. Comparative Serum Analyses Identify Cytokines and Hormones Commonly Dysregulated as Well as Implicated in Promoting Osteolysis in MMP2-Deficient Mice and Children. Frontiers in Physiology, 11:568718 (2020)". HS is the primary author and produced the first draft. HS and CFP designed the study, experiments and wrote the manuscript. HS and MAK conducted the experiments. AH and EH assisted in literature research and writing the manuscript. LDB, JAM and SSB recruited the patients and provided clinical data. All authors participated in the data analysis and performed critical revisions of the manuscript and approved the final version of the manuscript. This chapter contains research which received ethics approval from the University of Alberta Research Ethics Board, project names: "MMP2 deficiency syndrome" (study ID: Pro00068611 (human ethics)) and "Metalloproteinases in disease" (study ID AUP00000253 (animal use)); study investigator: Carlos Fernandez-Patron. The manuscript has been adapted to fit the format of this thesis.

2.1 Summary

Deficiency of matrix metalloproteinase 2 (MMP2) causes a multi-system syndrome characterized by multi-centric osteolysis, nodulosis and arthropathy (MONA) as well as cardiac valve defects, dwarfism and hirsutism. MMP2 deficient (*Mmp2*$^{-/-}$) mice are a model for this rare multisystem pediatric syndrome but their phenotype remains incompletely characterized. Here, we extend a phenotypic characterization of MMP2 deficiency to include cytokines and chemokines, soluble cytokine receptors, angiogenesis factors, bone development factors, apolipoproteins and hormones. Initial screening was performed on a representative case of MMP2 deficiency selected based on clinical assessment – an eight-year-old male MMP2 deficient patient diagnosed with MONA presenting a previously unreported deletion mutation c1294delC (Arg432fs) in the *MMP2* gene. Of eighty-one human serum biomolecules analyzed, eleven were upregulated (>4-fold), two were downregulated (>4-fold) and sixty-eight remained unchanged, compared to unaffected controls. Specifically, Eotaxin, GM-CSF, M-CSF, GRO-α, MDC, IL-1β, IL-7, IL-12p40, MIP-1α, MIP-1β and MIG were upregulated and EGF and ACTH were downregulated. Analysis of five different MMP2 deficient patients also showed upregulation in Eotaxin, IL-7, IL-12p40 and MIP-1α, and a downregulation in EGF. To establish whether these alterations are phenotypic traits of MMP2 deficiency (and not just patient-specific), we studied MMP2-deficient mice. Among 32 cytokines measured in plasma of *Mmp2*$^{-/-}$ mice, the cytokines Eotaxin, IL-1β, MIP-1α and MIG were commonly upregulated in mice as well as patients with MMP2 deficiency. Moreover, bioactive cortisol (a factor that exacerbates osteoporosis) was also elevated in MMP2-deficient mice and patients. Among the serum factors we have identified to be dysregulated in MMP2 deficiency many are osteoclastogenic and could potentially contribute to bone disorder in MONA. These new molecular phenotypic traits merit being targeted in future

research aimed at understanding the pathological mechanisms elicited by MMP2 deficiency in children.

2.2 Introduction

Matrix metalloproteinase 2 (MMP2), also known as gelatinase A or 72 kDa type IV collagenase, is a member of a family of 25 different Zn^{2+}-dependent endopeptidases that cleave a broad range of proteins including extracellular matrix proteins (such as collagens, laminin, fibrillin and aggrecan)(*1, 2*), cell surface receptors, growth factors as well as cytokines and chemokines (such as monocyte chemoattractant protein-3)(*12, 89-91*). Both excessive and defective MMP2 activity can be pro-inflammatory(*2, 72, 92-95*). In humans, deficiency of MMP2 due to biallelic inactivating mutations in the *MMP2* gene causes a multisystem inflammatory syndrome comprising multicentric osteolysis, nodulosis, and arthropathy (MONA, MIM# 259600 - also known as Torg Syndrome or Torg-Winchester Syndrome), cardiac valve defects, dwarfism and hirsutism(*2, 57, 95-98*).

Complete loss of MMP2 function due to inactivating *MMP2* gene mutations is rare and thus, epidemiological and clinical data on MMP2 deficiency in humans are limited. Nevertheless, there are reports of over 40 documented cases in the literature involving at least 20 different inactivating mutations in the *MMP2* gene (*98*). The pathogenesis of MONA in MMP2 deficient patients is unknown with treatment of patients being mostly limited to palliative symptom management and physiotherapy. The rarity of MMP2 deficiency in humans poses a great challenge when studying the pathological mechanisms elicited by this disorder. Limited access to the patients, who are young children receiving various medical treatments to manage symptoms, further limit the feasibility of studies and complicate the analyses and comparison among patients. Research on the pathogenesis of MMP2 deficiency frequently uses *Mmp2*$^{-/-}$ mice as a

study model (*57, 96, 99*). A thorough characterization of the commonalities and differences between MMP2 deficient patients and *Mmp2*$^{-/-}$ mice is requisite for translating findings in mice to humans. The molecular pathways connecting the loss of MMP2 activity through inactivating mutations to the subsequent development of the complex disease conditions described above are yet to be elucidated.

In previous studies, phenotypic comparisons of human and murine MMP2 deficiency have been mostly limited to clinical symptoms (including inflammation and pain in joints, a progressive decrease in bone mineral density and articular cartilage destruction), associated pathologies (such as congenital cardiac valve defects, dwarfism and hirsutism) and physical features (notably, craniofacial defects) observed in the murine and human conditions(*2, 57, 95-98*). The current lack of knowledge of the pathways by which MMP2 deficiency leads to the aforementioned disease phenotypes calls for studies, focused on cytokines, chemokines, angiogenesis and bone development factors, apolipoproteins and hormones, which are involved in mediating inflammation or bone remodeling and development(*54, 100*).

In this research, we report molecular phenotypic pathways previously unknown to be commonly dysregulated in murine and human MMP2 deficiency. Our analyses targeted cytokines, chemokines, angiogenesis and bone development factors, apolipoproteins and hormones in the circulation of MMP2-deficient patients and *Mmp2*$^{-/-}$ mice. Our results expose overlapping cytokine and chemokine expression profiles in *Mmp2*$^{-/-}$ mice and the case of human MMP2 deficiency. Among the serum components found to be dysregulated in both human and murine MMP2 deficiency, bioactive cortisol and several pro-inflammatory cytokines involved in bone loss (*101-104*), were significantly elevated. These identified factors are likely to be intermediaries in the poorly understood pathological mechanisms elicited by MMP2 deficiency.

Further research is needed to establish and clarify their roles in the causation of the multisystem syndrome of pediatric MMP2 deficiency. Although further research is needed to establish and clarify their roles in the causation of the multisystem syndrome of pediatric MMP2 deficiency, the present results (i.e., identification of new molecular phenotypic traits associated with human and murine MMP2 deficiency) are an essential first step to understanding the underlying biological mechanisms.

2.3 Results

2.3.1 Murine and human MMP2 deficiency result in distinct but overlapping expression of pro- and anti-inflammatory cytokines

Both murine and human MMP2 deficiency results in severe inflammation and bone loss (*2, 57, 95, 96*) but the MMP2-mediated molecular pathways through which these phenotypes occur are unknown. To identify dysregulated serum factors that could be associated with the inflammatory and arthritic phenotype in MMP2 deficiency, we first performed a targeted screen on the serum of an eight-year-old male patient with MMP2 deficiency caused by the inactivating mutation c1294delC (Arg432fs) in the *MMP2* gene. This patient was selected as a representative case of MMP2 deficiency for initial studies based on the presented symptoms, clinical assessment and absence of pharmacological intervention (materials and methods). We analyzed eighty-one serum biomolecules consisting of cytokines, chemokines, angiogenesis markers, bone development factors, hormones and apolipoproteins. Compared to unaffected controls, noteworthy differences in the MMP2 deficient patient include: i) the cytokines GM-CSF, GRO-α, IL-12p40, IL-1β, IL-4, IL-7, IL-9, IL-15, sCD40L and MIP-1α were substantially higher (> 4-fold) (**Figure 2.1a-c**); ii) IFN-α2 was 9-fold lower (**Figure 2.1c**); there were no notable differences in soluble cytokine

receptors (**Figure 2.1d**); iii) the vasoconstrictor Endothelin-1 (a substrate of MMP2)(*105*) was 13-fold higher (**Figure 2.1e**); iv) ACTH was 7-fold lower (**Figure 2.1f**); v) finally, there were no notable differences in apolipoprotein concentrations (**Figure 2.1g**).

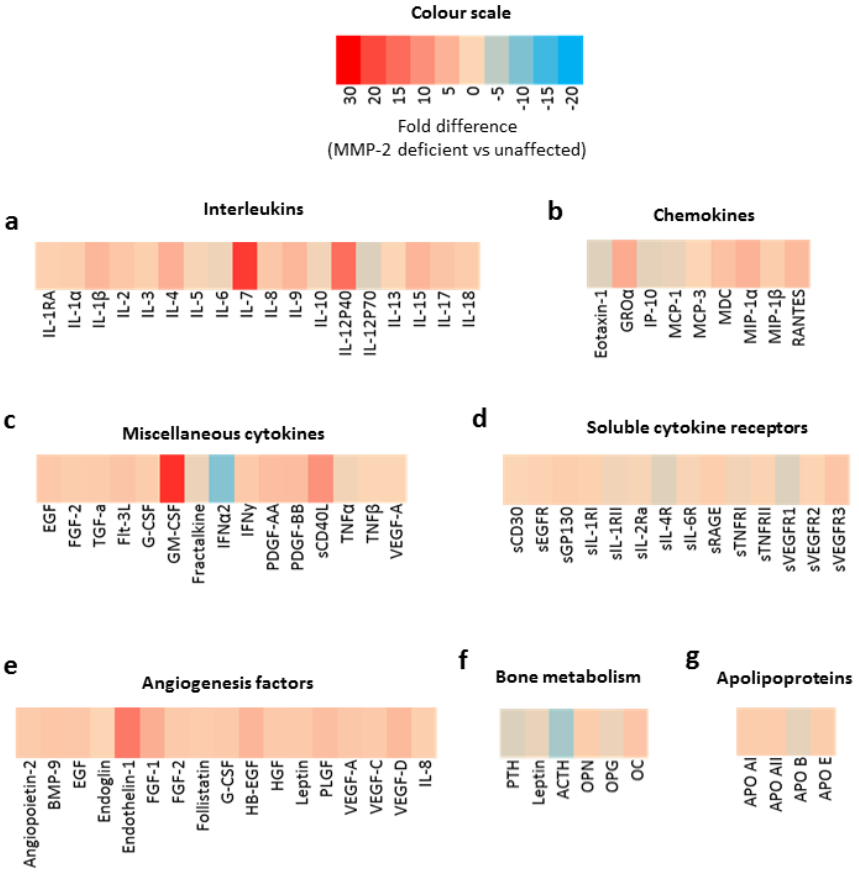

Figure 2.1: **Preliminary serological screening to identify dysregulated serum factors in a case of human MMP2 deficiency**.

(**a-g**) Heat map diagrams showing the relative serum levels of an array of (**a**) interleukins, (**b**) chemokines, (**c**) miscellaneous cytokines, (**d**) soluble cytokine receptors, (**e-f**) angiogenesis and bone development factors, and (**g**) apolipoproteins, in a case of human MMP2 deficiency (eight-year-old male MONA patient) compared to unaffected controls. Data are presented as fold difference between concentrations of each annotated biomolecule in the sera of MMP2 deficient patient *versus* unaffected controls (n=3). Measurements were taken in duplicate.

To increase confidence in the observed dysregulated cytokines in the initial screening, we conducted a second multiplex cytokine assay (48-plex) on the sera of the MMP2 deficient patient along with unaffected controls. We observed a significant upregulation in Eotaxin, GM-CSF, M-

CSF, GRO-α, MDC, IL-1β, IL-7, IL-12p40, MIP-1α, MIP-1β and MIG, whereas EGF was downregulated in the patient (**Figure 2.2**).

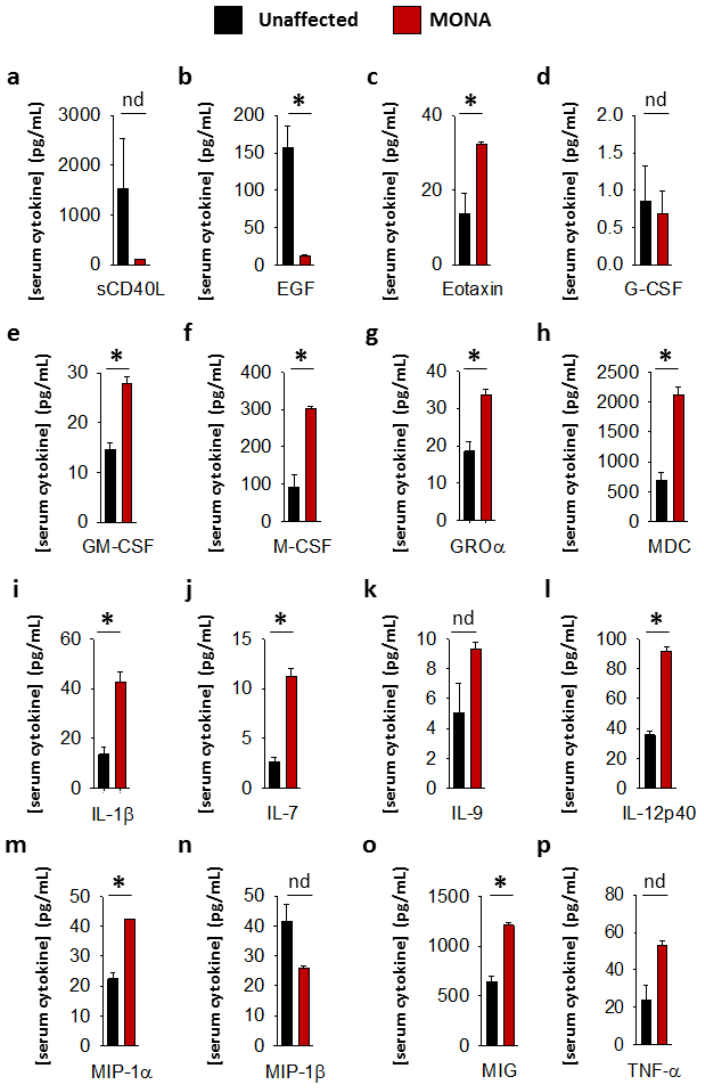

Figure 2.2: Complementary analyses of a panel of selected cytokines in the eight-years-old male MONA patient to confirm dysregulation.

(**a-p**) Bar graphs comparing concentrations of cytokines and chemokines in sera of MONA patient vs unaffected controls (n=3). The panel of selected cytokines was measured using a cytokine 48-plex assay (Eve Technologies). Data are presented as mean ± SE of the mean. Measurements were taken in duplicate. *$p<0.05$, comparisons MONA vs unaffected control group (One-way ANOVA/Holm–Sidak method); nd, no difference.

To determine whether these observations can be generalized to all the MMP2 deficient patients in the study, we conducted confirmatory multiplex cytokine analyses on the sera of a group of five MMP2 deficient patients diagnosed with MONA (four female and one male) compared to

six unaffected controls (five female and one male). These analyses showed a significant upregulation in Eotaxin, IL-7, IL-12p40 and MIP-1α, and a downregulation in EGF in the MMP2 deficient patients (**Table 2.1**).

Factor	Control	MONA	p-value	WT plasma	*Mmp2*$^{-/-}$ plasma	p-value
Eotaxin	19.5 ± 4.12	55.1 ± 11.5	0.009	49.8 ± 2.72	572 ± 6.72	<0.001
G-CSF	6.84 ± 3.61	0.721 ± 0.179	0.16	0.640 ± 0.00	38.8 ± 7.89	0.04
GM-CSF	24.4 ± 6.15	16.7 ± 3.03	0.317	36.1	45.21	--
IFNy	1.48 ± 0.312	0.664 ± 0.251	0.078	ND	2.37 ± 1.68	--
IL-1a	33.3 ± 6.90	34.0 ± 8.48	0.952	10.22 ± 0.00	59.9 ± 11.1	0.046
IL-1B	31.2 ± 10.5	29.7 ± 8.04	0.91	8.01 ± 3.40	23.4 ± 0.590	0.047
IL-2	1.83 ± 0.971	0.896 ± 0.320	0.425	3.86 ± 0.930	3.65 ± 0.658	0.874
IL-3	0.055 ± 0.0156	0.311 ± 0.165	0.122	ND	ND	--
IL-4	1.30 ± 0.267	0.845 ± 0.194	0.214	ND	0.12 ± 0.035	--
IL-5	5.07 ± 2.77	3.34 ± 1.09	0.603	4.70 ± 0.124	5.72 ± 0.0884	0.022
IL-6	0.633 ± 0.135	0.706 ± 0.0900	0.679	ND	1.34 ± 0.428	--
IL-7	3.54 ± 0.745	9.37 ± 1.54	0.005	12.3 ± 1.40	12.1 ± 2.28	0.935
IL-9	3.84 ± 1.40	7.51 ± 1.54	0.111	3.46 ± 2.44	ND	--
IL-10	0.908 ± 0.319	4.60 ± 1.99	0.074	7.22 ± 4.20	3.03 ± 1.02	0.434
IL-12p40	52.4 ± 12.3	140 ± 15.1	0.001	2.78 ± 1.28	3.84 ± 1.81	0.68
IL-12p70	1.74 ± 0.591	1.82 ± 0.631	0.928	9.96 ± 0.382	5.25 ± 1.09	0.055
IL-13	48.3 ± 5.91	37.9 ± 8.16	0.318	41.1 ± 24.5	72.4 ± 18.1	0.412
IL-15	11.3 ± 1.90	17.1 ± 6.34	0.367	1.28 ± 0.00	36.8 ± 13.7	0.122
IL-17	11.4 ± 6.51	17.3 ± 8.38	0.582	ND	0.885 ± 0.237	--
IP-10	43.1 ± 11.6	37.4 ± 9.32	0.718	13.4 ± 0.711	73.1 ± 3.83	0.004
MCP-1	387 ± 41.6	320 ± 39.8	0.286	ND	ND	--
M-CSF	105 ± 25.8	186 ± 65.5	0.28	25.6 ± 11.5	13.7 ± 9.47	0.507
MIG	1060 ± 202	1650 ± 521	0.292	13.0 ± 0.979	112 ± 4.96	0.003
MIP-1a	18.8 ± 2.20	45.5 ± 9.49	0.015	65.7 ± 2.676	8.16 ± 4.01	0.007
MIP-1B	45.2 ± 5.67	31.0 ± 3.87	0.078	14.5 ± 4.43	18.1 ± 3.15	0.578
RANTES	3800 ± 1120	11700 ± 8370	0.33	11.6 ± 3.79	50.8 ± 3.92	0.019
TNFa	28.6 ± 4.05	38.0 ± 6.15	0.22	7.49 ± 4.39	1.28 ± 0.00	0.293
VEGF	271 ± 70.6	152 ± 27.2	0.18	0.155 ± 0.103	0.595 ± 0.0247	0.053

Table 2.1: **Comparison of analyses of circulating cytokine levels in human and murine MMP2 deficiency**.

The panel of selected human cytokines and chemokines was measured in sera from MMP2 deficient MONA patients (n=5) and unaffected controls (n=6) using a cytokine 48-plex assay (Eve Technologies). The panel of selected murine cytokines and chemokines was measured in pooled plasma of *Mmp2*$^{-/-}$ (n=4) and WT (n=4) mice using the cytokine 32-plex assay (Eve Technologies). p-values obtained from comparisons of MONA vs unaffected control group and *Mmp2*$^{-/-}$ (n=4) vs WT (n=4) mice (One-way ANOVA/Holm–Sidak method); ND, not detected. Measurements were taken in duplicate.

Further determinations of serum factors that affect bone growth and development in the same group of MMP2 deficient patients (compared to unaffected controls) showed significant

upregulation in osteocalcin, osteopontin and FGF-23, and downregulation in osteoprotegrin and leptin, while DKK1, SOST, PTH and insulin showed no difference (**Fig 2.3**).

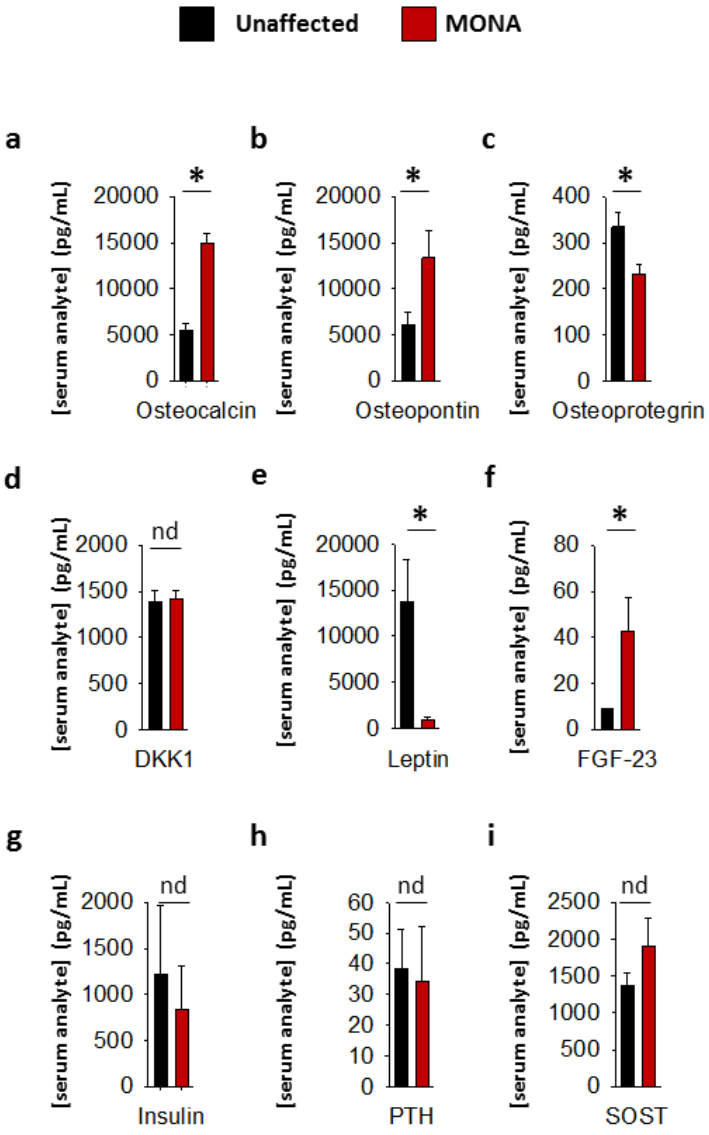

Figure 2.3: **Analyses of a panel of selected bone metabolism markers in the sera of MONA patients**.

(**a-i**) Bar graphs comparing concentrations of bone metabolism markers in the sera of MONA patients (n=5) vs unaffected controls (n=6). The panel of selected markers of bone development was measured using a 13-plex human bone array (Eve Technologies). Data are presented as mean ± SE of the mean. Measurements were taken in duplicate. *p<0.05, comparisons MONA vs unaffected control group (One-way ANOVA/Holm–Sidak method); nd, no difference.

Mmp2$^{-/-}$ mice are the standard study model for research on the pathogenesis of MMP2 deficiency (*57, 96, 99*). Thus, a thorough characterization of the commonalities and differences between MMP2 deficient patients and *Mmp2*$^{-/-}$ mice is requisite for translating findings in mice to humans. Identifying molecular phenotypic traits common to murine and human MMP2 deficiency would provide a starting point for research aimed at understanding the pathological mechanisms elicited in human MMP2 deficiency using the murine model.

To determine whether the dysregulated cytokines observed in the case of human MMP2 deficiency are also dysregulated in murine MMP2 deficiency, we measured the levels of thirty-two cytokines and chemokines in the plasma of age- and sex matched MMP2 knockout (*Mmp2*$^{-/-}$) mice (n=4) and compared them to wild type (WT) (n=4). The cytokines Eotaxin, MIG, IL-1α, IL-1β, IL-5, G-CSF, RANTES, KC, IP-10 and LIX (CXCL5) were significantly upregulated, whereas the cytokine MIP-1 α and LIF were significantly downregulated in the plasma of *Mmp2*$^{-/-}$ mice compared to WT (**Table 2.1**). There was no statistically significant difference between the two groups in M-CSF, TNF-α, IFN-γ, IL-2, IL-3, IL-4, IL-6, IL-7, IL-9, IL-10, IL-12 p40, IL-12p70, IL-13, IL-15, IL-17, MCP-1, MIP-2, and VEGF (**Table 2.1**). Together, these results reveal a distinct yet overlapping cytokine expression profiles in the circulation of MMP2 deficient mouse and human (**Figure 2.3a**). Indeed, Eotaxin, IL-1β, and MIG were upregulated in the circulation of *Mmp2*$^{-/-}$ mice and the MMP2 deficient patients (**Table 2.1 and 2.2**). The cytokines IL-1α, G-CSF and RANTES were uniquely upregulated in the circulation of *Mmp2*$^{-/-}$ mice. In contrast, IL-7, IL-12 p40, GM-CSF and M-CSF were uniquely dysregulated in the circulation of MMP2 deficient patients (**Figure 2.2**, **Table 2.1 and 2.2**).

Together, our results identify cytokines dysregulated in human and murine MMP2 deficiency that are implicated in bone loss(*101-103, 106-110*).

Factors	Action	Reference	MONA (serum)	*Mmp2*$^{-/-}$ (plasma)	*Mmp2*$^{-/-}$ (heart)
Eotaxin	Induces migration of pre-osteoclast and increases bone resorption	(*111*)	up	up	up
EGF	Stimulates proliferation of osteoblast progenitor cells	(*112, 113*)	down	-	-
IL-1α	Induces osteoclast differentiation	(*114*)	nd	up	nd
IL-1β	Induces RANKL expression and osteoclast differentiation	(*115, 116*)	up	up	nd
IL-7	Stimulates osteoclast formation by inducing RANKL and M-CSF expression and also via STAT5 activation	(*102, 117, 118*)	up	nd	up
IL-12p40	Subunit of IL-23; promotes osteoclastogenesis via inducing RANKL and RANK expression	(*119, 120*)	up	nd	up
G-CSF	Increases osteoclast bone-resorption activity	(*121*)	nd	up	up
GM-CSF	Increases formation of multi-nuclear bone-resorbing osteoclasts	(*103, 122*)	up	nd	nd
M-CSF	Induces osteoclast differentiation, survival, proliferation, and maturation	(*122*)	up	nd	nd
MIP-1α	Promotes migration and activation of osteoclasts	(*123*)	up	down	up
RANTES	Promotes cell migration and survival of osteoblasts	(*124*)	nd	up	up
MIG	Stimulates osteoclast migration and adhesion	(*125*)	up	up	up
OPG	Decoy receptor of RANKL; inhibits osteoclast differentiation	(*109, 126, 127*)	down	-	-

Table 2.2: **Summary of dysregulated cytokines in human and murine MMP2 deficiency.**

Upregulation or downregulation of cytokines in sera of MONA patients vs controls (**Figure 2.1-2.3, Table 2.1**), plasma of *Mmp2*$^{-/-}$ vs WT (**Table 2.1**) and heart tissue of *Mmp2*$^{-/-}$ vs WT (*128*); nd: no difference.

2.3.2 MMP2 deficiency is associated with increased circulatory levels of cortisol and decreased cortisol binding globulin

The initial serum screening of the eight-year-old male MMP2 deficient patient showed relatively lower levels of serum adrenocorticotropic hormone (ACTH) in MMP2 deficient serum compared to unaffected controls (**Figure 2.1f**). This raised the question whether circulating cortisol levels is dysregulated in the MMP2 deficient patient and if so, can this dysregulation be generalized to other MMP2 deficient patients and mice? To answer this question, we measured serum cortisol levels in MMP2 deficient patients as well as *Mmp2*$^{-/-}$ mice along with their respective unaffected controls by ELISA. The results showed that serum cortisol concentrations were significantly

higher in both MMP2 deficient humans and *Mmp2*$^{-/-}$ mice (**Figure 2.4a and 2.4b**) compared to their respective unaffected controls.

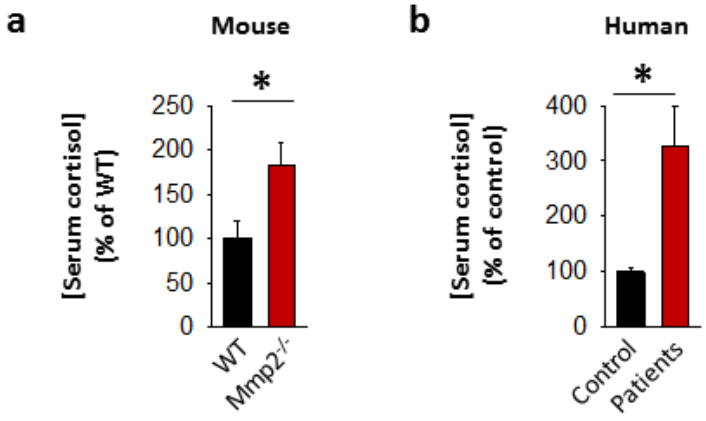

Figure 2.4: Quantitation of serum cortisol in humans and mice.

(**a**) Bar graph showing serum cortisol concentration in *Mmp2*$^{-/-}$ mice (n=6) compared to WT mice (n=6). (**b**) Bar graph showing serum cortisol concentration in MMP2 deficient humans (n=6) compared to unaffected controls (n=8). *$p < 0.05$, comparison of *Mmp2*$^{-/-}$ vs WT one-way ANOVA. Duplicate readings of standards taken to ensure technical reproducibility.

Approximately up to 90% of cortisol in circulation is bound to the cortisol binding protein (CBG) which keeps cortisol biologically inactive(*129*). Hence, we measured serum CBG protein levels in MMP2 deficient patients and mice to determine whether CBG is also elevated in response to cortisol elevation in MMP2 deficiency to suppress its biological activity. The results showed that there is no difference in CBG levels in MMP2 deficient patients tested compared to unaffected controls (**Figure 2.5a and 2.5b**), whereas *Mmp2*$^{-/-}$ mice had significantly lower serum CBG compared to wild type (**Figure 2.5c and 2.5d**). The results indicate that there is no compensatory increase in CBG in response to elevated cortisol to suppress its biological activity and hence overall biologically active cortisol is elevated in the sera of both MMP2 deficient mice and humans.

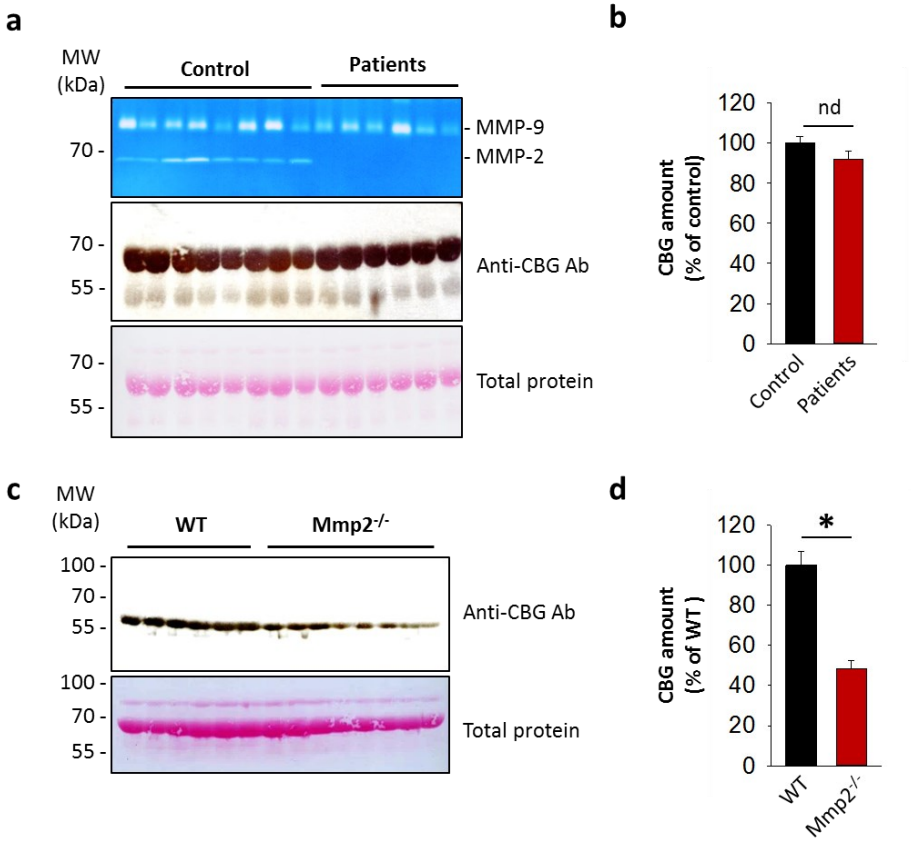

Figure 2.5: Serum cortisol binding protein in MMP2 deficient patients and mice.

(**a**) Quantitation of serum cortisol binding protein in MMP2 deficient humans and unaffected controls by western blot. Top: Gelatin zymogram of sera from MMP2 deficient humans (n=6) and unaffected controls (n=8). Middle: Immunoblot probed with anti-CBG antibody to detect CBG in sera from MMP2 deficient humans (n=6) and unaffected controls (n=8). Bottom: Membrane stained with ponceau red to determine total protein content. Blots shown are representative images of duplicate analyses. (**b**) Bar chart showing quantitation of band intensities of the blot in (a) by densitometric scanning. Band intensities of the blot probed with anti-CBG were divided by their corresponding total protein bands to normalize. *p<0.05 determined by one way ANOVA. (**c**) Quantitation of serum cortisol binding protein in *Mmp2*$^{-/-}$ and WT mice by western blot. Top: Immunoblot probed with anti-CBG antibody to detect CBG in sera from WT mice (n=6) and *Mmp2*$^{-/-}$ mice (n=8). Bottom: Nitrocellulose membrane stained with ponceau red to determine total protein content. (**d**) Bar chart showing quantitation of band intensities of the blot in (e) by densitometric scanning. Band intensities of the blot probed with anti-CBG were divided by their corresponding total protein bands to normalize. *p<0.05 determined by one way ANOVA.

2.4 Discussion

In this research, we aimed to advance the phenotypic characterization of MMP2 deficiency by identifying molecular traits that are similarly dysregulated in MMP2 deficient patients and *Mmp2*$^{-/-}$ mice which are the standard study model for the rare multisystem pediatric syndrome

elicited by MMP2 deficiency in humans. Due to the rarity of genetic MMP2 deficiency and limited access to patient samples, we adopted an approach where we selected an eight-year-old male MMP2 deficient MONA patient as a representative case for human MMP2 deficiency / MONA in the initial serum screening analyses. Our selection of this patient was based on the following: i) the patient presented with all the hallmark symptoms of MONA, ii) extensive clinical analyses including clinical blood tests have been done to rule out secondary diseases which could cause the observed symptoms (**Figure 2.6**), iii) the patient received no pharmacological drugs which could potentially affect the serum factors analyzed (the patient was prescribed joint mobilization – a physical therapy intervention – as treatment). MONA patients receive treatment with pharmacological drugs (such as bisphosphonates to reduce skeletal pain and increase bone mineral density (*130*)) which may have unpredictable side effects and affect the upregulation or downregulation of the serum factors analyzed. Therefore, it was necessary to adopt this unconventional approach of finding a representative case of human MMP2 deficiency where interfering factors such as pharmacological drugs and secondary diseases could be ruled out. We validated our findings from analyses of the representative case with *Mmp2*$^{-/-}$ mice and a cohort of five MMP2 deficient patients and found serum components that are similarly dysregulated in MMP2 deficient mice and patients.

The cytokines dysregulated in MMP2 deficiency include known inducers of osteoporosis.

The dynamic bone remodeling process is maintained by a balance and signaling between bone-forming osteoblasts (which produce bone matrix proteins) (*131*) and bone-resorbing multinucleated osteoclasts (*103, 108*). Chronic inflammation, as present in MMP2 deficiency (*2, 57, 94-98*), alters the balance between osteoclasts and osteoblasts favoring more bone resorption which then leads to osteoporosis (*55*). Among the panel of selected markers of bone metabolism

analyzed, FGF-23 was upregulated in MONA patients. Among the regulators of bone turnover, osteoprotegrin (OPG) was downregulated, whereas dickkopf-1 (DKK-1) and sclerostin (SOST) were unchanged in MONA patients. Although, further research is necessary to establish the consequences of the observed upregulation in FGF-23 and OPG in MMP2 deficiency, these two markers could potentially contribute to exacerbating osteolysis in the patients. FGF-23 is mainly secreted by osteocytes and osteoblasts and is upregulated in the circulation in cases of bone disorders characterized by softening and weakening of bones (low bone mineral density) including all types of hypophosphatemic rickets (*132*). FGF-23 inhibits bone mineralization (*133*), but the mechanism of action remains unclear. OPG acts as a decoy receptor for RANKL and inhibit osteoclastogenesis, and a downregulation in OPG (observed in MONA patients) is associated with increased osteoporosis (*109, 126, 127*).

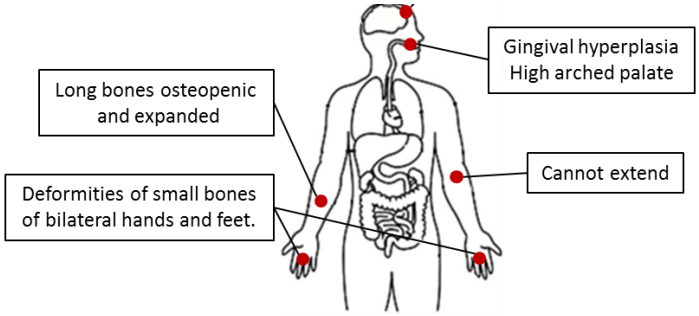

Summary of clinical assessment of eight-year-old MMP-2 deficient patient	
Physical exam	High arched palate, gingival hyperplasia and gynecomastia. Left elbow cannot be extended to 180 degrees. Ulnar deviation and abnormal creases on both hands. Contractures in both hands with shortened fingers and camptodactyly. Bone excess in plantar area right foot and camptodactyly of toes.
Clinical symptoms	Progressive contractures, subcutaneous nodules, osteolysis (on radiographs), pigmentary streaks, gynecomastia, gingival hyperplasia
Negatives	Normal eye and cardiac exams, no hepatosplenomegaly, no large joints contractures, normal development, no macrocephaly, normal testing for Morquio A (excluded by gene testing). Clinical blood tests: - normal complete blood count (CBC) - normal comprehensive metabolic panel (CMP): glucose, calcium, albumin, total protein, electrolytes (sodium, potassium, bicarbonate, chloride), kidney function tests (blood urea nitrogen and creatinine) and Liver tests (ALP, ALT-SGPT, AST-SGOT, bilirubin and hemoglobin) - normal rheumatoid factor - normal C-reactive protein, - CCP Antibodies IgG/IgA - normal erythrocyte sedimentation rate (ESR)
Clinical differential	Torg Winchester syndrome, Frank ter Haar (SH3PXD2B), Oligosaccharidosis (mannosidosis, mainly alpha), Aspartylgulcosaminuria, Fucosidosis, Multiple sulfatase deficiency, MPS disorders
Diagnosis	MONA (multicentric osteolysis, nodulosis, and arthropathy OMIM #259600), also known as Torg Winchester syndrome (confirmed by whole exome sequencing)
Exome/Genome	two mutations (compound heterozygote) in the MMP2 gene c.1160G>A (p.Trp387Ter) c.1294delC (Arg432fs)

Figure 2.6: Summary of clinical assessment of the eight-year-old MMP2 deficient patient.

Among the pro-inflammatory cytokines that were elevated in the circulation of *Mmp2*$^{-/-}$ mice and/or MMP2 deficient patients, IL-1α, IL-1β, IL-7, IL-12p40, G-CSF, GM-CSF, M-CSF, MIP-1α and MIG are implicated in the promotion of bone resorption by stimulating osteoclast migration, proliferation, differentiation or activation (**Table 2.2**) (*103, 104, 108, 109, 111, 112, 114-117, 119-121, 123, 125, 134*). Although further research is necessary to establish the consequences of the upregulation in these cytokines in the pathological mechanisms elicited in

MMP2 deficiency, a brief synthesis based on evidence from the literature on how these cytokines could contribute to increased osteolysis in MMP2 deficiency are as follows. Osteoclast maturation is regulated by factors such as the receptor activator of NF-κB ligand and M-CSF, in addition to TNF-α and GM-CSF (*108, 109*). IL-7, which was commonly elevated in the circulation of MONA patients and heart of *Mmp2*$^{-/-}$ mice (**Table 2.2**), stimulates osteoclast formation by up-regulating the T-cell production of soluble osteoclastogenic cytokines RANKL and M-CSF(*117*). Moreover, *in vivo* administration of IL-7 induces bone loss as well as blocks new bone formation in mice (*101, 102*). IL-12p40 was consistently elevated across all MONA patients (**Figure 2.1-2.2, Table 2.1**) and also upregulated in the heart of *Mmp2*$^{-/-}$ mice (*128*). IL-12p40 as a subunit of IL-23 is associated with osteolysis in mice (*135*) and functions to promote osteoclastogenesis by inducing RANKL and RANK expression (*119, 120*). The cytokine GM-CSF, elevated in the eight-year-old MMP2 deficient patient, induces the fusion of mononuclear osteoclasts to bone-resorbing multinuclear osteoclasts in mice (*103*). High levels of GM-CSF and M-CSF in systemic inflammatory diseases are suggested to increase osteoclast progenitor cell pools (in the bones, bone marrow and blood) which upon homing to the bones can lead to an increase in the number of osteoclasts and bone resorption (*122*) (**Figure 2.3c**). GM-CSF is a promising therapeutic target in the treatment of rheumatoid arthritis – an autoimmune disease characterized by joint inflammation which can lead to local and systemic osteoporosis (*136-138*). Mavrilimumab, a monoclonal antibody against GM-CSF receptor, has demonstrated promising results in the treatment of rheumatoid arthritis in clinical trials and is being considered as an additional therapeutic option for rheumatoid arthritis patients who are multi-resistant to the available targeted drugs (*137, 139-141*). Further research is necessary to establish the specific

consequences of GM-CSF in MMP2 deficiency, and to test the possibility of targeting GM-CSF to manage inflammation and prevent bone loss in MONA.

The variations in the dysregulated serum cytokines observed across MONA patients (**Figs. 2.1, 2.2 and Table 2.1**; eight-year-old male patient vs all five MONA patients) likely arise due to different medications and treatments the patients receive in to manage pain and inflammation among other uncontrollable factors. Three of these patients receive bisphosphonates to reduce skeletal pain and increase bone mineral density (*130*). Despite the existing variations in treatments between the patients, the cytokines Eotaxin, IL-7, IL-12p40 and MIP-1α were upregulated, and EGF was downregulated across all patients (**Figure 2.2 and Table 2.1**). Although the consequences of these changes specifically in MMP2 deficiency need to be established, the cytokines Eotaxin, IL-7, IL-12p40 and MIP-1α could contribute to increased osteolysis in MMP2 deficiency through their known osteoclastogenic functions causing increased bone resorption (**Table 2.2, Figure 2.7**). Also, an insufficiency of epidermal growth factor (EGF) in MONA could downregulate EGF's normal function of stimulating proliferation of bone marrow stromal stem cells (the progenitor cells for osteoblasts) (*113*).

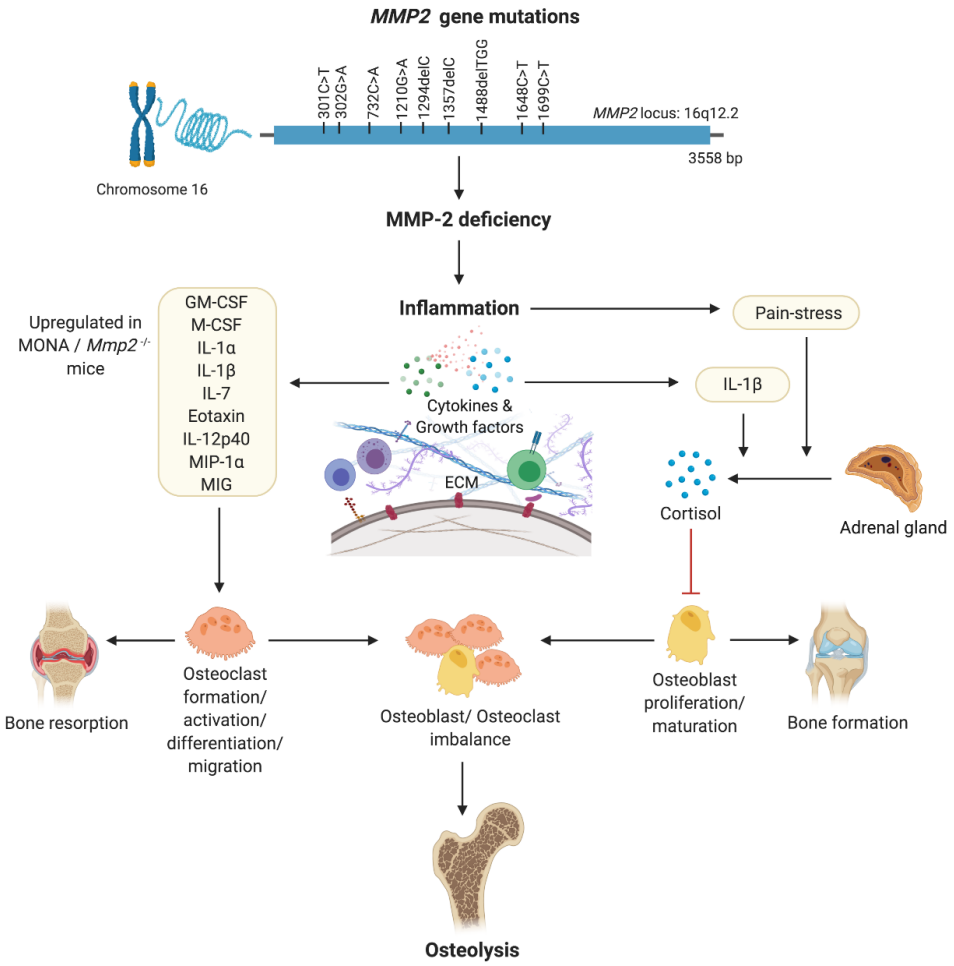

Figure 2.7: **A hypothesized pathway of MMP2 deficiency mediated osteoporosis**.

Denaturing mutations in the *MMP2* gene leading to MMP2 deficiency mediated inflammation results in increased circulating levels of pro-inflammatory cytokines known to increase the formation, migration, differentiation, and activation of osteoclasts. Pain-stress resulting from inflammation induces an increase in secretion of cortisol which has an inhibitory effect on osteoblast proliferation and maturation. Consequently, an imbalance in the population of bone forming osteoblasts and bone-resorbing osteoclasts results in osteolysis.

Glucocorticoid-induced osteoporosis may be a newly identified phenotype characteristic of MMP2 deficiency. The initial serum screening of the case of human MMP2 deficiency showing relatively low levels of serum ACTH prompted us to look at cortisol levels in MMP2 deficient patients. ACTH is a tropic hormone produced in the anterior pituitary gland and stimulates the release of steroid hormone cortisol from the adrenal gland(*142*). Interestingly, our data showed the presence of significantly higher levels of cortisol in MMP2 deficient patients compared to

unaffected controls. Low ACTH typically results in low cortisol being released from the adrenal gland, however presence of low ACTH could also imply presence of high serum cortisol which lowers ACTH release by a negative feedback mechanism(*142*).

Age, sex, pharmacological interventions, and procedure and time of blood collection (*143, 144*), may potentially affect serum cortisol levels in the patients. However, these factors are challenging to account for when studying a rare pediatric condition such as MMP2 deficiency because of the limited number of diagnosed patients in the world. Furthermore, there are practical difficulties in accessing to these patients and the various medical treatments prescribed to manage their inflammation and pain are likely to alter the expression of many cytokines.

In humans, circulating cortisol levels are higher on average during the day compared to night (*145, 146*), whereas in mice circulating cortisol levels are higher during night (*147*). For practical reasons, human sera collection in the clinic typically occurs during the day (when patients and healthy controls visit the hospital and follows strict protocol). The animal model of MMP2 deficiency, *Mmp2*$^{-/-}$ mice, allowed us flexibility in terms of controlling the aforementioned variables that may affect circulating cortisol. Yet, unaware of a possible influence of MMP2 levels on cortisol, we collected mice sera in the morning between the hours of 8:00 am to 11:00 am, a period of the day when circulating cortisol levels in mice are the lowest(*148*). Interestingly, we found that serum cortisol levels were significantly higher whereas CBG levels were significantly lower in *Mmp2*$^{-/-}$ mice, compared to WT mice. Our findings are in agreement with previous research (*149*), which had reported a strong association between lower levels of MMP2 protein in circulation with higher levels of plasma cortisol in humans. Thus, our data suggest a strong association between MMP2 deficiency and increased levels of circulating cortisol and decreased levels of the endogenous cortisol inhibitor CBG.

MMP2 deficient patients and *Mmp2*$^{-/-}$ mice present with chronic inflammation of the joints, and as such, upon movement, they experience chronic pain (*57, 98*) – a stressor capable of inducing the stress response and intensifying cortisol secretion which has acute anti-inflammatory effects (*150*). The chronic nature of the pain-related stressor could cause chronic reactivation of the stress response and repeated surges in cortisol secretion (*150*). Thus, chronic pain-related stress may have resulted in the elevated serum cortisol levels observed in MMP2 deficient patients and *Mmp2*$^{-/-}$ mice. Further, IL-1β was upregulated in both human and murine MMP2 deficiency (**Figs. 2.1, 2.2 and Table 2.1, 2.2**). While the specific effect of IL-1β upregulation in MMP2 deficiency need to be established, a likely effect of IL-1β upregulation is to directly stimulate the release of cortisol from the adrenal glands (**Figure 2.7**) (*151, 152*).

While our observations associate increased circulating bioactive cortisol with MMP2 deficiency, further studies are necessary to elucidate the molecular mechanisms of this association and the specific consequences of elevated cortisol in the pathogenesis of MONA. Conceivably, the potential consequences of increased cortisol in the MMP2 deficiency are likely to be through the known mechanisms by which cortisol affects bone metabolism. Glucocorticoids including cortisol inhibit calcium absorption, an increase of urinary calcium excretion (*104*), inhibit bone formation as well as increase bone resorption, which lead to osteoporosis after continued exposure to elevated cortisol (*107, 153, 154*). Cortisol increases the expression of the crucial osteoclastogenesis factor M-CSF (*155*) while decreasing the production of the anti-resorptive RANK-L decoy receptor osteoprotegrin (downregulated in MONA patients; **Figure 2.3c**) (*156*), therefore promoting bone resorption and osteoclastogenesis while disrupting the coupled osteoblast-osteoclast interaction (*104*). Cortisol can decrease osteoblasts replication and slow their differentiation into mature osteoblasts (*104, 157*). In addition, cortisol inhibits the synthesis

of type 1 collagen, the most abundant bone matrix protein and a major constituent in bone mineralization (*158*), by transcriptional and post-transcriptional mechanisms in osteoblasts (*159*). Further, cortisol increases the half-life of collagenase type III (MMP-13) transcripts in osteoblasts, resulting in increased matrix collagen degradation (*160*). Thus, further research is needed to establish cortisol as a target for therapeutic intervention in reducing osteoporosis in MMP2 deficiency.

2.5 Materials and Methods

The study was conducted in accordance with relevant guidelines and regulations of the Health Research Ethics Board (HREB) at the University of Alberta. All animal protocols were approved by the University of Alberta animal care committee and executed in compliance with institutional guidelines issued by the Canada Council on Animal Care. Serum was collected with informed consent from the donors.

2.5.1 Study cohort

Human: Initial screening of serum factors was performed on an eight-year-old male MMP2 deficient patient presenting a previously unreported inactivating deletion mutation c1294delC (Arg432fs) in *MMP2* gene and clinically diagnosed with MONA. We selected this patient as a representative case for human MMP2 deficiency / MONA in the initial serum screening analyses because of the following reasons: i) the patient presented with all the hallmark symptoms of MONA, ii) extensive clinical analyses including clinical blood tests have been done to rule out secondary diseases which could cause the observed symptoms, iii) the patient received no pharmacological drugs which could potentially affect the serum factors analyzed (the patient was prescribed joint mobilization – a physical therapy intervention – as treatment). Due to the rarity

of genetic MMP2 deficiency and limited access to patient samples, we deemed this unconventional approach necessary for this study. We followed the initial screening with analyses of selected serum factors in five other MONA diagnosed MMP2 deficient patients of both sexes (four females and one males – including MMP2 deficiency cases previously described (*97, 130*)) of ages between eight to fifteen years were used for subsequent analyses of serum factors. The second male patient present a homozygous mutation a c.301C > T, predicting the amino acid change p.Arg101Cys (*97*). The female patients present a homozygous mutation c.1699C > T in exon 11 of the *MMP2* gene that introduces a premature stop codon (p.Arg567Ter) (*130*). Sera from a total of thirteen different unaffected controls, which included donors of both sexes of ages between ten to forty-five years (including unaffected siblings and parents of the MMP2 deficient patients), were used in this study (number of controls used in each experiment is stated in the figure legends). Unaffected controls were confirmed to express MMP2 by gelatin zymography. Human serum samples were collected, frozen, transported from the sites of collection in dry ice and stored at -80°C before subsequent analysis.

Mouse: Plasma (EDTA-treated) from four *Mmp2*$^{-/-}$ and four WT male mice aged ten to fifteen weeks were used for multiplex assays. Sera from eight Mmp2$^{-/-}$ and six WT male mice aged ten to fifteen weeks were used for cortisol analyses. Plasma samples were collected in the morning between 8:00 am to 11:00 am and stored at -80°C until subsequent analyses.

2.5.2 Multiplex Assays to quantify serum components

Multiplex assays for measuring serum proteins were outsourced to Eve Technologies (Calgary, AB, Canada) who collected the following data. Sample preparation and data analysis was done by me in the CFP lab.

Assessment of markers of inflammation in Mmp2$^{-/-}$ mice: Mouse plasma and chemokine concentrations were determined using a multiplex immunoassay (Millipore MILLIPLEX; cat# MCYTMAG-70K-PX32) analyzed with a BioPlex 200 (BioRad, USA). Mouse cytokines and chemokines measured include: Eotaxin, G-CSF, GM-CSF, IFN-γ, IL-1α, IL-1β, IL-2, IL-3, IL-4, IL-5, IL-6, IL-7, IL-9, IL-10, IL-12p40, IL-12p70, IL-13, IL-15, IL-17, IP-10, KC, LIF, LIX, MCP-1, M-CSF, MIG, MIP-1α, MIP-1β, MIP-2, RANTES, TNFα, and VEGF.

Assessment of inflammation markers in MMP2 deficient patient: Human serum cytokine and chemokine concentrations were determined using a 42-plex (Millipore MILLIPLEX; cat# HCYTOMAG-60K) and a 48-plex (Eve Technologies, Canada, cat#HD48) multiplex immunoassays including: sCD40L, EGF, Eotaxin, FGF-2, Flt-3 ligand, Fractalkine, G-CSF, GM-CSF, GROα, IFNα2, IFNγ, IL-1α, IL-1β, IL-1ra, IL-2, IL-3, IL-4, IL-5, IL-6, IL-7, IL-8, IL-9, IL-10, IL-12p40, IL-12p70, IL-13, IL-15, IL-17A, IL-17E/IL-25, IL-17F, IL-18, IL-22, IL-27, IP-10, MCP-1, MCP-3, M-CSF, MDC (CCL22), MIG, MIP-1α, MIP-1β, PDGF-AA, PDGF-AB/BB, RANTES, TGFα, TNFα, TNFβ, VEGF-A. Serum concentrations of a panel of human soluble cytokine receptors consisting of sCD30, sEGFR, sgp130, sIL-1RI, sIL-1RII, sIL-2Rα, sIL-4R, sIL-6R, sRAGE, sTNFRI, sTNFRII, sVEGF-R1, sVEGF-R2 and sVEGF-R3 were measured using a multiplex immunoassay (Millipore MILLIPLEX; cat# HSCRMAG32KPX14).

Assessment of vascular growth mediators: Human angiogenesis/growth factor array (Millipore MILLIPLEX; cat# HAGP1MAG-12K) was used to measure serum levels of Angiopoietin-2, BMP-9, EGF, Endoglin, Endothelin-1, FGF-1, FGF-2, Follistatin, G-CSF, HB-EGF, HGF, IL-8, Leptin, PLGF, VEGF-A, VEGF-C, VEGF-D.

Assessment of bone metabolism markers: Serum concentrations of factors affecting bone development – ACTH, DKK-1, FGF-23, IL-1B, IL-6, Insulin, Leptin, PTH, OC, OPG, OPN,

SOST and TNF-α – were measured using a human bone array (Eve Technologies, Canada, cat# HBN-13-36).

Assessment of lipid carrier proteins: Concentrations of apolipoproteins ApoA1, Apo A2, ApoB and ApoE were measured using a human apolipoprotein 4-Plex assay (Eve Technologies, Canada).

2.5.3 Measuring serum cortisol concentration by enzyme linked immunosorbent assay (ELISA)

We used an ELISA kit (Enzo Life Sciences, cat# ADI-900-071) to quantitate the concentrations of cortisol in mice and human sera, following the standard manufacturer's protocol provided with the kit.

2.5.4 Western Immunoblotting to detect cortisol binding globulin

Serum CBG was detected by Western immunoblot. Human or mouse sera were mixed with a reducing sample buffer in a 1:20 ratio (150 mM Tris-HCL, pH 6.8, 15% (w/v) SDS, 30% (v/v) Glycerol and 10% (v/v) 2-Mercaptoethanol), heated at 95°C for 10 min; 3 µL of the resultant sample mixture was analyzed by SDS/10%-PAGE. For Western immunoblotting, the proteins were transferred from the SDS-PAGE gel onto a 0.2 µm nitrocellulose membrane (BioRad, USA). The membrane was then probed with a rabbit polyclonal anti-CBG antibody (Abcam, cat# ab107368), followed by horseradish-peroxidase-conjugated goat anti-rabbit secondary antibody (BioRad, USA) and the Amersham ECL Western Blot detection reagents (GE Healthcare, cat# RPN2106) as per manufacturer's instructions.

2.5.5 MMP2/MMP9 detection by substrate zymography

Gelatin zymography system: porcine skin gelatin (Sigma, cat# G8150) was copolymerized with the 10% SDS-PAGE gel (at a final gelatin concentration of 0.2% v/v). A non-reducing sample buffer (62.6 mM Tris-HCl, pH 7.4, 25% (v/v) Glycerol, 4% (w/v) SDS and 0.01% Bromophenol blue) was mixed with serum samples in a serum/buffer ratio of 1:10 (v/v). Serum proteins were separated by gel electrophoresis in a vertical gel electrophoresis apparatus (Amersham Biosciences), at 200V constant for 2 hours. The gel was washed thrice with 2.5% (v/v) Triton X-100 for 20 min each time and incubated at 37 °C overnight (12 h) submerged in an enzyme assay buffer (25 mM Tris-HCl pH 7.4, 150 mM NaCl and 5 mM CaCl2). The gel was stained with Coomassie blue and de-stained in 25% (v/v) methanol / 10% (v/v) acetic acid. MMP2 and MMP9 were detected as clear substrate-lysis bands contrasting against a blue background (from Coomassie staining) in the gel.

2.5.6 Statistical analysis

SigmaPlot 13 (Systat Software, San Jose, CA) was used to analyze the results and plot graphs. Data are presented as mean ± standard error of mean. One way ANOVA was performed, where appropriate (indicated in the figure legends), to determine statistical significance in the difference between two groups.

3 Chapter 3: Identification of fibrinogen as a natural inhibitor of MMP2

Hassan Sarker, Eugenio Hardy, Ayman Haimour, Walter P. Maksymowych, Lorenzo D. Botto, Carlos Fernandez-Patron

Preface

This chapter represents the work accepted for publication in *Scientific Reports* in 2019 as "Sarker, H., Hardy, E., Haimour, A., Botto, L., Maksymowych, W., Fernandez-Patron, C. Identification of fibrinogen as a natural inhibitor of MMP2. Scientific Reports 9, 4340, (2019)". HS is the primary author and performed the experiments, analyzed the data, and produced the first draft. HS and CFP designed the study and experiments and edited the manuscript. CFP provided funding and supervision. HS and AH conducted the *in silico* analyses. EH, LDB, WPM and CFP participated in the data analysis and performed critical revisions of the manuscript. This chapter contains research which received ethics approval from the University of Alberta Research Ethics Board, project names: "MMP2 deficiency syndrome" (study ID: Pro00068611 (human ethics)); study investigator: Carlos Fernandez-Patron. The manuscript has been adapted to fit the format of this thesis.

3.1 Summary

Non-genetic MMP2 insufficiency is a relatively unexplored condition which could be induced by pathological overexpression of endogenous MMP2 inhibitors such as TIMPs and/or the acute phase reactant alpha-2-macroglobulin. Here, we investigate the hypothesis that human fibrinogen (FBG) – an acute phase reactant – inhibits human MMP2. Following an unexpected observation where sera from human donors including arthritis patients with increased levels of serum FBG exhibited reduced binding of serum proMMP2 to gelatin, we found that human FBG (0 to 3.6 mg/mL i.e., 0 to 10.6 μM) concentration-dependently inhibited human proMMP2 and MMP2 from binding to gelatin. Moreover, at normal physiological concentrations, FBG (5.29-11.8 μM)

concentration-dependently inhibited (40-70% inhibition) the cleavage of fluorescein-conjugated gelatin by MMP2, but not MMP9. Indicative of a mixed-type (combination of competitive and non-competitive) inhibition mechanism, FBG reduced the V_{max} (24.9±0.7 min^{-1} to 17.7±0.9 min^{-1}, $P<0.05$) and increased the Michaelis-Menten constant K_M (204±6 nM to 478±50 nM, $P<0.05$) for the reaction of MMP2 cleavage of fluorescein-conjugated gelatin. *In silico* analyses and studies of FBG neutralization with anti-FBG antibodies implicated the domains D and E of FBG in the inhibition of MMP2. In conclusion, FBG is a natural selective MMP2 inhibitor, whose pathological elevation could lead to MMP2 insufficiency in humans.

3.2 Introduction

Matrix metalloproteinase 2 (MMP2), also known as gelatinase A or 72 kDa type IV collagenase, is a member of a family of 25 different Zn^{2+}-dependent endopeptidases involved in the degradation of extracellular matrix proteins (such as collagens)(*1, 2*) as well as cytokines (such as monocyte chemoattractant protein-3)(*12, 89, 90*). MMP2 consists of a pro-peptide domain, a catalytic domain, three fibronectin-like repeats (collagen binding domain) inserted into the catalytic domain and a hemopexin-like (PEX) domain linked to the catalytic domain via a hinge region(*3, 161*). Proteolytic activity of MMP2 is regulated at the levels of *MMP2* gene transcription (mRNA synthesis) and translation (protein synthesis), by post translational modifications (such as cleavage of the pro-peptide domain by MT1-MMP) as well as by endogenous inhibitors(*1*). These regulatory mechanisms are imperative since both excessive and defective MMP2 activity can be pro-inflammatory and are implicated in cardiovascular diseases and comorbidities(*2, 72, 92-95*).

Increased MMP2 protein expression levels have been associated with increased risk and all-cause mortality in patients with hypertension, ischemic heart disease, heart failure and

comorbidities thereof including diabetic and arthritic conditions (particularly rheumatoid arthritis)(*72, 92, 93, 162*). Unfortunately, most previous studies have not specifically correlated MMP2 expression with MMP2 activity as determined by MMP2 binding to or cleavage of important physiological substrates (such as collagens or cytokines). Therefore, it remains unknown whether MMP2 activity is elevated or not in these conditions despite the reported increase in MMP2 protein levels, due to a simultaneous increase in levels of endogenous MMP2 inhibitors. Also, autosomal recessive inactivating mutations of the *MMP2* gene (MMP2 deficiency) predispose to congenital heart defects, such as transposition of the great arteries to bicuspid aortic valve and septal defects in the atria and ventricles(*94*) as well as to a multi-centric osteolysis and arthritis syndrome (MONA; OMIM #259600)(*95, 98*) – characterized by progressive bone demineralization, destruction of cartilage in joints and abnormal long bone and craniofacial development(*57*). Among the endogenous inhibitors of MMP2 are tissue inhibitors of metalloproteinases (TIMPs)(*163, 164*) and circulating factors, such as alpha-2-macroglobulin (a positive acute-phase reactant and an anti-protease in the circulation with a broad-spectrum specificity for proteases including MMP2)(*22, 24, 165-167*). Pathological overexpression of these inhibitors could reduce MMP2 proteolytic activity below normal physiological levels, thus causing MMP2 insufficiency as observed in liver cirrhosis and pancreatitis patients with high TIMP-2 levels(*168*). Similar to alpha-2-macroglobulin, fibrinogen (FBG) is another positive acute-phase reactant in the circulation, where its concentration can increase by up to 10 folds in response to inflammatory stimuli(*32*). FBG is a 340 kDa dimeric glycoprotein comprised of two sets of three polypeptide chains (Aα, Bβ and γ) that are interconnected by 29 disulfide bridges(*30*). It is unknown whether human FBG inhibits or not human MMP2 proteolytic activity.

In the present work, we report that high serum FBG levels exhibit impaired binding of serum proMMP2 to gelatin and selectively inhibits human MMP2 (but not MMP9) proteolytic activity by a mixed-type mechanism (i.e., a combination of non-competitive and competitive modes of inhibition). With the aid of *in silico* molecular docking analyses, we found that FBG target domains of MMP2 involved in catalysis and binding of MMP2 substrates (collagen peptides). We conclude that FBG is a natural selective MMP2 inhibitor, whose pathological elevation could contribute to a state of non-genetic MMP2 activity insufficiency with as-yet poorly understood pathophysiology.

3.3 Results

3.3.1 Impaired binding of serum proMMP2 and recombinant MMP2 to gelatin in the presence of high FBG concentrations

While studying human MMP2 deficiency involving a cohort of MMP2 deficient patients, rheumatoid arthritis patients and healthy controls (Table S1), we made a serendipitous observation where we identified a control blood donor (denoted herein as abnormal) whose serum proMMP2 demonstrated an unusual lack of binding to gelatin. To quantitate proMMP2 protein levels in the serum of these test-blood donors, we first subjected the serum samples (10 µL undiluted) to a protein separation step using gelatin cross-linked agarose beads (containing 43 µg of immobilized gelatin) to isolate the collagen-binding proteins including proMMP2. Subjecting the gelatin – bound and unbound fractions to gelatin zymography analysis showed thatproMMP2 bound to immobilized gelatin – as expected for a gelatinase – for all the tested sera samples except for one serum sample (referred to as abnormal) (**Figure 3.1a**, left). Most of the proMMP2 of the abnormal sample remained in the gelatin-unbound fraction (**Figure 3.1a**, right), indicating a lack of binding of MMP2 to gelatin. To confirm this result, we conducted

Western blot analyses on the gelatin-bound fractions using two anti-MMP2 antibodies against two different domains of MMP2 – the PEX domain (epitope at amino acids 475-490) and the catalytic domain (a region around amino acid P117). Western blots (**Figure 3.1a**, left) detected proMMP2 in the gelatin-bound fractions of all the sera samples except for the abnormal sample, confirming the results of the zymography analyses, namely that proMMP2 binding to the immobilized gelatin was reduced in the abnormal sample but not in any of the other serum samples tested (a representative sample is shown in **Figure 3.1** denoted as control). The donor of the abnormal serum indicated that he was asymptomatic at the time of blood collection and was not clinically investigated.

Next, SDS-PAGE analysis of the sera indicated two prominent protein bands unique to the abnormal serum (not prominent in the other samples), one above 55 kDa and the other at 47 kDa (**Figure 3.1b**, left). Mass spectrometry analysis revealed them to be FBG beta chain (Bβ) and FBG gamma chain (γ) with a high degree of confidence (**Figure 3.1b**, right). FBG concentration in the abnormal serum sample was 67900 ± 212 ng/mL (as determined by ELISA). These data showed that FBG was elevated in the abnormal serum sample (the average serum concentration of FBG in control samples was <1000 ng/mL (**Figure 3.3a**); whereas reported normal plasma concentration of FBG is 1.8-4 mg/mL (5.29-11.8 μM))(*31*).

To ascertain whether the impairment in binding of serum MMP2 to gelatin (in the donor of the abnormal serum) was reversible (e.g., caused due to a transient elevation of MMP2 interactors such as FBG in the circulation of the donor) rather than permanent (e.g., due to an inactivating *MMP2* gene mutation), we retested the donor approximately three months after the first blood collection and made the following observations: (i) Serum FBG levels in the donor of the abnormal serum significantly decreased from 67900 ± 212 ng/mL to 1409 ± 247 ng/mL. (ii)

MMP2 binding to gelatin was restored (**Figure 3.2**). These results demonstrated that the binding between MMP2 and gelatin was restored when FBG was no longer elevated in the serum of the same individual. The cause for the transient elevation in circulating FBG in the donor is unknown and was not investigated.

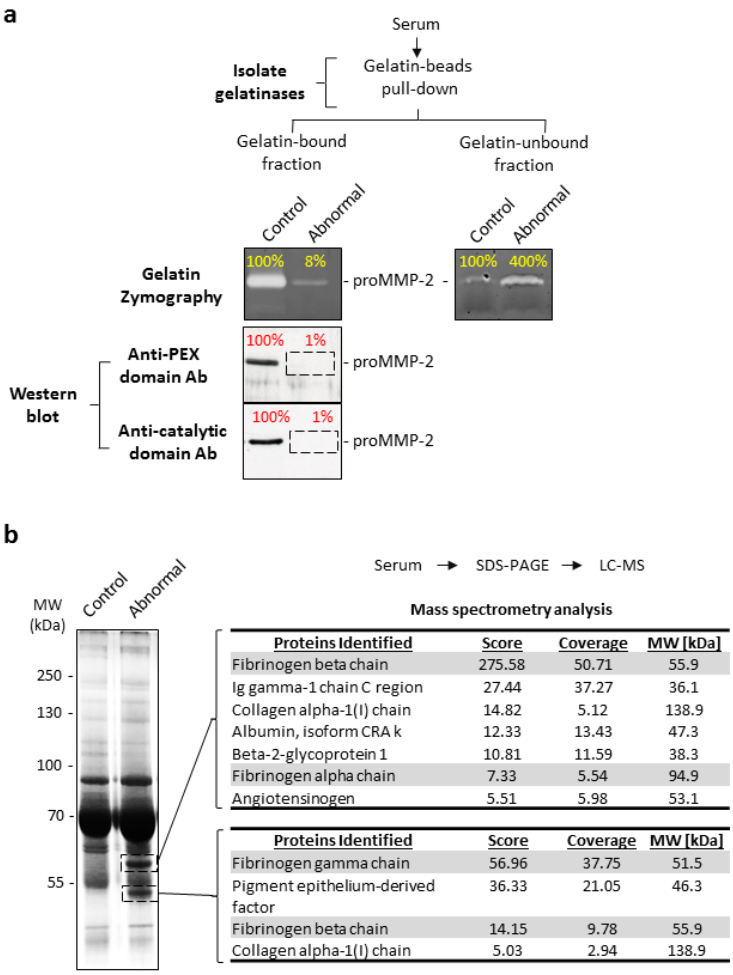

Proteins Identified	Score	Coverage	MW [kDa]
Fibrinogen beta chain	275.58	50.71	55.9
Ig gamma-1 chain C region	27.44	37.27	36.1
Collagen alpha-1(I) chain	14.82	5.12	138.9
Albumin, isoform CRA k	12.33	13.43	47.3
Beta-2-glycoprotein 1	10.81	11.59	38.3
Fibrinogen alpha chain	7.33	5.54	94.9
Angiotensinogen	5.51	5.98	53.1

Proteins Identified	Score	Coverage	MW [kDa]
Fibrinogen gamma chain	56.96	37.75	51.5
Pigment epithelium-derived factor	36.33	21.05	46.3
Fibrinogen beta chain	14.15	9.78	55.9
Collagen alpha-1(I) chain	5.03	2.94	138.9

Figure 3.1: Identification of a blood donor with elevated serum fibrinogen exhibiting impaired binding of MMP2 to gelatin.

(a) Analysis of serum samples by gelatin zymography and Western blot to detect MMP2 and/or to quantitate its gelatinolytic activity. Undiluted serum samples (10 µL) were incubated with an estimated 43 µg of immobilized gelatin at 4°C for 1 hour. Gelatin-bound and gelatin-unbound proteins were subjected to gelatin zymography to quantitate MMP2 activity. Gelatin-bound proteins were subjected to Western blot to detect MMP2 using anti-PEX and anti-catalytic domain (MMP2) antibodies. **Top**: Gelatin zymogram showing the majority of activity of serum MMP2 of the abnormal sample remained in the gelatin-unbound fraction. **Bottom**: Western blots showing serum MMP2 of the abnormal sample was undetected in the gelatin-bound fraction by both the anti-PEX domain and anti-catalytic domain antibodies. Band intensities are shown as a percentage relative to the band of the representative control serum sample. Uncropped gels and blots are presented in supplementary figure S7. **(b)** SDS-PAGE coupled

with LC-MS (ESI) was used to identify the compositions of two unique protein bands in the abnormal sample as indicated. LC-MS, liquid chromatography – mass spectrometry; ESI, electrospray ionization; PEX, hemopexin-like; Ab, antibody; MMP2, matrix metalloproteinase 2.

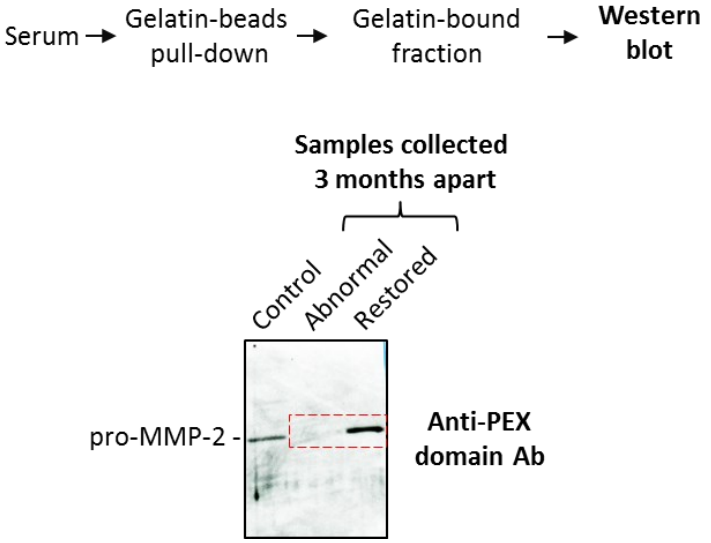

Figure 3.2: Restoration of binding of serum MMP2 to gelatin when serum fibrinogen levels normalized.

Western blot (using the anti-PEX domain antibody) showing MMP2 in the gelatin-bound fraction indicating the restoration of binding of MMP2 to gelatin in a second serum sample from the donor of the abnormal serum collected three months after the first collection. PEX, hemopexin-like domain; Ab, antibody.

Moreover, we screened sera from rheumatoid arthritis patients and healthy controls to identify samples with elevated serum FBG and performed the gelatin binding assay as described. Rheumatoid arthritis patients exhibiting higher serum FBG levels relative to healthy controls (**Figure 3.3a**) also demonstrated relatively reduced binding of serum MMP2 to gelatin (**Figure 3.3b**).

To test whether FBG indeed disrupted the interaction between MMP2 and gelatin, we incubated recombinant pro-MMP2 (0.001 mg/mL; 13.9 nM) with immobilized gelatin (43 μg) in the presence of increasing concentrations of FBG (0 to 3.6 mg/mL; 0 to 10.6 μM) and observed that FBG concentration-dependently inhibited the binding of MMP2 to its substrate gelatin (**Figure 3.4**).

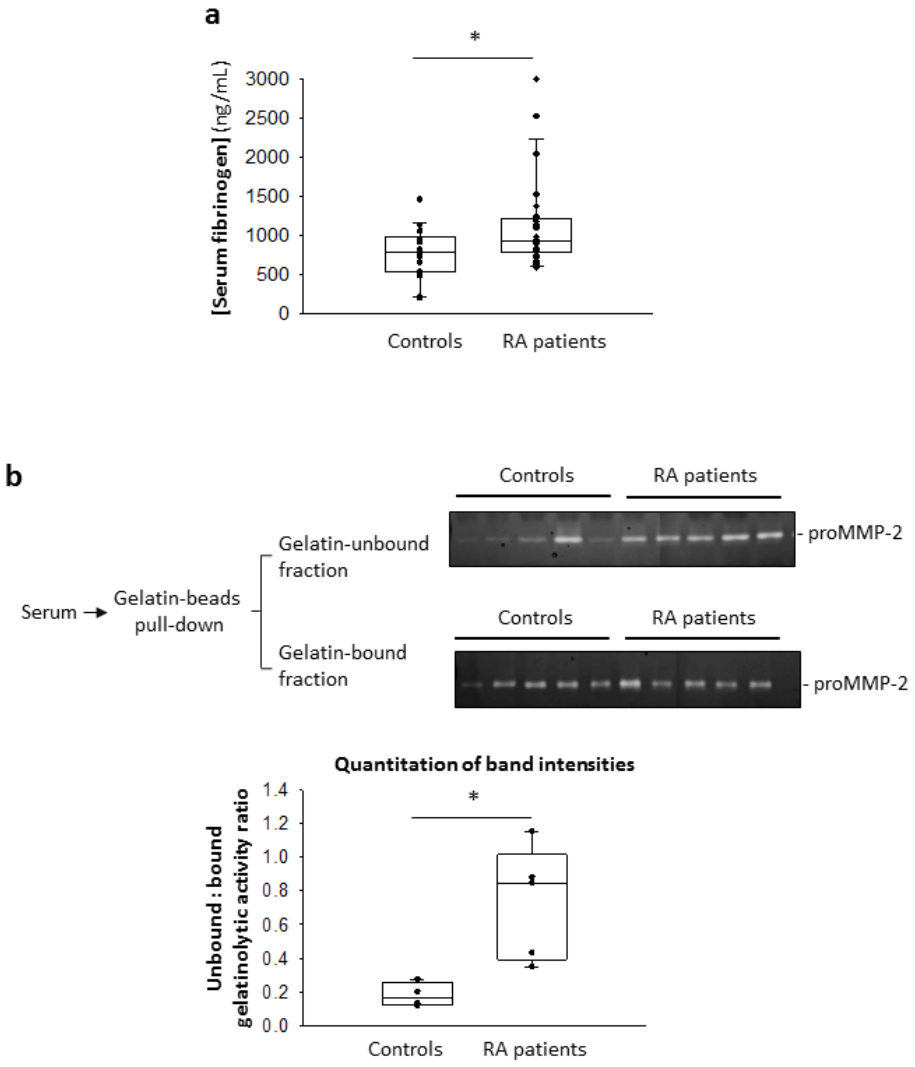

Figure 3.3: **Reduced binding of serum proMMP2 to gelatin in sera with higher fibrinogen concentrations.**

(a) Quantitation of serum fibrinogen concentrations of rheumatoid arthritis patients (n=25) and healthy controls (n=19) by ELISA. P=0.019 controls vs RA patients, determined by Mann-Whitney Rank Sum Test. **(b) Top:** Gelatin binding assay of selected RA patient (high FBG) and control (low FBG) serum samples, followed by gelatin zymography shows the gelatinolytic activity of proMMP2 in the gelatin-unbound fraction and the gelatin-bound fraction. **Bottom**: Quantitation and comparison of the intensities of the lysis bands in the gelatin zymograms above by densitometry. *P<0.05 controls vs RA patients, determined by Mann-Whitney Rank Sum Test.
ELISA, enzyme-linked immunosorbent assay; RA, rheumatoid arthritis; FBG, fibrinogen.

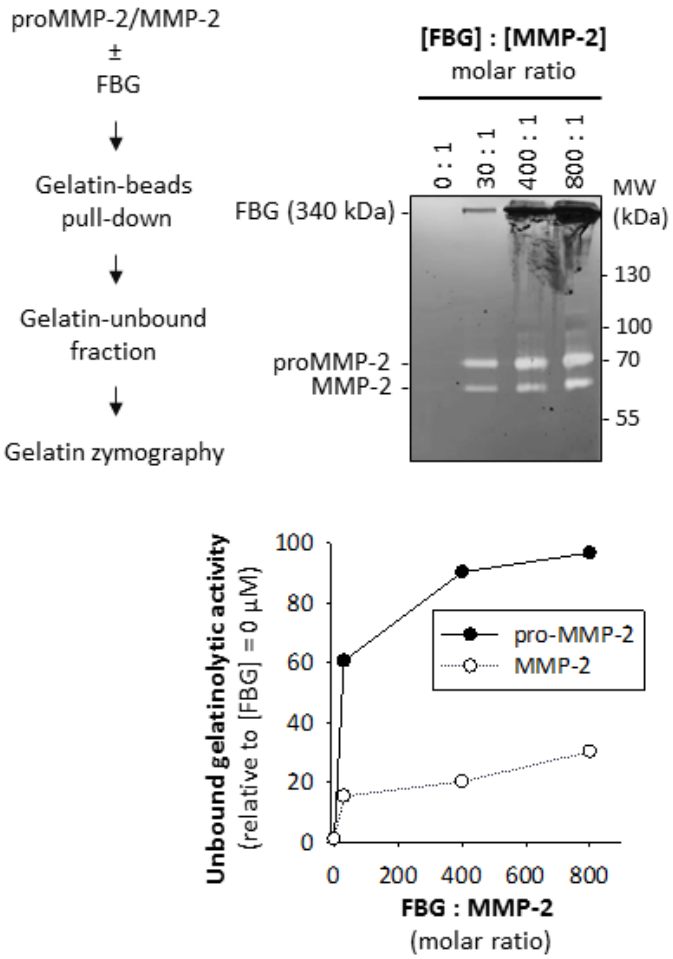

Figure 3.4: Purified fibrinogen concentration-dependently reduces binding of recombinant MMP2 to gelatin.

Top left: Strategy for assessing a lack of binding of MMP2 to gelatin in the presence or absence of FBG. **Top right:** Gelatin binding assay followed by gelatin zymography shows an increase in gelatinolytic activity of MMP2 remaining in the gelatin-unbound fraction with increasing FBG concentration. Gelatin zymogram showing gelatinolytic activity of MMP2 in the gelatin-unbound fraction for varying [FBG] : [MMP2] ratios (0 : 1 to 800 : 1). **Bottom**: Quantitation of the intensities of the lysis bands in the gelatin zymogram (left) by densitometry. Relative intensity for each band was calculated by dividing the absolute intensity of each band by the absolute intensity of the band at [FBG] = 0 µM ([FBG] : [MMP2] = 0 : 1).

3.3.2 Human FBG is not cleaved by recombinant human MMP2

To test whether any of the three subunits of FBG is cleaved by MMP2, we incubated purified FBG (3 mg/mL or 8.82 µM) with MMP2 (12 nM) at 37°C for 24 hours followed by SDS-PAGE analysis. None of the FBG subunits were cleaved by MMP2 (nor by MMP9) whereas all three

subunits were degraded by plasmin (12 nM) – a protease that degrades FBG and fibrin in normal physiology(*169*) (**Figure 3.5**).

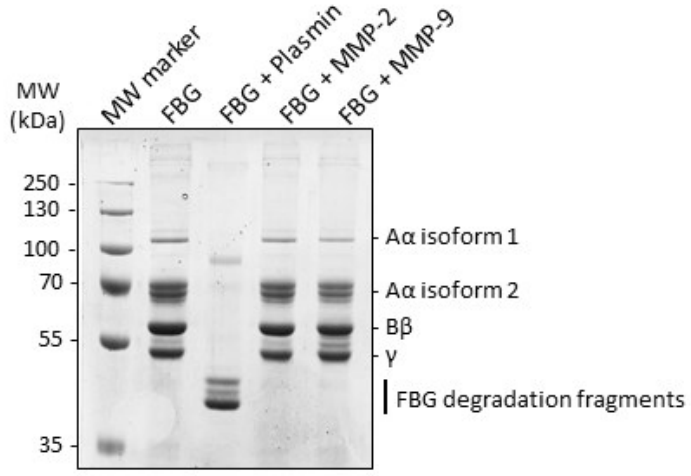

Figure 3.5: Human fibrinogen is not cleaved by recombinant human MMP2 or human MMP9.

Proteolysis of human FBG by plasmin, MMP2 and MMP9. FBG (3 mg/mL) was incubated with near physiological concentrations of either plasmin (12 nM) or MMP2 (12 nM) or MMP9 (12 nM) for 24 hours at 37°C. The reaction mixtures were analysed by SDS-PAGE.

As a control to ensure the recombinant MMP2 used was active when incubated at 37°C for 24 hours, we included a cleavage reaction with collagen type I as substrate in parallel with FBG (**Figure 3.6**).

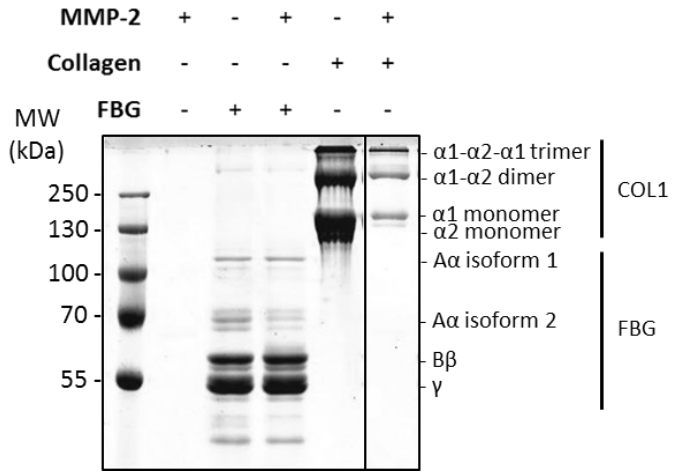

Figure 3.6: Cleavage of purified collagen type I and FBG by MMP2.

SDS-PAGE of fibrinogen (50 µg) and collagen type I (50 µg) degradation by recombinant MMP2 (12 nM) after incubation for 24 hours at 37°C.

Although, previous research(*170*) reported that the Aα and Bβ chains of bovine FBG are cleaved by MMP2, the cleavage reported was highly inefficient relative to plasmin mediated degradation of FBG. Our results show that human FBG is not cleaved by recombinant active MMP2 at physiological concentrations and conditions. This observed lack of cleavage of human FBG by MMP2 suggests that FBG is not likely to be a physiological target for MMP2 mediated degradation. Rather, the interaction between FBG and MMP2 may cause an inhibition of MMP2 activity – a hypothesis we tested in subsequent experiments.

3.3.3 FBG inhibits MMP2 proteolytic activity

To determine whether FBG inhibits MMP2 activity, we incubated recombinant active MMP2 with increasing concentrations of a fluorogenic substrate (fluorescein-conjugated gelatin) in the absence or presence of FBG. Concentrations of MMP2 and FBG used in the assay – 0.001 mg/mL (16.1 nM) and 3 mg/mL (8.82 µM) respectively – were close to their reported normal circulating physiological ranges: 0.00017-0.00049 mg/mL (2.74-8.06 nM) MMP2(*171*) and 1.8-4

mg/mL (5.29-11.8 μM) FBG(*31*). The double reciprocal plot (**Figure 3.7a**) of substrate concentration and rate of reaction (change in relative fluorescence unit over time) demonstrates inhibition of MMP2 activity by FBG. The V_{max} decreased from 24.9 ± 0.7 min^{-1} to 17.7 ± 0.9 min^{-1} ($P<0.05$) and the K_M increased from 204 ± 6 nM to 478 ± 50 nM ($P<0.05$) with the addition of FBG (**Table 3.1**), indicating that the mode of inhibition is mixed – a combination of competitive and non-competitive inhibition. As a negative control, substituting human serum albumin (HSA) – the most abundant protein in serum(*172*) – in place of FBG did not inhibit MMP2 activity (**Figure 3.7b**). Next, we demonstrated that after FBG undergoes plasmin-mediated degradation (**Figure 3.7c**, left), the resulting FBG fragments are unable to inhibit MMP2 and MMP2 activity was restored (**Figure 3.7c**, right), also suggesting that FBG is required to be intact in order to inhibit MMP2. Furthermore, neutralization of FBG using an anti-FBG antibody (but not non-immune IgG) lifted inhibition of MMP2 by FBG, restoring MMP2 activity (**Figure 3.7d**). A concentration-response experiment (**Figure 3.7e**) showed that FBG concentration-dependently inhibited MMP2 and the IC_{50} to inhibit the proteolytic activity of 0.001 mg/mL (16.1 nM) MMP2 was found to be 2.31 ± 0.04 mg/mL (6.76 ± 0.12 μM) FBG. Together, these results clearly demonstrated that FBG inhibits MMP2 proteolytic activity.

To test whether the inhibitory actions of FBG may also be applicable to other MMPs, we tested using the same flourometric gelatinase activity assay the effects of FBG on MMP9 – another gelatinase of the MMP family that is structurally homologous to MMP2(*4*). The double reciprocal plot (**Figure 3.8a**) of substrate concentration and rate of reaction showed no significant change in either the V_{max} (111 ± 4 min^{-1} *versus* 98 ± 3 min^{-1}; $P>0.05$) or the K_M (272 ± 7 nM *versus* 240 ± 10 nM; $P>0.05$) with the addition of FBG (**Table 3.1**), demonstrating that

intact FBG does not inhibit MMP9 activity. Also, MMP9 proteolytic activity was not inhibited by plasmin-cleaved FBG (**Figure 3.8b**).

MMP2

Kinetic constants	- FBG	+ FBG	P-value
$\mathbf{K_M}$ (nM)	204 ± 6	478 ± 50	0.007
$\mathbf{V_{max}}$ (min^{-1})	24.9 ± 0.7	17.7 ± 0.9	0.003

MMP9

Kinetic constants	- FBG	+ FBG	P-value
$\mathbf{K_M}$ (nM)	272 ± 7	240 ± 10	0.118
$\mathbf{V_{max}}$ (min^{-1})	111 ± 4	98 ± 3	0.0815

Table 3.1: **Summary of kinetic constants of MMP2 and MMP9 activity in the absence or presence of fibrinogen.**
Maximum velocity (V_{max}) and the Michaelis-Menten constant (K_M) derived from the Lineweaver-burk plots presented in figures 5a and 6a. Data are presented as mean ± standard error of mean (n=3). Comparison of +FBG vs –FBG, P-value determined by two-tailed student's t-test.

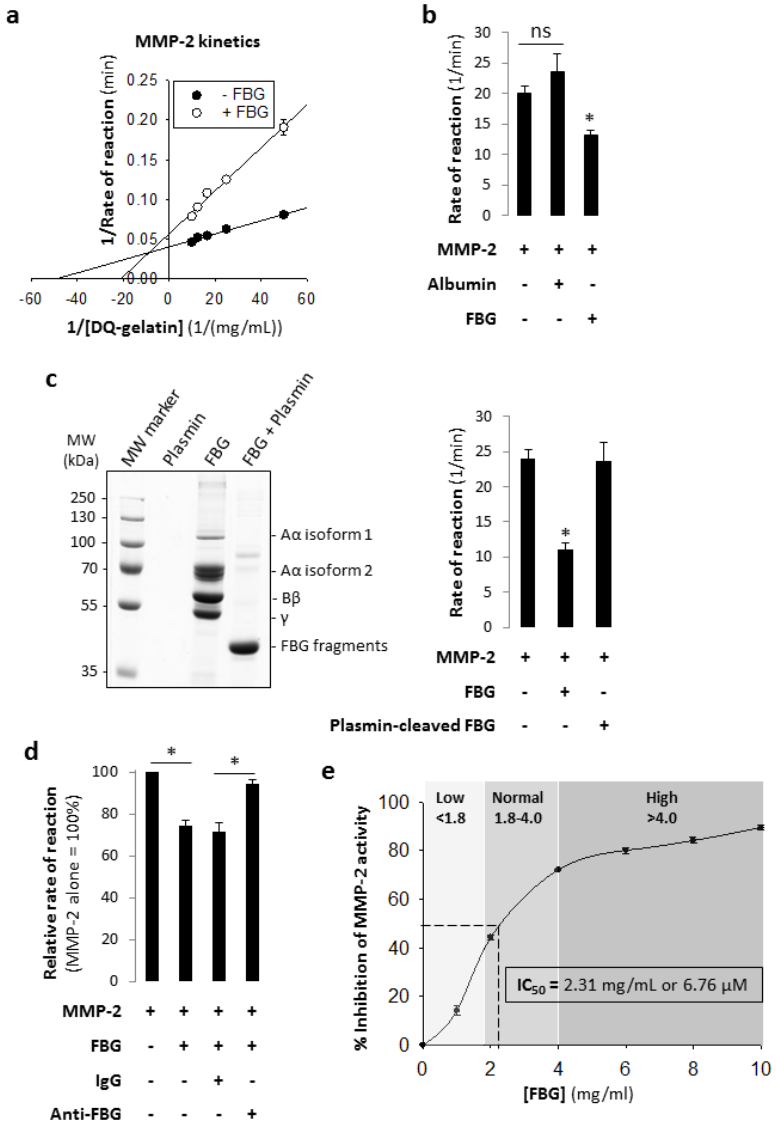

Figure 3.7: **Purified human fibrinogen inhibits gelatinolytic activity of recombinant human MMP2.** **(a)** Lineweaver-Burk plot of the proteolytic processing of DQ-gelatin by MMP2 in the absence or presence of 3 mg/mL FBG; [MMP2] = 0.001 mg/mL (13.9 nM) and [DQ-gelatin] = 0.02, 0.04, 0.06, 0.08 or 0.1 mg/mL. **(b)** Bar graphs showing the effect of intact fibrinogen (3 mg/mL) on the activity of MMP2 (0.001 mg/mL); MMP2 alone and human serum albumin (3 mg/mL) plus MMP2 were used as a control. *P<0.05 vs MMP2 determined by student's t-test. ns, not significant. Data are shown as mean of triplicates. **(c) Left**: SDS-PAGE confirming complete degradation of fibrinogen (6 mg/mL) when incubated with plasmin (0.001 mg/mL) for 12 hours at 37 °C. **Right**: Bar graphs showing that and plasmin-degraded fibrinogen fragments (3 mg/mL) *vs* intact fibrinogen (3 mg/mL) have no effect on the activity of MMP2 (0.001 mg/mL). *P<0.05 vs MMP2 determined by student's t-test. ns, not significant. **(d)** Bar graph showing restoration of MMP2 activity when FBG is selectively removed from solution by an anti-FBG antibody. [MMP2] = 0.001 mg/mL (13.9 nM); [DQ-gelatin] = 0.05 mg/mL; [FBG]= 2 mg/mL (5.88 µM); [IgG] and [anti-FBG] = 5.88 µM. *P<0.05; determined by two-tailed student's t-test (n=4). **(e)** Plot showing the effect of increasing fibrinogen concentrations (0.0 to 10 mg/mL) on MMP2 (0.001 mg/mL) activity. Note that high circulating FBG concentrations (as those found in RA patients (**Figure 3.2a**)) effectively inhibit MMP2 activity by more than 50%. Data are presented as mean ± standard error of mean. FBG, fibrinogen; RFU, relative fluorescence unit.

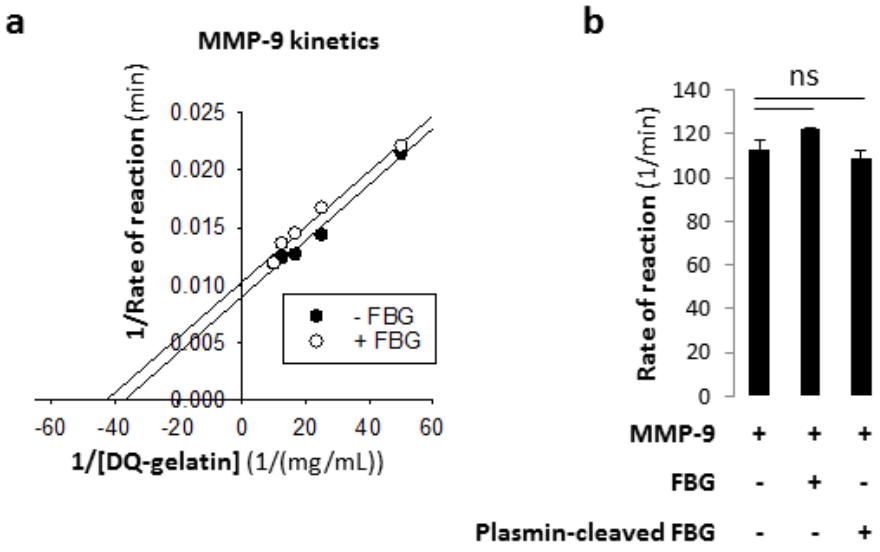

Figure 3.8: **Gelatinolytic activity of recombinant human MMP9 is not inhibited by purified human fibrinogen.**
(a) Lineweaver-Burk plot of the proteolytic processing of DQ-gelatin by MMP9 in the absence or presence of 3 mg/mL FBG; [MMP9] = 0.001 mg/mL (12.0 nM) and [DQ-gelatin] = 0.02, 0.04, 0.06, 0.08 or 0.1 mg/mL. **(b)** Bar graphs showing that intact fibrinogen (3 mg/mL) or plasmin-degraded fibrinogen fragments (3 mg/mL) has no effect on the activity of MMP9 (0.001 mg/mL). ns, not significant. Data are presented as mean ± standard error of mean. FBG, fibrinogen; RFU, relative fluorescence unit.

3.3.4 FBG targets the catalytic domain of MMP2

To understand the molecular mechanism of interaction between FBG and MMP2 which results in the inhibition of MMP2 activity, we performed *in silico* molecular docking analyses which revealed that FBG binds MMP2 at the catalytic domain. Docking of FBG to MMP2 showed that the interaction between FBG and MMP2 is stabilized via hydrogen bonds and non-polar interactions between residues in the catalytic domain of MMP2 and the D domain of FBG (**Figure 3.9a, Figure 3.10, Table 3.3**). Docking of Marimastat – a synthetic MMP2 inhibitor that targets the catalytic domain – to MMP2 revealed two MMP2 residues (His413 and Pro423) that form hydrogen bonds with Marimastat (**Figure 3.9b, Table 3.3**). These two MMP2 residues are also involved in stabilizing FBG-MMP2 interactions via hydrogen bonds, thus showing that FBG and Marimastat bind at a common region of the catalytic domain of MMP2. Moreover, comparing docking models of the FBG-MMP2 complex and the collagen peptide-MMP2

complex (**Figure 3.11, Table 3.4**) revealed that FBG and collagen interact with several common MMP2 residues at the catalytic domain, namely R127, G165, E166, M170, D180, G200, V201 and D204. Together, these results predict FBG to interact with MMP2 at regions in the catalytic domain where the synthetic MMP2 inhibitor Marimastat and the MMP2 substrate collagen (peptide) bind.

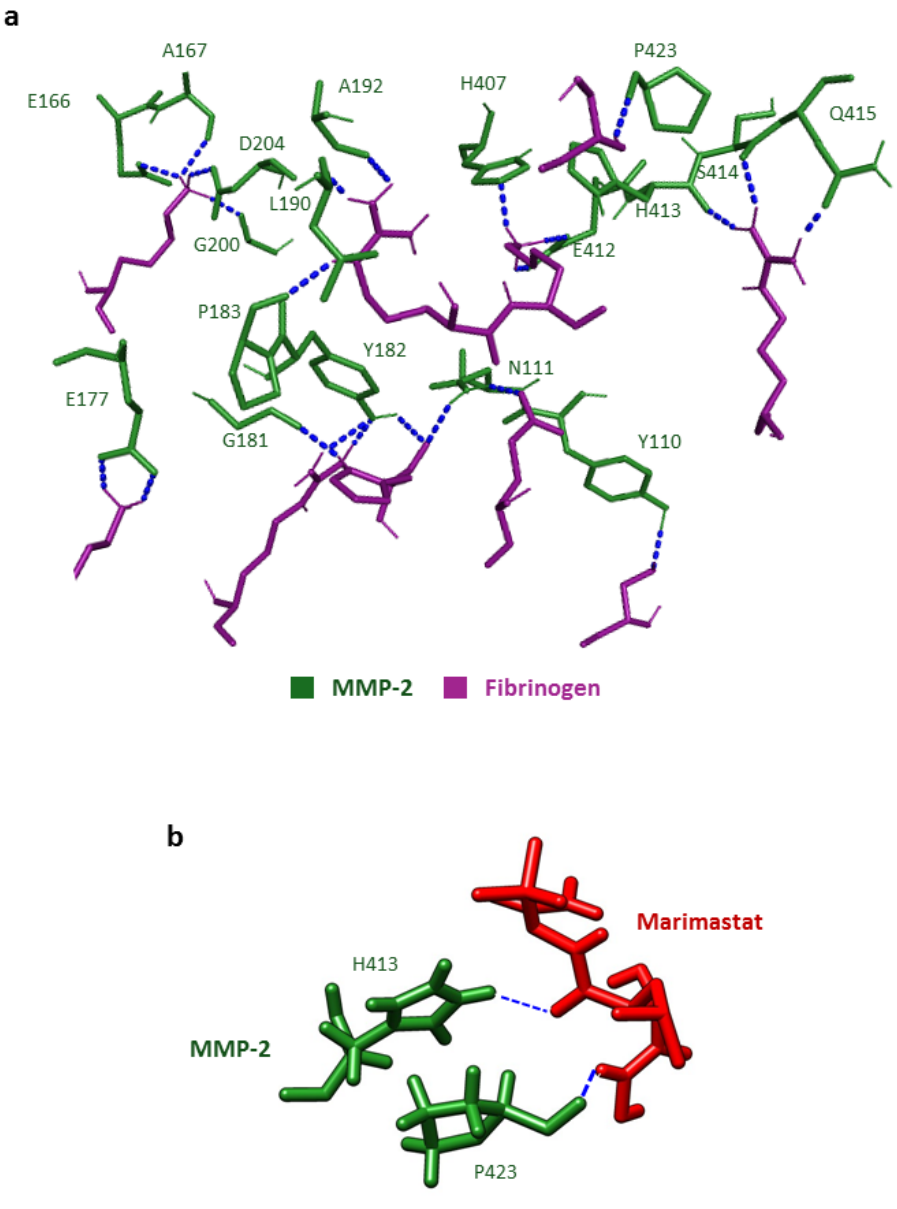

Figure 3.9: Fibrinogen and Marimastat bind at a common region of the catalytic domain of MMP2.

(a) Molecular docking of MMP2 to FBG. Labelled residues of MMP2 (green) that form hydrogen bonds (blue dotted lines) with FBG residues (magenta) are presented. **(b)** Molecular docking of MMP2 to Marimastat. Labelled residues of MMP2 (green) that form hydrogen bonds (blue dotted lines) with Marimastat (red) are presented.

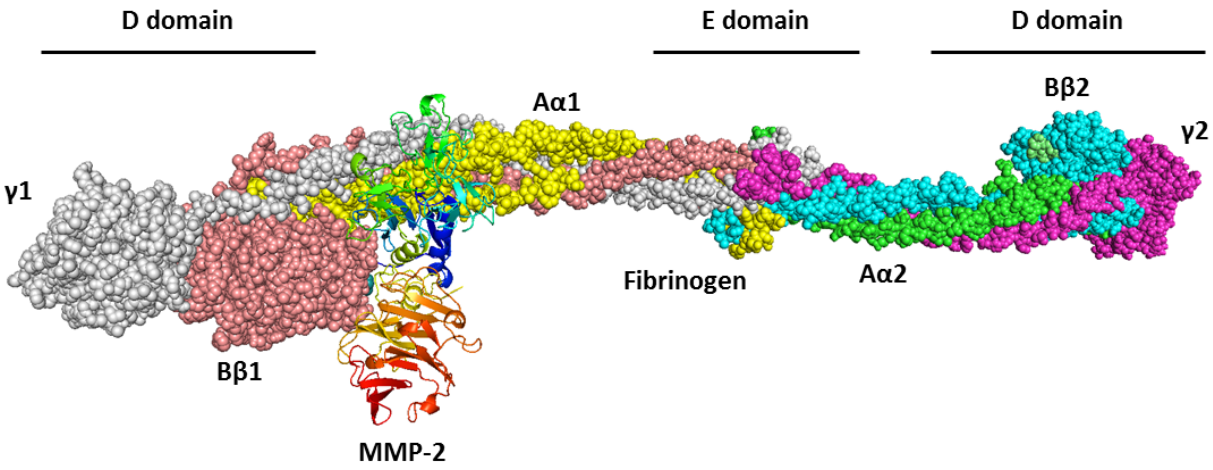

Figure 3.10: Molecular docking of FBG and MMP2.

Whole annotated image of molecular interactions between MMP2 and FBG presented in Figure 7a.

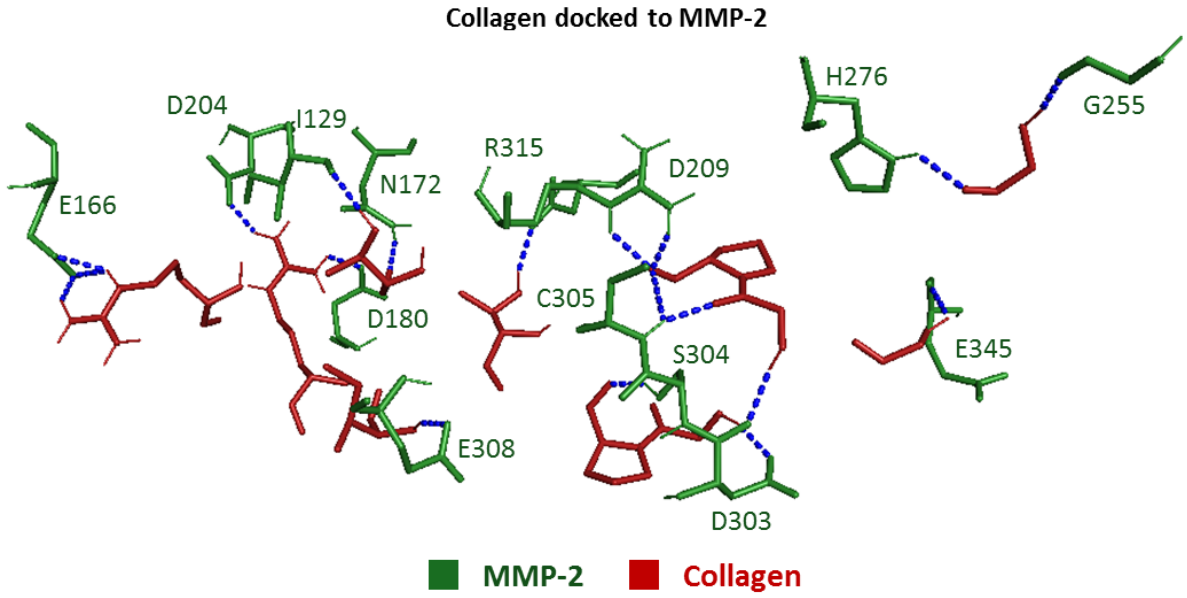

Figure 3.11: **Molecular docking of collagen to MMP2.**

Labelled residues of MMP2 (green) that form hydrogen bonds (blue dotted lines) with collagen residues (red) are presented. Interacting MMP2 residues span over the catalytic domain and the fibronectin type II repeats 1,2 and 3.

	Fibrinogen docked to MMP2	Marimastat docked to MMP2
Hydrogen bonds	Y110, N111, E166, A167, E177, G181, Y182, P183, L190, A192, G200, D204, H407, E412, H413, S414, Q415, P423	H413, P423
Other interacting residues	F112, F113, P114, R115, R127, D164, G165, D168, I169, M170, H178, G179, D180, F184, D185, G189, L191, H193, V201, T311, I424, Y425	F184, G189, L190, A192, H193, A194, L399, V400, H403, H407, L420, A422, I424, Y425, T426
Target domain(s) of MMP2	Catalytic Fibronectin type II repeat 2	Catalytic

Table 3.2: **A comparison of MMP2 residues interacting (within 5Å) with FBG and Marimastat**

	Collagen docked to MMP2
Hydrogen bonds	I129, E166, N172, D180, D204, D209, G255, H276, D303, S304, C305, E308, R315, E345
Other interacting residues	R127, G130, Y131, T132, P133, G165, M170, F173, H178, G200, V201, A278, C291, F293, S301, Y302, T306, T307, G309, R310, D312, G313, T335, S344, G346, A347, K386
Target domain(s) of MMP2	Catalytic Fibronectin type II repeat 1 Fibronectin type II repeat 2 Fibronectin type II repeat 3

Table 3.3: **A comparison of MMP2 residues interacting (within 5Å) with collagen in the presence or absence of FBG**.

3.4 Discussion

We began this investigation when we made the serendipitous observation that a blood donor with abnormally high concentration of serum FBG displayed reduced binding of serum proMMP2 to gelatin-coated beads. To clarify whether pathological elevation of FBG leads to reduced binding of serum proMMP2 to gelatin, we further tested sera from rheumatoid arthritis patients – a pathology associated with high serum FBG levels. Interestingly, binding of proMMP2 to gelatin-coated beads was significantly reduced in the rheumatoid arthritis patients as well. Based on these observations, we hypothesized that FBG is an inhibitor of MMP2. Through *in vitro* studies, we further confirmed reduced binding of recombinant human proMMP2 (72 kDa) as well as active MMP2 (62 kDa) to gelatin-coated beads in the presence of purified human FBG. Subsequent Lineweaver-burk enzyme kinetics analyses demonstrated that human FBG is a natural mixed-type (i.e., competitive and non-competitive) selective inhibitor of MMP2 (but not MMP9). *In silico* analyses and studies of FBG neutralization with anti-FBG antibodies implicated the domains D and E of FBG in the inhibition of MMP2.

Interestingly, we have found that normal physiological concentrations of circulating FBG are sufficient to inhibit circulating concentrations of MMP2 (by 40-70%). Conceivably, the inhibition of circulating MMP2 activity by FBG serves to downregulate platelet activation and aggregation. Indeed, at sites of vascular injury, platelets release MMP2 which, in turn, potentiates platelet activation by interacting with integrin $\alpha_{IIb}\beta_3$ on the platelet surface via its PEX domain(*173-175*). Active MMP2 is also able to facilitate platelet aggregation triggered by agonists such as adenosine diphosphate (ADP), collagen or thrombin(*176*). FBG displaces MMP2 and binds to the ectodomains of integrin $\alpha_{IIb}\beta_3$ molecules on the surface of platelets to tether platelets together, thus stabilizing platelet aggregates(*174, 177*). The binding of free FBG

molecules to proteolytically active MMP2, resulting in inhibition of MMP2 activity, could lead to downregulation of the potentiation of platelet activation via MMP2 activity dependent mechanisms. We have demonstrated that FBG has no effect on MMP9 activity, which might favour the downregulation of platelet activation as MMP9 is able to counteract the pro-aggregatory effects of MMP2(*173, 178, 179*). In line with previous research(*174, 177*), FBG, while stabilizing platelet aggregates, might also play an anti-aggregatory role in MMP2 mediated platelet activation by inhibiting MMP2 activity – a hypothesis worth investigating in future studies (**Figure 3.12**).

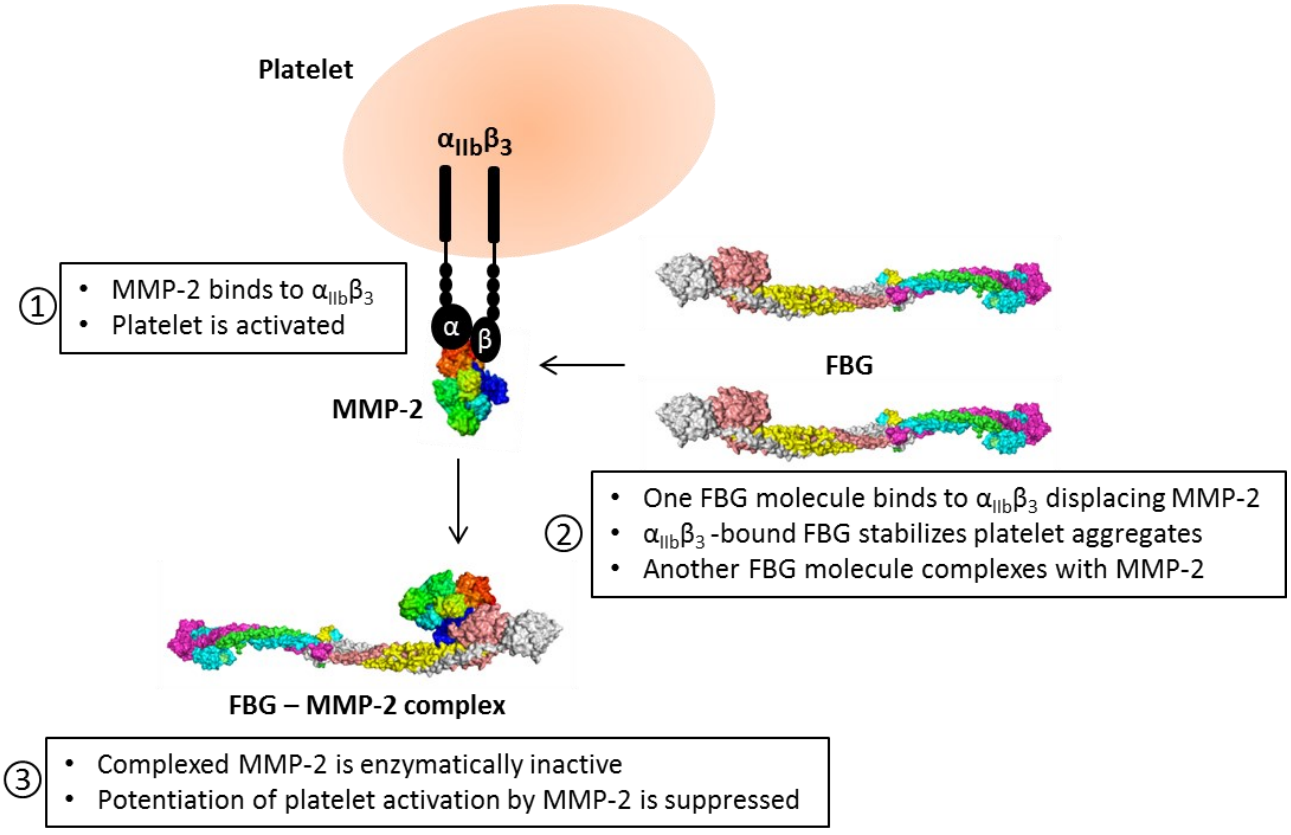

Figure 3.12: Illustration of a hypothesized anti-aggregatory function of FBG-mediated inhibition of MMP2 activity.

Besides the inhibition of circulating MMP2, FBG may also inhibit interstitial MMP2 activity in conditions where FBG is deposited in the extracellular matrix without subsequent conversion to fibrin, such as at sites of tumorigenesis(*180-182*). Interstitial MMP2 activity downregulates fibrosis – excess deposition of a collagen-rich extracellular matrix that can occur in most organs(*183*). Moreover, accumulation of interstitial FBG upregulates fibrosis by acting as a pro-fibrotic ligand(*184*), by increasing TGF-β1 production in resident macrophages in skeletal muscles(*185*) as well as by binding to ICAM-1 in target cells(*186*). Conceivably, a possible mechanism by which FBG upregulates fibrosis could be via inhibition of anti-fibrotic action of MMP2 – a hypothesis that warrants further investigation.

How selective is human FBG as an inhibitor for human MMP2? To address this question, we tested human MMP9 – the closest member of the MMP protein family to MMP2 in terms of structural homology as well as sequence identities of their catalytic domain, fibronectin type II repeats and the PEX domain(*4*). We found that human MMP9 activity was not inhibited by human FBG. Sequence alignments of the catalytic domain and the PEX domain of different members of the MMP family showed low similarity between MMP2 and other MMPs (**Figure 3.13**). Based on the sequence alignments, we predict that human FBG selectively inhibits human MMP2 and does not inhibit other human MMPs, as we have confirmed for human MMP9.

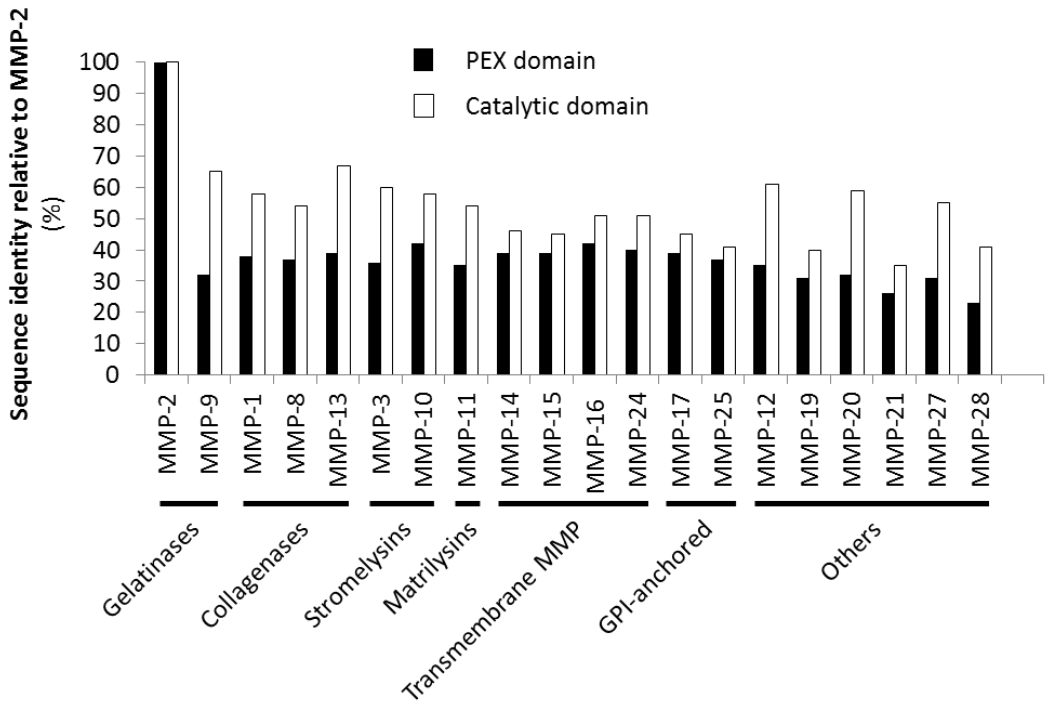

Figure 3.13: Comparison of amino acid sequence similarity of MMPs relative to MMP2.

The amino acid sequences of catalytic and the hemopexin-like domains of MMPs were aligned with MMP2. The data is presented as percent identity relative to MMP2.

Of note, we are aware that Monaco, S. et al.(*170*) investigated the hydrolysis of bovine FBG by human MMP2. However, our study has focused on the interaction between human FBG and human MMP2. To explain a potential inter-species difference in the ability of MMP2 to cleave FBG of bovine but not of human origin, we examined the alignment of amino acid sequences of the subunits of bovine *versus* human FBG. The analyses show that the sequence similarities of Alpha, Beta and the Gamma subunits are at 58.2%, 82.4% and 83%, respectively. We think that the differences in the amino acid sequences between human and bovine FBG are likely responsible for the different sensitivities to MMP2 cleavage exhibited by FBG from these species.

Having investigated the selectivity of FBG for MMP2, we explored the interaction mechanism between FBG and MMP2 using *in silico* molecular docking analyses and domain-specific anti-FBG antibodies. Our *in silico* analyses showed that FBG binds to MMP2 at the catalytic domain and interacts with the same MMP2 residues that interact with the synthetic MMP2 inhibitor – Marimastat. Specifically, both FBG and Marimastat interact with the MMP2 residues F184, G184, A192, H193, H407, H413, P423, I424 and Y425 via either polar or non-polar bonds. Moreover, FBG and collagen interact with several common MMP2 residues, namely R127, G165, E166, M170, D180, G200, V201 and D204, indicating that FBG, when bound to MMP2, could block collagen (and perhaps other MMP2 substrates) from accessing the active site in the catalytic domain of MMP2. The interaction of FBG with MMP2 spans over the active site in the catalytic domain as well as the fibronectin type II repeat 2, supporting the conclusion we derived from our experimental data that the mode of MMP2 inhibition by FBG is mixed-type (FBG competes with MMP2 substrates for the catalytic domain as well as binds to residues in the fibronectin type II repeat 2 domain). A plausible mechanism of the non-competitive inhibition is that FBG binds to MMP2 or MMP2-substrate complex at the fibronectin type II repeat 2 (or at a different site not predicted by the *in silico* analyses) and prevents catalysis by altering the molecular conformation of MMP2. Further, our data indicate that adding anti-FBG antibody but not IgG enables MMP2 to exert gelatinase activity in the presence of FBG. Anti-FBG binds to domains D and E of FBG (as per the manufacturer of this antibody). The *in silico* data gathered in this investigation predicts domain D to be involved in the interactions between FBG and MMP2. Together, these data further support the notion that FBG inhibits MMP2 via domains D or E. Consistently, complexation of FBG with anti-FBG inhibits FBG-mediated inhibition of MMP2, whereas non-immune IgG (control) has no such effect.

In conclusion, this investigation identifies human FBG as a selective mixed-type inhibitor of human MMP2. Our discovery leads to the formulation of potentially important hypotheses to be tested in future investigations, including: 1) FBG mediated inhibition of MMP2 plays an anti-aggregatory role MMP2 activity-dependent platelet activation and aggregation pathways (**Figure 3.12**). 2) FBG upregulates fibrosis via inhibition of the anti-fibrotic action of MMP2. 3) The pathological elevation of circulating FBG, together with other known MMP2 inhibitors, could lead to a state of non-genetic MMP2 insufficiency which may cause pathologies including arthritic and cardiac disorders reminiscent of those described for patients with genetic MMP2 deficiency(*57, 95*). We believe that this study is a starting point in a new direction of research on the possible occurrence of conditions caused by MMP2 activity insufficiency amid apparently normal levels of MMP2 expression – the potential clinical implications of such conditions are yet unknown and merit further research.

3.5 Materials and Methods

3.5.1 Study cohort

The serum samples used in this study were collected at the University of Utah Hospital (Salt Lake City, UT) and the University of Alberta Hospital (Edmonton, AB) with informed consent from the donors. The study was conducted with approval from the Health Research Ethics Board (HREB) at the University of Alberta. Healthy controls consisted of 17 females and 5 males whereas RA patients consisted of 20 females and 5 males, between the ages of 34 and 77 years (**Table 3.2**). The abnormal serum sample belonged to an asymptomatic 30-year-old male. Collagen derivatives (gelatin and fluorescein-conjugated gelatin) were used as surrogate for collagen in *in vitro* assays. All (following) methods were performed in accordance with the relevant guidelines and regulations.

Denotation	Condition	Age	Sex	Denotation	Condition	Age	Sex
C1 (abnormal)	Asymptomatic	30	M	R4	RA	70	F
C2	Control	69	F	R5	RA	76	F
C3	Control	41	M	R6	RA	36	F
C4	Control	69	F	R7	RA	64	M
C5	Control	60	M	R8	RA	68	F
C6	Control	77	F	R9	RA	35	F
C7	Control	44	M	R10	RA	42	F
C8	Control	35	F	R11	RA	40	M
C9	Control	43	F	R12	RA	69	F
C10	Control	59	F	R13	RA	45	F
C11	Control	42	F	R14	RA	34	F
C12	Control	53	F	R15	RA	56	F
C13	Control	34	F	R16	RA	66	M
C14	Control	37	F	R17	RA	57	F
C15	Control	65	F	R18	RA	40	F
C16	Control	71	M	R19	RA	36	F
C17	Control	36	F	R20	RA	66	F
C18	Control	69	F	R21	RA	69	F
C19	Control	45	F	R22	RA	74	F
C20	Control	67	F	R23	RA	44	M
R1	RA	53	F	R24	RA	58	F
R2	RA	58	M	R25	RA	47	F
R3	RA	38	F				

Table 3.4: Demographic information of the total cohorts of sera donors assessed.

3.5.2 Serum MMP2 isolation using immobilized gelatin

Serum MMP2 was isolated on gelatin immobilized on cross-linked 4% agarose beads (Sigma, Missouri, USA, cat# G5384). The beads suspension was spun down at 2000 x g for 2 mins in a bench-top centrifuge (Mandel mini, Mandel Scientific, CA) and the supernatant was removed. 40 µL of packed gelatin-beads were washed three times with 1 mL of ice-cold phosphate-buffered saline (PBS; pH 7.4, Thermo Fisher Scientific, Massachusetts, USA) and resuspended in 120 µL of PBS. 10 µL of each serum sample was added to 40 µL of the beads suspension (1 : 4 , v:v) in separate 0.5 mL microcentrifuge tubes and incubated at 4°C for 1.5 hours with shaking at 1300 rpm in a Thermomixer R (Eppendorf^{TM}). After centrifugation (at 2000 x g for 2 mins), the

supernatant (containing proteins not bound to gelatin-beads) was separated (using a pipette) from the beads (containing gelatin-bound proteins including MMP2) and collected in new microcentrifuge tubes. The beads remaining in the tubes were washed 3 times with 1 mL of PBS, resuspended in 50 µL of PBS and stored on ice until subsequent zymography and Western blot analyses.

3.5.3 Quantitation of serum FBG concentration

We used an enzyme-linked immunosorbent assay (ELISA) kit (cat# ab208036, Abcam) to quantitate the concentrations of serum FBG in the donors, following manufacturer's instructions provided with the kit.

3.5.4 MMP2 quantitation by substrate zymography analyses

Gelatin zymography system: porcine skin gelatin (Sigma, cat# G8150) was copolymerized with the 10% SDS-PAGE gel (at a final gelatin concentration of 0.2% v:v). Equal volumes of a non-reducing sample buffer (62.6 mM Tris-HCl, pH 7.4, 25% (v/v) Glycerol, 4% (w/v) SDS and 0.01% Bromophenol blue) were added to the samples (unfractionated serum, recombinant MMP2 or gelatin- bound or unbound fraction). Gels were run using vertical gel electrophoresis apparatus (Amersham Biosciences), at 200V constant for 2 hours. The gel was washed three times with 2.5% (v/v) Triton X-100 for 20 mins each time and incubated at 37 °C overnight (12 h) in an enzyme assay buffer (25 mM Tris-HCl pH 7.4, 5 mM $CaCl_2$, 150 mM NaCl, 0.05% (v/v) Brij^{TM}-35). The gels were stained with Coomassie blue and destained in 25% (v/v) methanol / 10% (v/v) acetic acid. MMP2 activity towards either gelatin or fibrinogen resulted in clear substrate-lysis bands contrasting against a blue background (from Coomassie staining) in the gel. Intensities of the lysis bands were determined by densitometric scanning using the software ImageJ (NIH, Bethesda, MD).

3.5.5 Protein binding assay to assess effect of FBG on gelatin - MMP2 interaction

Lyophilised human FBG (Sigma, cat# F3879) was reconstituted in PBS at 10 mg/mL concentration (estimated [FBG] = 6 mg/mL or 17.6 µM) to make a working solution. 40 µL of packed gelatin-beads were washed three times with 1 mL of PBS and resuspended in 40 µL of PBS. Increasing concentrations of FBG (0, 1.2, 1.8, 3.6 mg/mL) were pre-incubated with a constant 0.001 mg/mL recombinant proMMP2 (Calbiochem) at 4 ºC for 30 mins in 0.5 mL centrifuge tubes with shaking (1100 rpm) in a thermomixer R (Eppendorf^{TM}). Equal volumes of gelatin-beads (containing an estimated 43 µg gelatin in 10 µL) were then added and the mixture was incubated for a further 1.5 hours in the same conditions. The mixture was then centrifuged (2000 x g, 1-2 mins) - until all the beads had settled at the bottom of the centrifuge tubes. The supernatant (the gelatin-unbound fraction) was separated and analyzed for gelatinase activity using the substrate zymography method described above.

3.5.6 Western immunoblotting to detect MMP2

Serum and recombinant MMP2 were detected by Western blot. Recombinant proMMP2 (Calbiochem) was included as a positive control for detection by primary anti-MMP2 antibodies. Equal volumes of samples were mixed with a reducing sample buffer (150 mM Tris-HCL, pH 6.8, 15% (w/v) SDS, 30% (v/v) Glycerol and 10% (v/v) 2-Mercaptoethanol), heated at 95°C for 10 mins and run on a SDS/10%-PAGE. The gel was stained with the Zn-Imidazole reverse stain technique previously described by us(*187, 188*). After imaging the gel, the Zn-Imidazole stain was removed from the gel by Zn chelation; i.e., by incubating the gel in 50 mM EDTA/ 1X running buffer (25 mM Tris, 192 mM Glycine and 3.4 mM SDS). For Western immunoblotting, the proteins were transferred from the gel onto a 0.2 µm nitrocellulose membrane (BioRad,

USA). The membrane was then probed with a rabbit polyclonal anti-MMP2 antibody (Abcam, cat# ab37150) or a rabbit monoclonal anti-MMP2 (D2O4T) antibody (CellSignalling, cat# 87809). These primary antibodies were then detected using a horseradish-peroxidase-conjugated goat anti-rabbit secondary antibody (BioRad, USA) and the Amersham ECL Western Blot Detection Reagent (GE Healthcare, cat# RPN2106).

3.5.7 Serum protein identification by LC–MS

Identification of proteins in serum was done by liquid chromatography/mass spectrometry starting with SDS-PAGE-resolved Zn-Imidazole stained protein bands. The gel was excised and de-stained in 50mM EDTA (pH 8) for 10 mins and washed in deionized water. The gel pieces were washed with 100 mM ammonium bicarbonate/acetonitrile (v/v, 50:50), reduced (with 10 mM BME in 100 mM bicarbonate) and alkylated (with 55 mM iodoacetamide in 100 mM bicarbonate). Gel pieces were dehydrated using 100% acetonitrile for 10 mins and protein in the gel was digested with trypsin (6 ng/μL) for 16 hours at 25°C. Eluted tryptic peptides were collected. Residual peptides in the gel pieces wererecovered by two consecutive extractions in i) extraction buffer A (97% water/2% acetonitrile/1% formic acid) and ii) extraction buffer A and acetonitrile in a 1:1 (v/v) ratio. For protein identification, the peptides were analysed using conventional liquid chromatography (Easy-nLC II, Thermo Scientific) and mass spectrometry (LTQ XL-Orbitrap hybrid mass spectrometer (Thermo Scientific)) aided with Proteome Discoverer 1.4 / SEQUEST platform for proteome analysis (Thermo Scientific), at the Alberta Proteomics and Mass Spectrometry Facility (University of Alberta).

3.5.8 MMP2 activity determination by a flourometric enzyme activity assay

The effect of human plasma FBG (Sigma) on the proteolytic activity of recombinant human MMP2 (Abcam, cat# ab81550) was determined using the Enzcheck® gelatinase/collagenase assay kit (Thermo Fisher Scientific). DQ^{TM} gelatin from pig skin conjugated with fluorescein was used as the MMP2 substrate whose final concentrations were varied from 0.02 mg/mL to 0.1 mg/mL. The concentrations of MMP2 and FBG used in the assay were kept constant at 0.001 mg/mL and 3 mg/mL respectively. The final assay volume was 100 µL and contained 50 mM Tris-HCl (pH 7.6), 150 mM NaCl, 5mM $CaCl_2$, 0.2 mM NaN_3. The assay was performed in SpectraPlate^{TM}-384 MB microplates (PerkinElmer). MMP2 was pipetted to wells containing increasing concentrations of the gelatin substrate (0.02, 0.04, 0.06, 0.08 and 0.1 mg/mL) either in the presence or absence of FBG. Corresponding negative controls (no MMP2 added) were set up. The contents of each well were mixed by pipetting the mixture up and down. Fluorescence was measured using the Synergy^{TM} H4 hybrid microplate reader (BioTek), at 37°C for 5 hours with fluorescence readings taken every 60 seconds. Read mode was set to top optic with gain 50, and the excitation and emission wavelengths were set to 485 nm and 528 nm, respectively. For each time point, the background fluorescence was corrected by subtracting the measured fluorescence value derived from the no-enzyme (negative) control. The corrected fluorescence values of each reaction condition were plotted against time and the rates of reaction were determined by calculating the initial gradient once the curves reached linearity (when the rate of product formation is highest). As a negative control, human serum albumin (HSA; Sigma, cat# A3782) was used instead of FBG.

3.5.9 Restoration of MMP2 activity by neutralization of FBG

We tested the effect of neutralizing FBG in solution on MMP2 activity using two complimentary methods: i) FBG (6 mg/mL in 1X PBS, pH 7.4) was degraded by incubating with 0.001 mg/mL purified human plasmin (Sigma, cat# P1867) for 12 hours at 37 °C. The degradation of FBG was confirmed by SDS-PAGE and the fragments were subsequently used to assess their effect on MMP2 activity in the gelatinase activity assay described above. ii) FBG (4 mg/mL in 1X PBS, pH 7.4) was incubated with equimolar concentrations (11.76 μM) of polyclonal rabbit anti-human fibrinogen (anti-FBG; Agilent Dako) at 37 °C for 2 hours to form an immunocomplex. In a control experiment, we incubated FBG with non-immune negative control rabbit immunoglobulin (IgG; Dako Agilent) which does not complex with FBG. Following brief centrifugation (2000x g for 2 mins), the FBG solutions (final [FBG] = 2 mg/mL) containing either anti-FBG or IgG were subsequently used to assess their effect on MMP2 activity in the gelatinase activity assay described above.

3.5.10 In silico molecular modelling and protein-protein docking

Crystal structures of full length proMMP2 (PDB ID: 1CK7)(*11*), dimeric form of human fibrinogen (PDB ID: 3GHG)(*189*) and a collagen model peptide (PDB ID: 1BKV)(*190*), and Marimastat (PubChem CID: 119031)(*191*) were used for *in silico* molecular protein-protein docking analyses. To simulate a catalytically active MMP2, the propeptide (amino acids 30 – 109) of full length proMMP2 was removed using Python Molecular Viewer (MGLTools software, The Scripps Research Institute). The generated structure was then refined using 3Drefine server(*192, 193*) and used for subsequent docking with FBG, collagen and Marimastat. Docking of MMP2 with FBG and collagen was done using the online server ClusPro with no manual changes in default settings described by the developers(*194-198*). We selected the best

model based on the most negative binding energy and the highest cluster size. Marimastat docking to MMP2 was performed following the procedure previously described by Jha et al.(*199*) using Chimera UCSF(*200*) and AutoDock Vina 1.1.2(*201*). The structure of Marimastat was minimized using the default parameters (steepest descent steps: 100; steepest descent step size (Å): 0.02, conjugate gradient steps: 10; conjugate gradient step size (Å): 0.02; update interval: 10; fixed atoms: none) on Chimera, hydrogens were added and Gasteiger charges were assigned for a net charge of +0. MMP2 structure preparation included solvent deletion, addition of hydrogens and assignment of Gasteiger charges. The AutoDock Vina docking grid map was set to cover the full structure of MMP2 with the maximum number of binding modes (set at 10) and maximum exhaustiveness of search (set at 8). The best ranked model was selected based on the predicted binding affinity in kcal/mol, RMSD values and hydrogen bonds. Polar contacts in the docked models of collagen with MMP2, FBG with MMP2 and FBG with MMP2 docked to collagen were identified using PyMOL (Schrödinger, LLC, NY). Molecular interactions were determined using the software CONTACT of CCP4(*202*) to find potential interacting residues within 5Å. Interactions were classified as hydrogen bonds or other (polar or non-polar) interactions.

3.5.11 Sequence alignment

The sequences of the PEX and the catalytic domains of MMPs were obtained from UniProt (The UniProt Consortium). Sequences were aligned using the protein alignment tool blastp (NCBI, Bethesda, MD, USA).

3.5.12 Statistical analysis

The results were analyzed and the graphs were plotted using SigmaPlot 13 (Systat Software, San Jose, CA). Data are presented as mean ± standard error of mean. Student's t-test analysis or

Mann-Whitney Rank Sum Test was conducted, where appropriate (indicated in the figure legends), to determine statistical significance in the difference between two groups.

4 Chapter 4: ApoA1 transports and regulates MMP2 in the blood

Hassan Sarker, Rashmi Panigrahi, Ana Lopez-Campistrous, Todd McMuellen, Ken Reyes, Elena Anderson, Vidhya Krishnan, Samuel Hernandez-Anzaldo, J N Mark Glover, Eugenio Hard, Carlos Fernandez-Patron

Preface

This chapter represents our work deposited as a preprint manuscript in Research Square (https://doi.org/10.21203/rs.3.rs-3897886/v1), under a CC BY 4.0 license. The manuscript is currently being peer-reviewed for publication. The study was directed by CFP. HS, RP, ALC, TM, EH and CFP participated in the design of the experiments. HS, RP, ALC, KR, VK, EA and SHA conducted the experiments and collected the data. RP conducted the *in silico* AlphaFold-aided structural studies under the supervision of MG. ALC conducted the thin-film visual interference color assay. HS, RP and CFP wrote the manuscript. HS, EH and CFP edited the manuscript. All the authors participated in the data analysis, performed critical revisions of the manuscript, and approved the final version of the manuscript. The manuscript has been adapted to fit the format of this thesis.

4.1 Summary

Synthesized in the liver and intestines, apolipoprotein A1 (ApoA1) is the major protein component of high-density lipoprotein (HDL) particles and transports cholesterol from peripheral organs to the liver. This interorgan communication strategy may protect against atherogenesis by sequestering cholesterol from atherosclerotic lesions. Here, we found that ApoA1 has high affinity for the catalytic groove and fibronectin-like repeats of matrix metalloproteinase 2 (MMP2), the most abundant MMP in human blood. In healthy humans and ApoA1-expressing mice, we found that MMP2 is associated with ApoA1 in HDL. We confirmed the ApoA1/MMP2 interactions using five orthogonal interaction proteomics assays. Strikingly, we found that Apoa1 can allosterically increase the proteolytic activity of MMP2—an effect not

observed in ApoA1-deficient plasma from ApoA1 KO mice. This finding was not predictable, as MMP2 was not previously known to be an allosteric enzyme. Using a high-confidence artificial intelligence (AlfaFold)-based structural model of the ApoA1/MMP2 complex, we explain how ApoA1 binds and allosterically regulates MMP2. We speculate that ApoA1 sequesters MMP2 in the blood circulation and redistributes it to ApoA1 target organs, such as the liver. This interorgan communication mechanism is independent of canonical reverse cholesterol transport by ApoA1/HDL and may prevent MMP2-mediated rupture of atherosclerotic plaques.

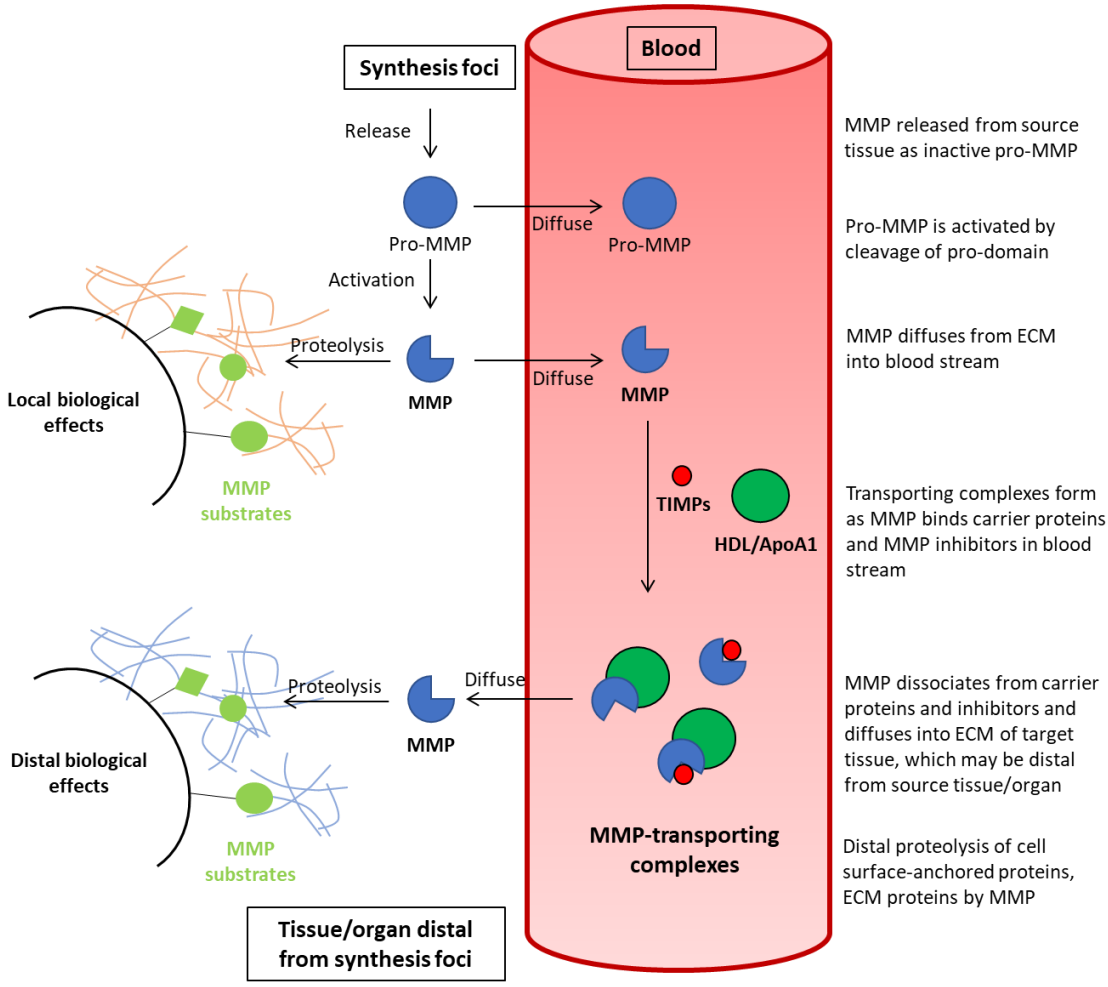

4.2 Introduction

Interorgan communication is an evolutionarily conserved mechanism in all animals that serves to maintain homeostasis in response to changing external conditions(*203*). Organs synthesize and release diverse molecular signals that can reach distal target organs through the blood circulation. These signals include (i) metabolites such as glucose and lactate that mediate the cross-talk between skeletal muscle and liver tissue during vigorous exercise, (ii) peptides such as insulin released from the pancreas to promote glucose uptake by other organs, and (iii) proteins such as proteases released from the pancreas to digest dietary proteins in the small intestine, which provide the organism with free amino acids for protein synthesis(*203-206*). Among the proteases found in the blood circulation are matrix metalloproteinases (MMPs).

At least 25 different MMPs have been identified in vertebrates; twenty-four are present in *Homo sapiens*(*1, 2*). MMPs are expressed as inactive zymogens (pro-MMPs) and generally consist of an N-terminal signal peptide, catalytic domain, and C-terminal hemopexin-like domain(*1, 3*). Proteolytic removal of the propeptide domain by autolysis or by other MMPs (e.g., membrane-anchored MMP14) or non-MMP endopeptidases (e.g., plasmin) yields active MMPs(*1*). Active MMPs have many substrates, including extracellular matrix components, proinflammatory cytokines, growth factors, and cell-surface receptors(*1, 85, 105, 207*). The diversity of substrates allows MMPs to regulate extracellular matrix integrity, inflammatory signaling, cell growth, and metabolism in the organs where they are synthesized(*1, 2, 85*). MMP activity is strongly regulated by endogenous inhibitors, including tissue inhibitors of matrix metalloproteinases (TIMPs)(*18, 25, 85, 105, 207-209*), whose N-terminus binds noncovalently to the catalytic domain of MMPs, effectively blocking substrate access(*210-212*).

In normal cells and organs, small amounts of MMPs are constitutively synthesized and secreted into the extracellular space and blood circulation(*2, 85*). In disease conditions, affected organs often become foci of MMP synthesis and secretion—this has been documented, for example, for ischemic failing hearts and tumors(*3, 84*). However, the impact of increased secretion of MMPs from one organ on other organs (interorgan communication) is unclear. Plausibly, increased circulating MMP levels can promote (or exacerbate) adverse extracellular matrix remodeling, inflammatory signaling, cell migration and organ dysfunction, leading to comorbidities. Currently, how MMP activity is regulated in the blood is unclear. This is, at least in part, because the molecular interactome of MMPs in the blood is largely unknown.

Within the MMP family, gelatinase A (MMP2) is the most abundant member in the blood (as shown by our data here). Clarifying the transport and regulation of MMP2 in the blood circulation was the focus of this research. We report hitherto unknown interactions of MMP2 with apolipoprotein A1 (ApoA1). ApoA1 (28 kDa) is the major protein component of high-density lipoprotein (HDL) particles and transports cholesterol from peripheral organs to the liver(*213, 214*). We found that ApoA1 has high affinity for the catalytic groove and fibronectin-like repeats of MMP2. Consistent with these findings, we observed that MMP2 is associated with HDL particles in healthy humans and ApoA1-expressing mice. Strikingly, we also found that ApoA1 can allosterically increase the proteolytic activity of MMP2 to very high levels—an effect not observed in ApoA1-deficient plasma from ApoA1 KO mice. This finding was not predictable, as MMP2 was not previously known to be an allosteric enzyme. Therefore, we thoroughly characterized the structural basis underlying the interactions between MMP2 and ApoA1 using artificial intelligence (AlphaFold)-based structural modeling of the ApoA1/MMP2 complex. Based on our findings, we postulate a novel hypothesis: ApoA1 in HDL acts as a

"transporter and regulator of the activity potential (TRAP)" of MMP2. Given that this mechanism is likely not specific for MMP2, we propose the new term "TRAP of MMPs" to define multiprotein complexes that transport MMPs in the blood and may additionally cause MMP activity to increase, decrease or remain unchanged—without immediate biological effects—while simultaneously enabling secreted MMPs in the blood to reach distal target organs and participate in interorgan communication. As proof-of-principle, we identified blood-borne proteins with the potential to serve as components of TRAP complexes of MMP2.

4.3 Results

4.3.1 MMP2 circulates in the blood as a large MW complex with HDL

We fractionated freshly isolated human plasma by fast-performance liquid chromatography (FPLC) using a Superose® 6 10/300 gel-filtration FPLC column isocratically developed with NaCl (50 mmol/l) buffer as the mobile phase, a technique routinely used for the analysis of lipoprotein particles. We identified fractions containing HDL-C by characteristic retention times and confirmed the results by detecting ApoA1 (the major protein component and marker of HDL) via western immunoblotting (**Figure 4.1A**).

Fractions containing the column eluent were analyzed for the presence of MMP2 (by gelatin zymography). MMP2 was concentrated in the FPLC fractions containing HDL, as determined by the presence of its unique protein constituent ApoA1 (**Figure 4.1A**, fractions 13-15, with retention times <43 minutes and a MW >158 kDa; **Figure 4.2**). We did not detect MMP2 in FPLC fractions containing complexes larger than HDL (175-500 kDa, 6-12 nm), such as LDL (2.93 MDa, 22-29 nm) or VLDL (6-27 MDa, 25-90 nm), which excluded the presence of MMP2 in these lipoprotein particles in the specimens analyzed.

Studies with mouse and human plasma showed that MMP2 was concentrated in FPLC fractions containing HDL in both species (**Figure 4.1B**). Neither the use of serum (instead of plasma) nor frozen specimens (instead of freshly isolated specimens) altered the cofractionation of plasma MMP2 with HDL in either mice or humans.

Subjecting plasma to BN–PAGE, an electrophoretic technique capable of resolving large protein complexes, followed by the detection of MMP2 (by gelatin zymography) or ApoA1 (by western immunoblotting) showed that MMP2 activity appears in a band which also exhibits ApoA1 immunoreactivity (**Figure 4.1C**).

We investigated whether MMP2 forms a complex with ApoA1 in HDL and whether other MMPs in plasma share this feature with MMP2. To determine whether all the plasma MMPs were associated with ApoA1/HDL, we measured their quantity in selected FPLC fractions 13-17, which contained ApoA1 and represented a wide range of sizes of proteins/complexes, from <44 kDa in fractions >17 to >158 kDa in fractions <15 (**Figure 4.1E, Figure 4.3**). MMP2 and MMP9 were most abundant in high-MW fractions 13-15 (**Figure 4.1E**) and were resolved from MMP1, MMP3, MMP7, and MMP10 (mostly found in low-MW fractions 16-17). Consistent with the findings in the present study, TIMPs were also detected in fractions containing MMPs (**Figure 4.1E**). MMP8, MMP12, and MMP13 were not detected.

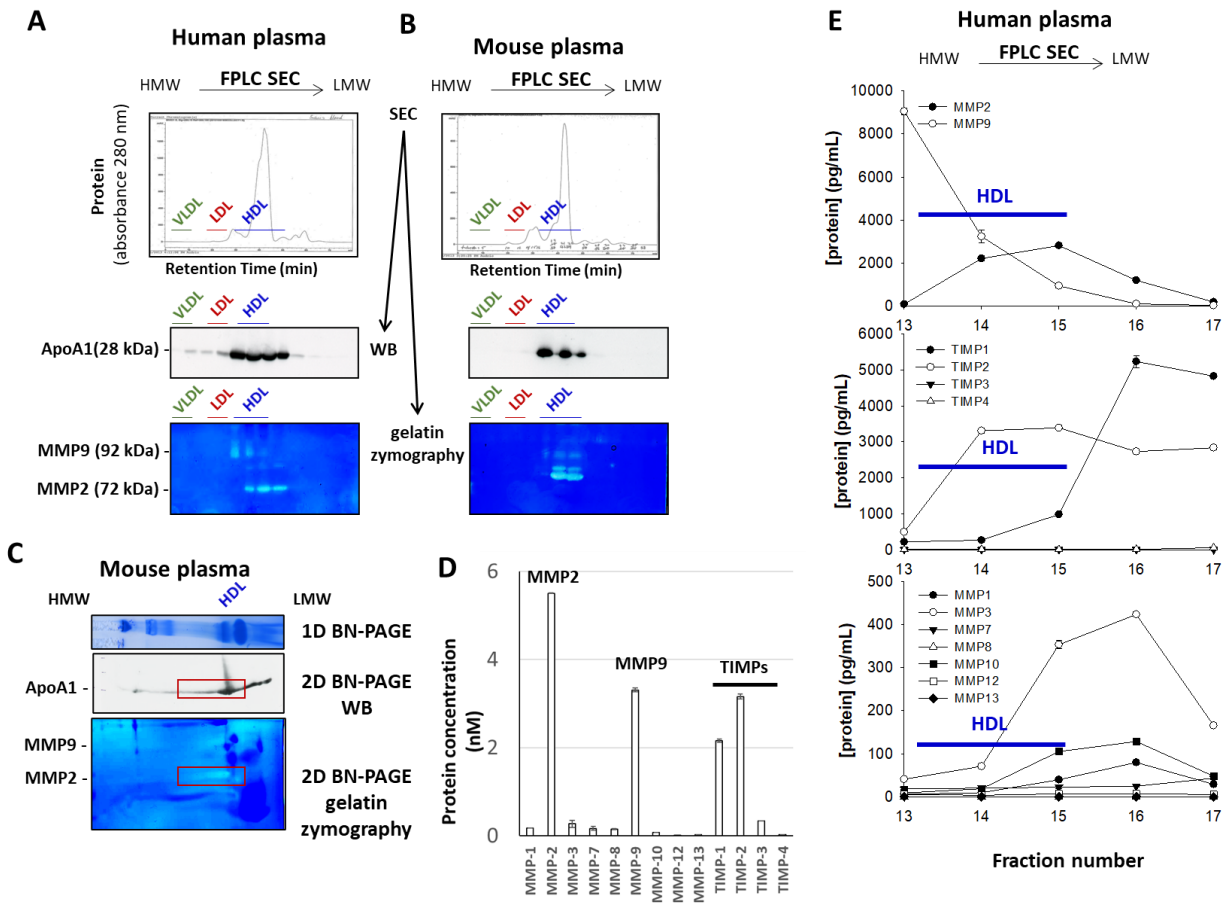

Figure 4.1: FPLC analyses of human and mouse plasma samples showing that MMP2 associates with HDL in the blood.

(A) Size-exclusion chromatography data showing that human plasma MMP2 cofractionates with ApoA1. Plasma from a healthy adult human donor was subjected to FPLC (size-exclusion) fractionation, and the fractions were analyzed for the presence of ApoA1 (by western blot) and MMP2 (by in-gel gelatin zymography). (B) Mouse plasma MMP2 cofractionated with ApoA1 according to size-exclusion chromatography. A pooled sample of plasma from WT male mice (CBL57/B6, n=9) aged 12-15 weeks was subjected to size-exclusion (FPLC) fractionation, and the fractions were analyzed for the presence of ApoA1 (by western blot) and MMP2 (by in-gel gelatin zymography). (C) Mouse plasma MMP2 comigrated with ApoA1 according to native PAGE (BN-PAGE). A pooled sample of plasma from WT male mice (CBL57/B6, n=9) aged 12-15 weeks was subjected to 2-dimensional electrophoretic separation: 1st dimension native BN–PAGE to separate complexes, followed by 2nd dimension SDS–PAGE/WB (to detect ApoA1) or gelatin zymography (to detect MMP2) to separate subunit proteins. (D) Quantitation of MMPs and TIMPs in human plasma. Pooled plasma samples from healthy adult human donors (n=5) were subjected to multiplex immunoassay to quantify plasma MMPs and TIMPs. Measurements were taken in duplicate. (E) Size-exclusion fractionation profile of MMPs and TIMPs in human plasma. The size exclusion (FPLC) fractions obtained from the pools of plasma samples from healthy adult human donors (n=5) were subjected to multiplex immunoassay to quantify all the MMPs and TIMPs. Measurements were taken in duplicate. The data are presented as the mean ± standard error.

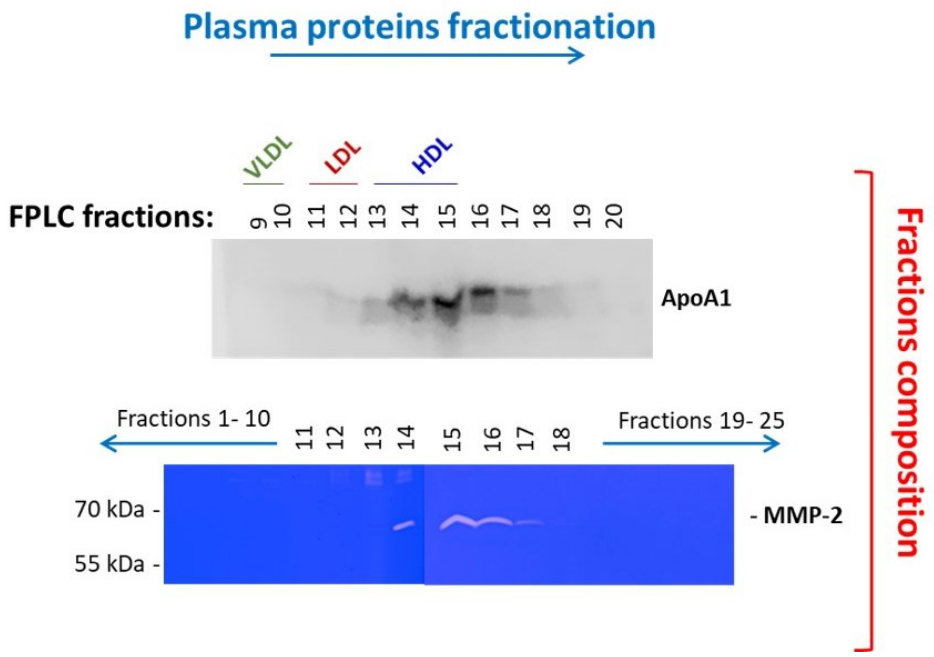

Figure 4.2: FPLC analyses of human plasma show that MMP2 co-fractionates with ApoA1.

A pooled sample of plasma from healthy adult human donors (n=5) was subjected to FPLC (size-exclusion) fractionation and the fractions were analyzed for presence of ApoA1 (by western immunoblot) and MMP2 (in-gel gelatin zymography).

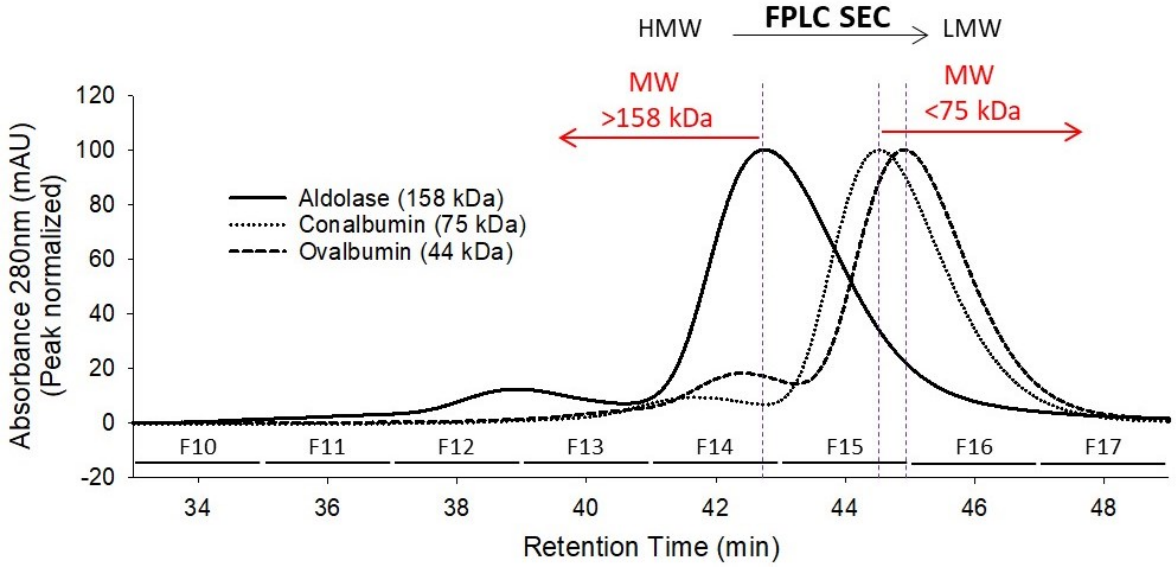

Figure 4.3: FPLC traces of standard proteins for reference of molecular weights in collected fractions.

To determine the requirement of ApoA1 for the formation of high-MW MMP2 complexes, we subjected plasma from ApoA1 KO and WT mice to the same FPLC fractionation procedure (**Figure 4.5A**). A lack of ApoA1 did not affect the total quantity of MMP2 in plasma (**Figure 4.5B**). However, we observed a shift in MMP2 fractionation toward low-MW FPLC fractions in ApoA1 KO plasma compared to that in WT plasma (**Figure 4.4A, B**). The proportion of MMP2 in the high-MW fractions 13 and 14 containing ApoA1/HDL relative to the low-MW fractions 16 and 17 was lower in the ApoA1 KO plasma than in the WT plasma (**Figure 4.4A, B**). The proportion of MMP2 co-migrating with HDL (fractions 13 and 14) was 51.1% in the WT strain and 32.6% in the ApoA1 KO strain (**Figure 4.4A**). In the absence of ApoA1 in ApoA1 KO plasma, ApoE is the major apolipoprotein associated with HDL(*214*) (**Figure 4.4C**), and the total plasma HDL and total cholesterol in HDL-containing fractions were decreased (**Figure 4.4D, Figure 4.5C**).

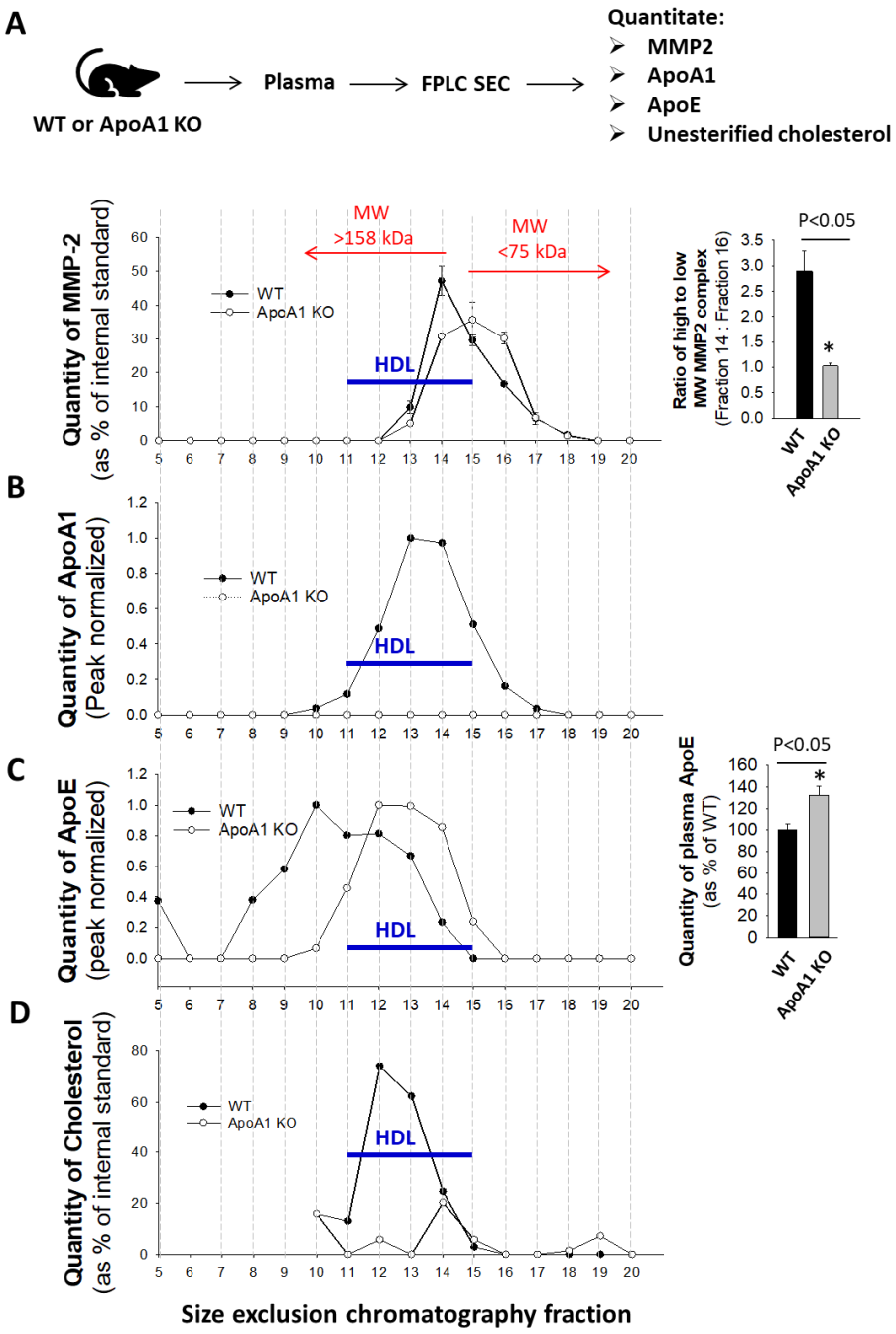

Figure 4.4: FPLC analyses of plasma from ApoA1 KO and WT mice indicate that plasma MMP2 interacts with HDL via ApoA1.

Pooled samples of plasma from WT (n=6) or ApoA1 KO (n=6) mice were fractionated by FPLC (size-exclusion) and fractions were analyzed to detect and quantitate: (**A**) MMP2 by in-gel gelatin zymography (bar plot to the right shows a comparison of the abundance of MMP2 in a high molecular weight fraction (F14) relative to low molecular weight fraction (F16) in WT and ApoA1 KO mouse plasma), (**B**) ApoA1 by western immunoblot, (**C**) ApoE by western immunoblot (bar plot to the right shows quantitation of total plasma ApoE), and (**D**) total cholesterol by a standard cholesterol-SL assay. The data are presented as the mean ± standard error (triplicate). *p<0.05 vs WT (1-way ANOVA).

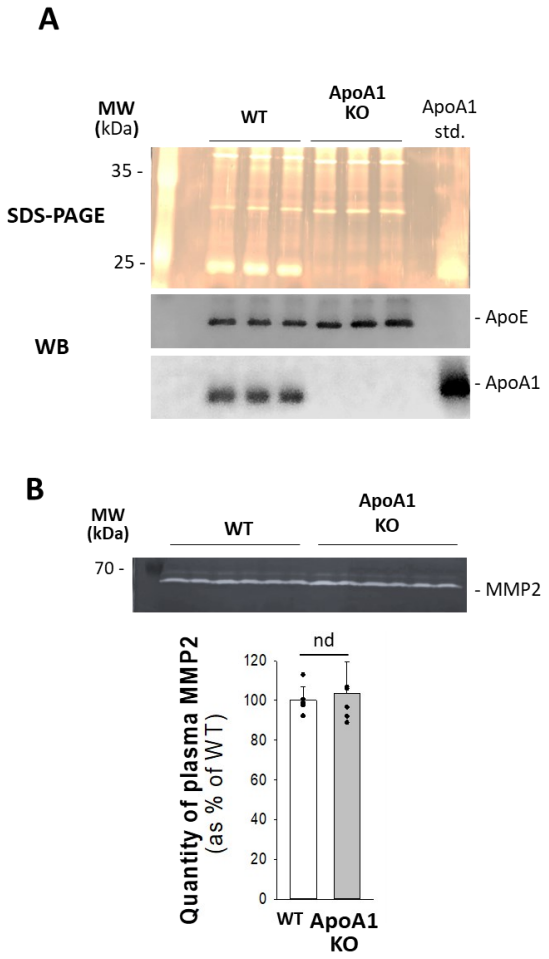

Figure 4.5: Analysis of ApoA1 KO and WT mouse plasma.

(**A**) SDS-PAGE and WB analyses of mouse plasma confirming absence of ApoA1 in the plasma of ApoA1 KO mice compared to WT. (**B**) Quantitation of plasma MMP2 in ApoA1 KO and WT mice by gelatin zymography.

The shift in MMP2 fractionation toward low-MW fractions in ApoA1 KO plasma compared to WT plasma suggested that ApoA1 is an interactor of MMP2 in HDL. We incubated recombinant active MMP2 with HDL purified from human plasma and subjected the mixture to native BN–PAGE (1st Dimension) to separate proteins and complexes by size, followed by SDS–PAGE/western blot or gelatin zymography (2nd dimension) to locate HDL (by probing for ApoA1) and MMP2 (by gelatinolytic activity). We found that, in the absence of HDL, MMP2 can (i) form complexes with itself and (ii) undergo autolysis (**Figure 4.6A**). In the presence of increasing HDL

concentrations, MMP2 tended to form high-MW complexes, with a prominent continuum of MMP2 activity (from low to high MW) across the gel at the highest concentration of HDL tested (MMP2:HDL = 1:20); the detected intensities of the MMP2 activity bands (both intact and cleavage products) were greater in the presence of HDL than in the presence of vehicle (**Figure 4.6A**). These studies unexpectedly revealed that active MMP2, when incubated alone, formed homomultimeric complexes with itself and underwent autolysis. HDL inhibited autolysis and increased the proteolytic activity of MMP2.

4.3.2 ApoA1 in HDL inhibits MMP2 autolysis

To directly test the effect of HDL on MMP2 stability, we incubated recombinant active MMP2 with vehicle, EDTA (an inhibitor of MMP2) or HDL for 0, 30 or 60 minutes. Next, we measured the quantity of MMP2 remaining at each time point. Compared with the control, MMP2 incubated with vehicle underwent autolysis at 30 and 60 minutes (0 minutes). However, MMP2 activity was preserved in the presence of either TIMP2 (an inhibitor of MMP2) or HDL (a noninhibitor interactor of MMP2) (**Figure 4.6B, Figure 4.7**). No MMP2-mediated proteolysis of ApoA1 in HDL was observed.

We compared the effects of equimolar preparations of albumin (a nonspecific interactor of MMP2), α-2-macroglobulin (A2MG; a protein inhibitor of MMP2 activity), purified HDL or ApoA1 on MMP2 activity. We incubated MMP2 with vehicle, albumin, A2MG, HDL or ApoA1 for 30 minutes at 37°C and compared the quantity of active MMP2 remaining (in-gel gelatin zymography assay) to that of the control (MMP2 at 0°C – no autolysis). The relative quantities of active MMP2 remaining after incubation with vehicle, albumin, A2MG, HDL or ApoA1 were 18%, 60%, 80%, 100% and 100%, respectively (**Figure 4.6C**). Both HDL and ApoA1 effectively inhibited MMP2 autolysis. We made a similar observation when we preincubated active MMP2 with ApoA1

(compared to vehicle or albumin) or at 37°C for 60 minutes and subsequently measured the proteolytic activity of MMP2 by an in-solution gelatinase assay (**Figure 4.6D**). Therefore, HDL inhibited MMP2 autolysis, at least in part through ApoA1.

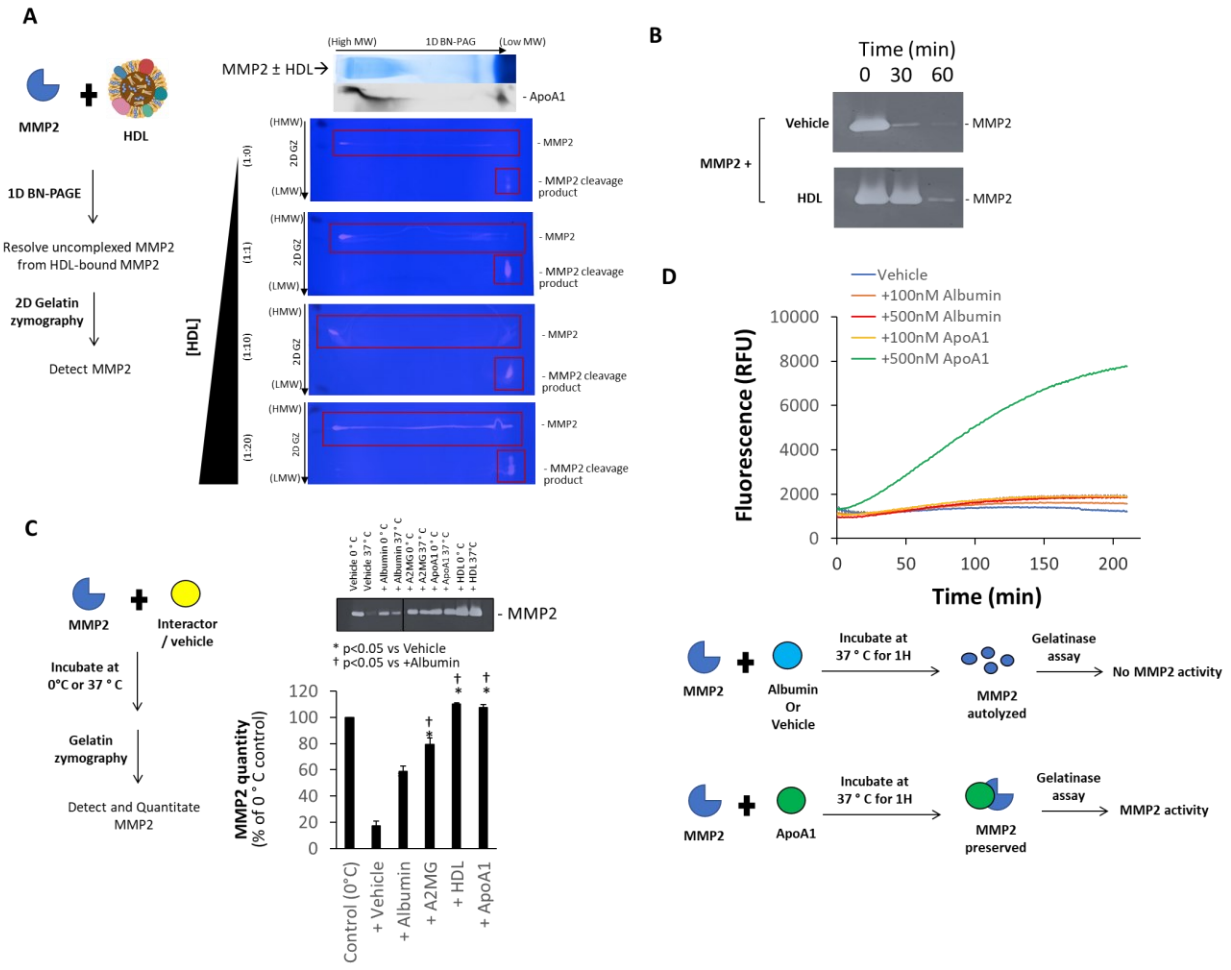

Figure 4.6: Autolysis of MMP2 is inhibited by HDL and ApoA1.

(**A**) Recombinant human active MMP2 was incubated with increasing concentrations of plasma-derived HDL, and the mixture was subjected to 2-dimensional electrophoretic separation: 1st dimension native BN-PAGE followed by 2nd dimension gelatin zymography to detect MMP2. (**B**) Recombinant active MMP2 was incubated with vehicle or HDL at a 1:10 (MMP2:reagent) molar ratio and incubated at 37°C for 0, 30 or 60 minutes, after which MMP2 was detected by in-gel gelatin zymography. (**C**) Recombinant active MMP2 was incubated with vehicle, albumin, A2MG, HDL or ApoA1 at a 1:10 (MMP2:reagent) molar ratio at 0°C or 37°C for 30 minutes, after which MMP2 was detected via in-gel gelatin zymography. (**D**) Recombinant active MMP2 (10 nM) was incubated with vehicle, albumin or ApoA1 at concentrations of 100 nM or 500 nM at 37°C for 60 minutes, after which MMP2 activity was measured via an in-solution gelatinase assay.

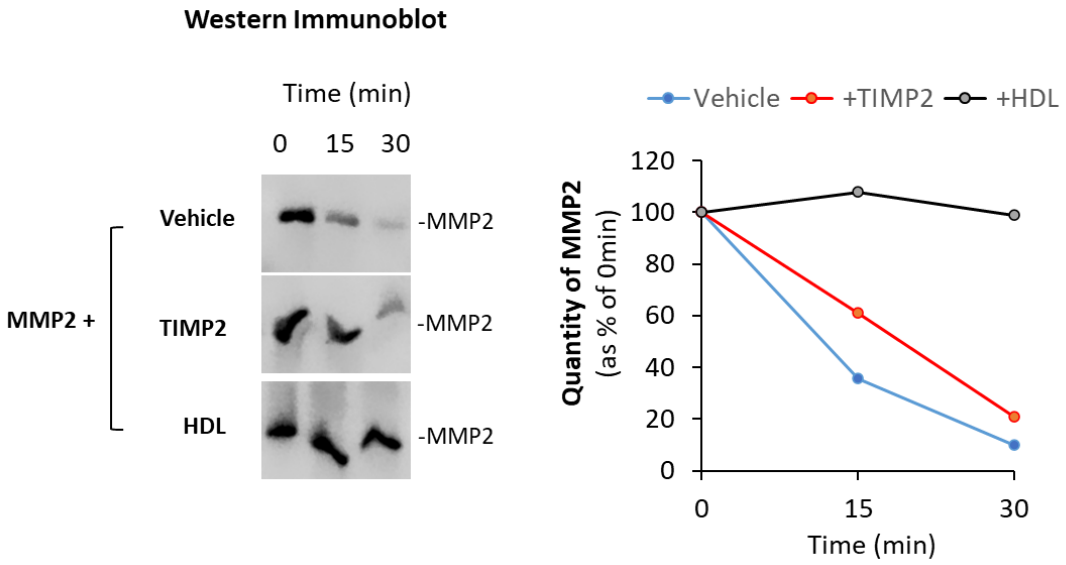

Figure 4.7: The effect of vehicle, TIMP2 or HDL on the autolysis of MMP2.

Recombinant active MMP2 was incubated with vehicle or HDL at a 1:10 (MMP2 : reagent) molar ratio and incubated at 37°C for 0, 30 or 60 minutes followed by detection of MMP2 by SDS-PAGE/ Western immunoblot.

4.3.3 ApoA1 directly interacts with MMP2

To clarify how ApoA1 influences MMP2 activity, we tested the interaction between recombinant active MMP2 and plasma-derived or recombinant ApoA1 using several complementary methods. Microscale thermophoresis (MST) analyses of active MMP2 (ligand) and ApoA1_6xHis (labeled with fluorophore) confirmed that MMP2 indeed directly binds ApoA1 with a dissociation constant (K_d) of 58.3 nM, indicating high binding affinity (**Figure 4.8A**). The structural integrity and native conformation of MMP2 are maintained by Ca^{2+} ions(*11*)—we found that MMP2 does not bind to ApoA1 in the absence of Ca^{2+} ions (negative control; **Figure 4.8A**), indicating that the MMP2-ApoA1 interaction is specific and dependent on the conformational and structural integrity of MMP2. We confirmed these MST data using a thin-film visual interference color assay in which the interaction between ApoA1 and MMP2 reproducibly generated changes in the observed color upon binding (**Figure 4.8B)**. A positive control of a known binding pair (with the MMP2 catalytic

domain and anti-MMP2 antibody) confirmed the immobilization of the protein on the film surface **(Figure 4.9**). Consistently, the thermal stability of MMP2 was also drastically increased by ApoA1, indicating that MMP2 forms a stable complex with ApoA1 (**Figure 4.10**). To clarify the stoichiometry of the MMP2-ApoA1 complex, we utilized a chemical cross-linker to stabilize the complex. We found that MMP2 (62 kDa) and ApoA1 (28 kDa) formed two distinct complexes at approximately 100 kDa and 130 kDa, suggesting that ApoA1 may bind MMP2 at a 1:1 or 2:1 ratio (**Figure 4.11A**). Together, our binding data, obtained using five different complementary techniques, clearly demonstrated that MMP2 directly interacts with ApoA1. As shown in **Figure 4.11B**, MMP2 also binds to ApoA2 and ApoE (two apolipoproteins present in HDL), as well as TIMP2.

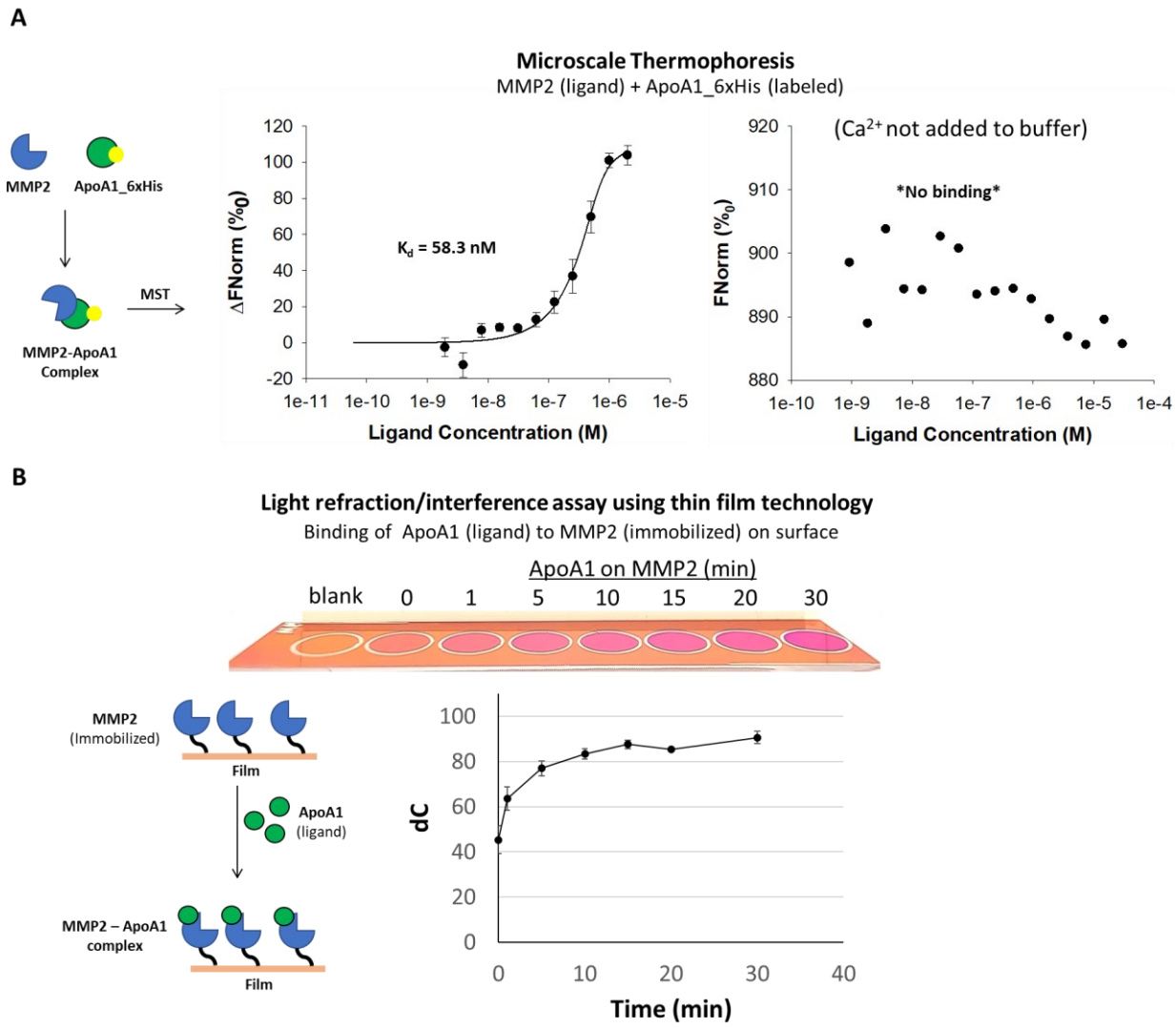

Figure 4.8: Interaction studies showing that MMP2 directly interacts with ApoA1.

(**A**) MST analyses of increasing concentrations of recombinant active MMP2 (0.9 nM to 30 µM) and 0.6 µM ApoA1_6xHis labeled with RED-Tris-NTA dye in the presence or absence of calcium ions in the assay buffer. The experiments were performed in triplicate. (**B**) A visual interference color binding assay was used to test the binding of ApoA1 to MMP2. ApoA1 (a ligand) at 100 µg/mL was added to recombinant active MMP2 (75 µg/mL) immobilized on the film, which was subsequently incubated for 0, 1, 5, 10, 15, 20 or 30 minutes, followed by color detection (see "Supplementary Methods"). The experiments were performed in triplicate.

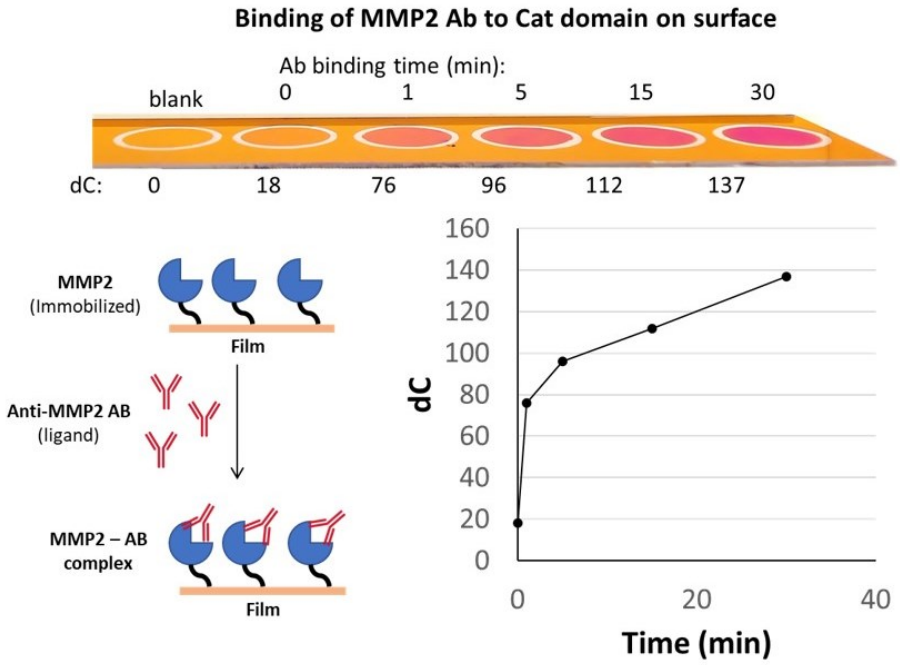

Figure 4.9: visual interference colour binding assay validation using the binding of MMP2 antibody to MMP2 catalytic domain.

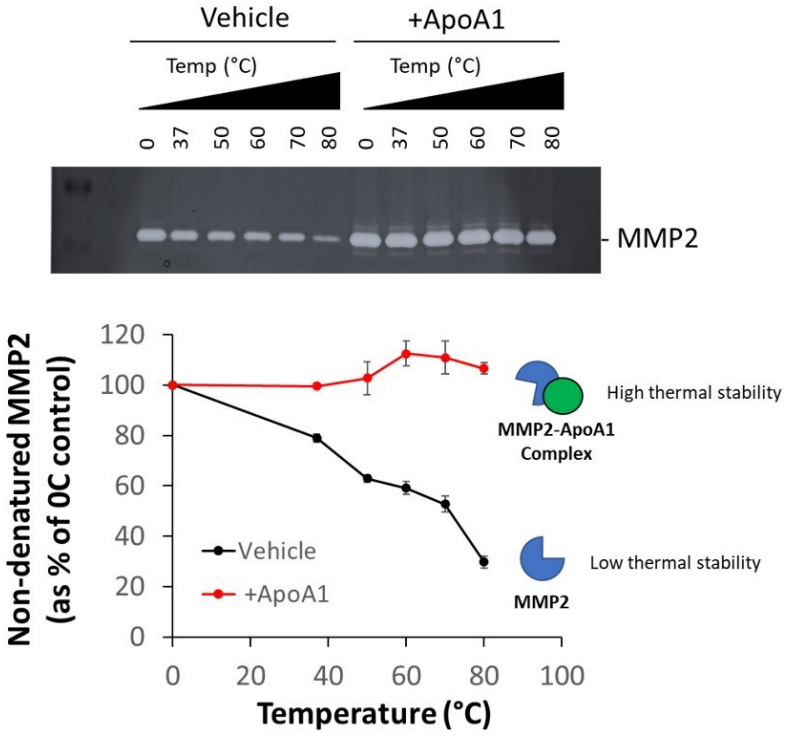

Figure 4.10: Thermal stability assay demonstrating the effect of ApoA1 on the thermal stability of recombinant active MMP2.

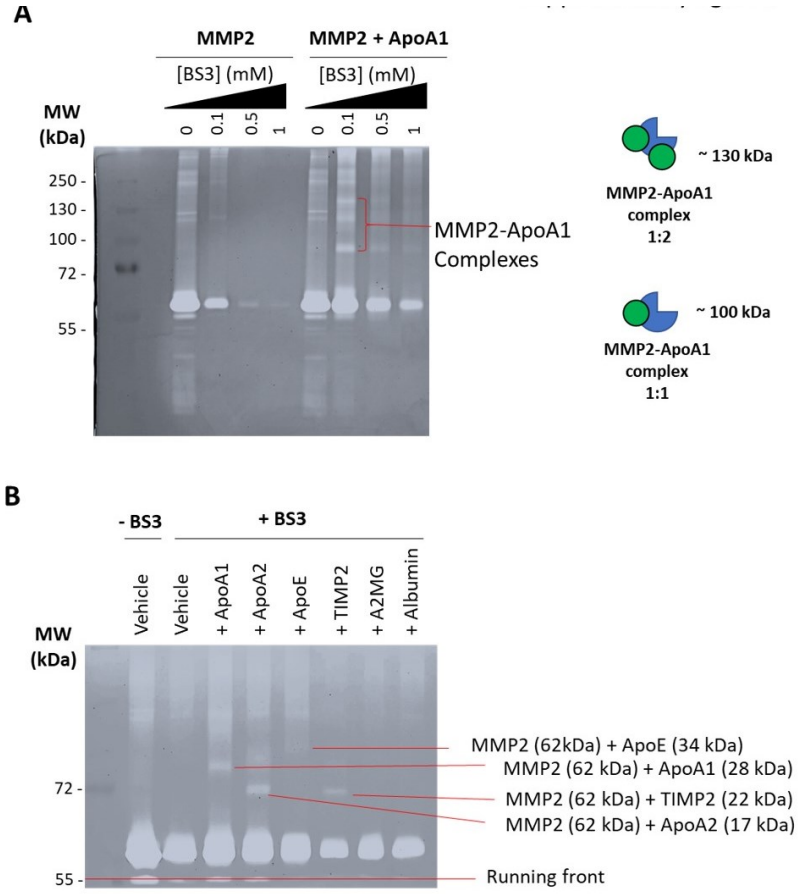

Figure 4.11: Chemical cross-linking experiments to determine the stoichiometry of MMP2-Apolipoprotein complexes.

(**A**) Zymogram showing MMP2 complexes formed with BS3 cross-linker in the absence or presence of ApoA1. (**B**) Zymogram showing MMP2 complexes formed with BS3 cross-linker in the presence of ApoA1, ApoA2, ApoE, TIMP2, A2MG or Albumin.

4.3.4 ApoA1 in HDL increases the proteolytic activity of MMP2

We applied an in-solution gelatinase activity assay to measure the rate of cleavage of fluorescein-conjugated gelatin (substrate) by MMP2 in the presence of HDL compared to that of albumin, TIMP2, A2MG (two plasma MMP2 inhibitors) or vehicle (enzyme assay buffer). TIMP2 and A2MG inhibited MMP2 activity (as expected), but albumin had no effect (**Figure 4.12A**). However, HDL concentration-dependently increased the rate of MMP2 activity (**Figure 4.12A, B**). Like HDL, ApoA1, ApoA2 and ApoE concentration-dependently increased MMP2 activity (**Figure 4.12C**), although ApoA1 and ApoE were more effective than ApoA2 was (**Figure 4.12D**).

Control studies using purified ApoA1 generated by recombinant technology confirmed the ability of ApoA1 isolated from plasma to increase MMP2 activity (**Figure 4.13**). Interestingly, ApoA1/HDL-containing fractions obtained from size-exclusion chromatography analyses of plasma from WT mice, but not from ApoA1 knockout mice, increased the proteolytic activity of recombinant MMP2, as we observed with purified HDL and ApoA1 (**Figure 4.12D, Figure 4.14**). Notably, ApoA1 inhibited MMP2 autolysis at an ApoA1:MMP2 molar ratio > 1 and increased MMP2 proteolytic activity at an ApoA1:MMP2 molar ratio > 5 (**Figure 4.15**). This experiment indicated that the increase in the proteolytic activity of MMP2 induced by ApoA1 or HDL cannot be entirely explained by the inhibition of MMP2 autolysis.

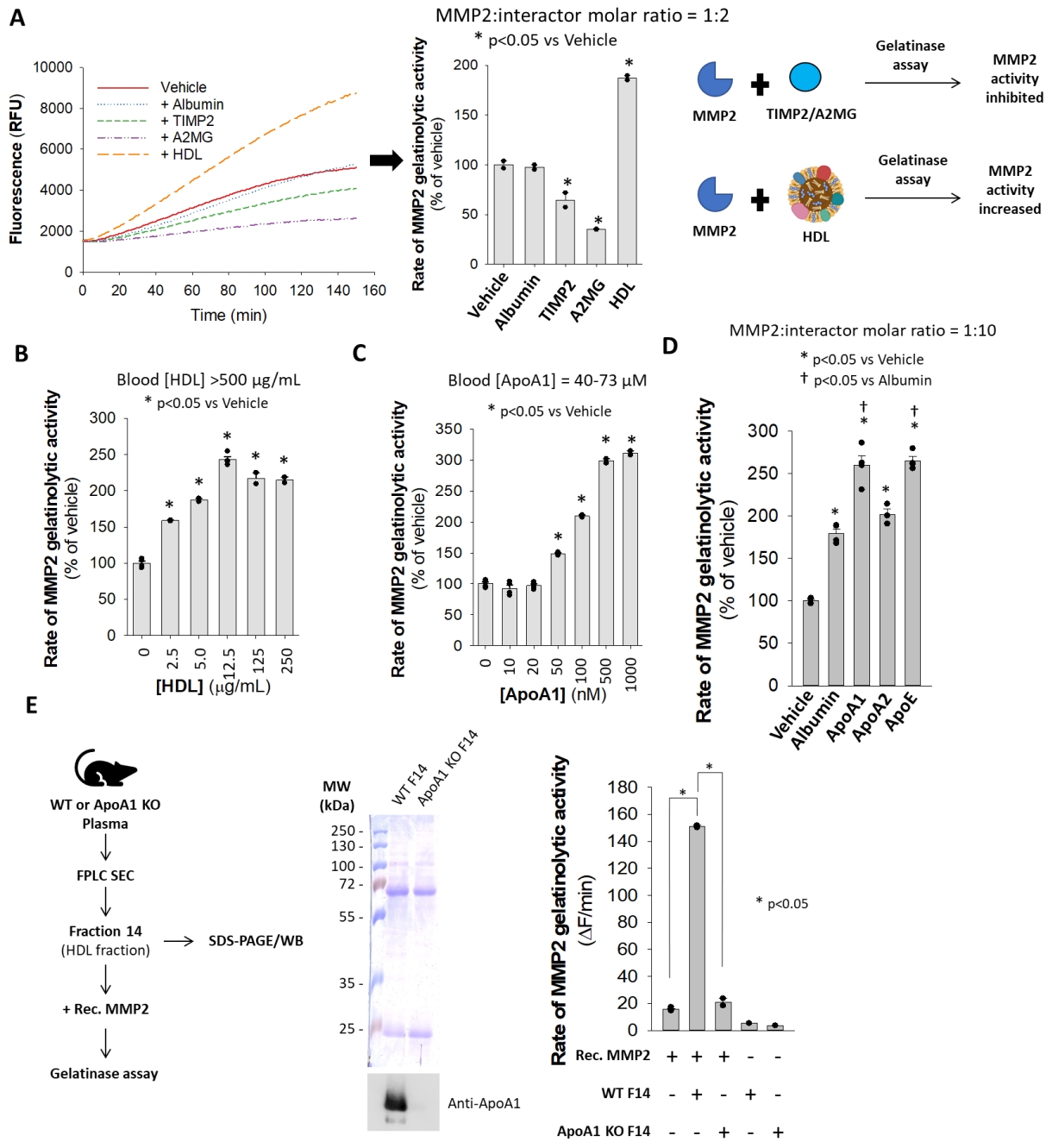

Figure 4.12: ApoA1 in HDL increases the proteolytic activity of MMP2.

(**A**) Recombinant active MMP2 was mixed with vehicle, albumin, TIMP2, A2MG or HDL at a 1:2 (MMP2:reagent) molar ratio, and the mixtures were subjected to an in-solution gelatinase assay to measure the proteolytic activity. Measurements were taken at least in triplicates. Data presented as the mean ± standard error. *p<0.05 vs vehicle (1-way ANOVA). (**B-C**) Increasing concentrations of HDL or ApoA1 were added to recombinant active MMP2, after which an in-solution gelatinase assay was used to measure MMP2 activity. Measurements were taken at least in triplicates. Data presented as mean ± standard error. *p<0.05 vs vehicle (1-way ANOVA). (**D**) Recombinant active MMP2 was mixed with vehicle, albumin, ApoA1, ApoA2, or ApoE at a 1:10 (MMP2:reagent) ratio, after which an in-solution gelatinase assay was used to measure MMP2 activity. Measurements were taken at least in triplicates. Data presented as mean ± standard error. *p<0.05 vs vehicle, †p<0.05 vs albumin (1-way ANOVA). (**E**) WT or

ApoA1 KO mouse plasma was subjected to size-exclusion chromatography fractionation, a selected fraction containing HDL (confirmed by the presence of ApoA1 via SDS–PAGE/Western blot) was added to recombinant active MMP2, and the gelatinolytic activity was measured. The bar plot compares the effect of the selected WT and ApoA1 KO fraction on the rate of MMP2-related gelatinolytic activity. Measurements were taken at least in duplicates. The data are presented as the mean ± standard error. *p<0.05 vs vehicle (1-way ANOVA).

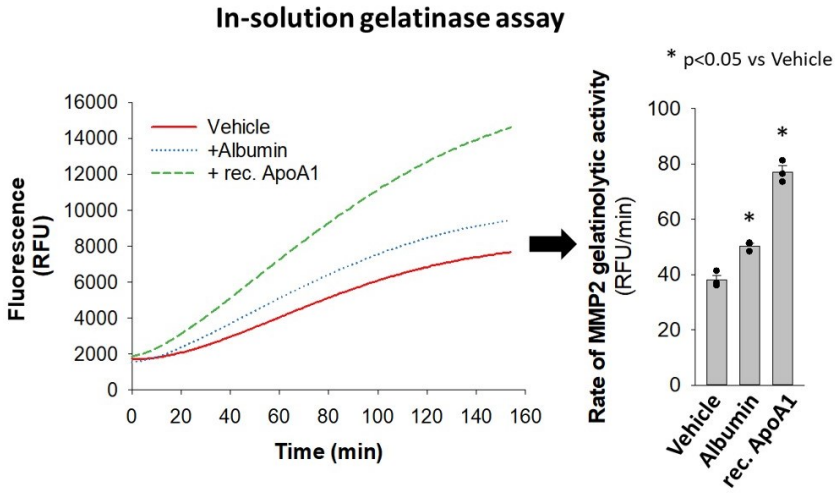

Figure 4.13: Quantitation of MMP2 activity using in-solution gelatinase assay in the presence of vehicle, Albumin or recombinant ApoA1.

MMP2 activity was measured in the presence of albumin or recombinant ApoA1 at a 1:10 molar ratio. Measurements were taken in triplicates. Data are presented as mean ± standard error.

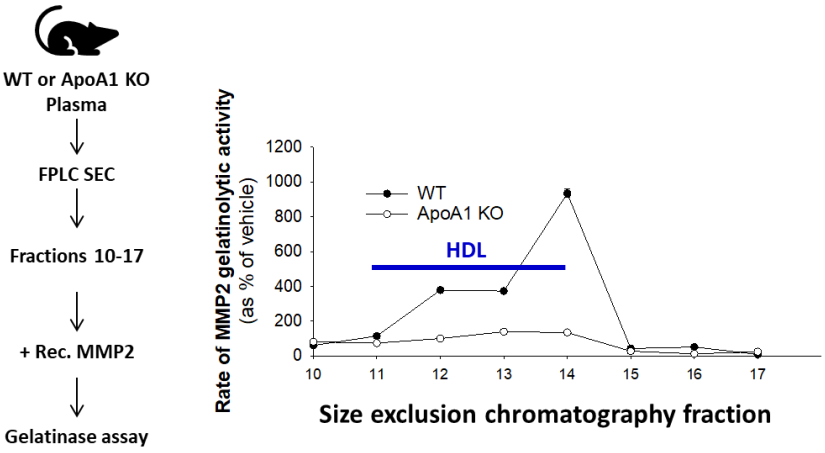

Figure 4.14: Effect of SEC/FPLC fractions of WT or ApoA1 KO mice plasma on MMP2 activity.

WT or ApoA1 KO mice plasma were subjected to size-exclusion chromatography fractionation and a range of fractions including fractions containing HDL were added separately to recombinant active MMP2 and gelatinolytic activity was measured. The line plot compares the effect of the selected WT and ApoA1 KO fractions on the rate of MMP2 gelatinolytic activity.

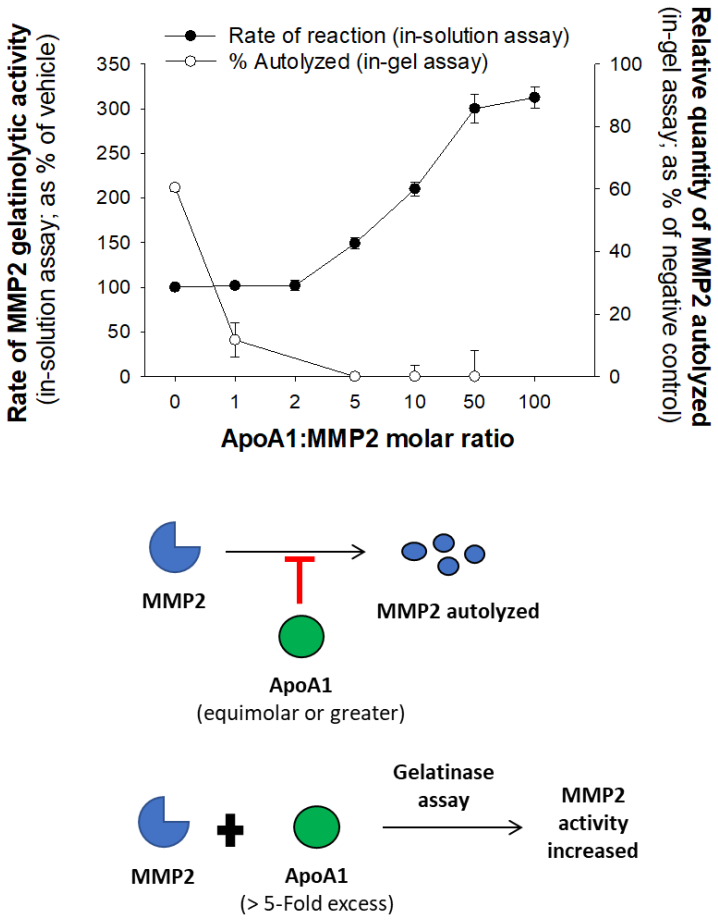

Figure 4.15: Comparison of the effects of ApoA1 on MMP2 autolysis inhibition and allosteric activation.

Line-plots showing the effect of increasing concentrations of ApoA1 on the proteolytic activity of MMP2 (measured by in-solution gelatinase assay) and inhibition of MMP2 autolysis (measured by in-gel zymography). Measurements were taken at least in triplicates. Data presented as mean ± standard error.

To reveal the mechanism by which ApoA1 increases MMP2 activity, we measured MMP2 proteolytic activity in the presence of ApoA1 or vehicle (enzyme assay buffer) with increasing substrate concentration and fit the data into sigmoidal and Michaelis–Menten kinetic models (**Figure 4.16, Figure 4.17**). The sigmoidal kinetic model was a better fit for the data with higher confidence levels for V_{max} and K_m or K_{half} determinations than was the Michaelis–Menten kinetic model (**Figure 4.16A, Figure 4.17**). In both models, the V_{max} was significantly greater in the presence of ApoA1 than in the presence of vehicle, but there was no change in the K_m or K_{half}. These data suggested that ApoA1 increases MMP2 activity through disrupting MMP2-MMP2

homomultimeric complexes (**Figure 4.18**). This unmasks MMP2 active sites making them available for substrate binding and, hence, effectively increases V_{max} without altering the affinity of MMP2 for the substrate (represented by K_m or K_{half}, **Figure 4.16B**).

A

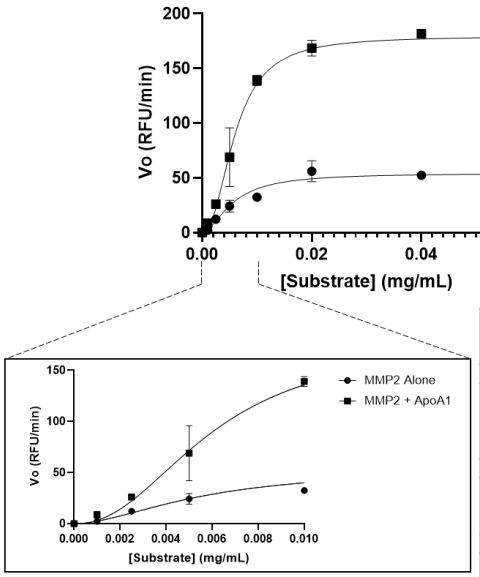

Allosteric Sigmoidal kinetics	MMP2 Alone	MMP2 + ApoA1
Best-fit values		
Vmax	54.41	179.5
Hill slope (h)	1.767	2.230
Khalf	0.005619	0.006013
Kprime	0.0001054	1.114e-005
95% CI (profile likelihood)		
Vmax	48.21 to 63.39	164.6 to 197.9
Hill slope (h)	1.152 to 2.790	1.563 to 3.322
Khalf	0.004281 to 0.008082	0.005174 to 0.007252
Goodness of Fit		
Degrees of Freedom	14	16
R squared	0.9543	0.9717
Sum of Squares	357.8	2654
Sy.x	5.055	12.88

B

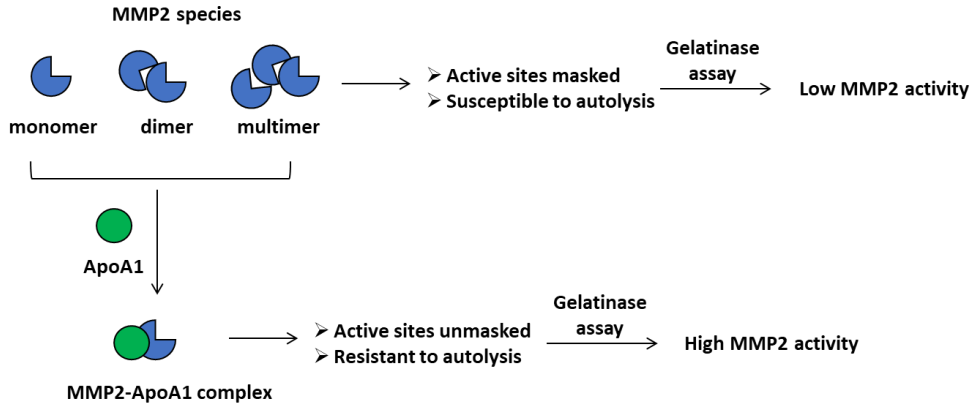

Figure 4.16: Kinetic analyses (sigmoidal model) of the effect of ApoA1 on MMP2 activity.

(**A**) MMP2 proteolytic activity was measured in the presence of vehicle or ApoA1 (at a 1:10 molar ratio) with increasing concentrations of substrate (fluorescein-conjugated gelatin). The data were fit into a sigmoidal model and are presented as line/scatter plots. Measurements were taken at least in triplicates. Data presented as mean ± standard error. (**B**) Illustration of the proposed mechanism by which ApoA1 increases MMP2 activity in solution.

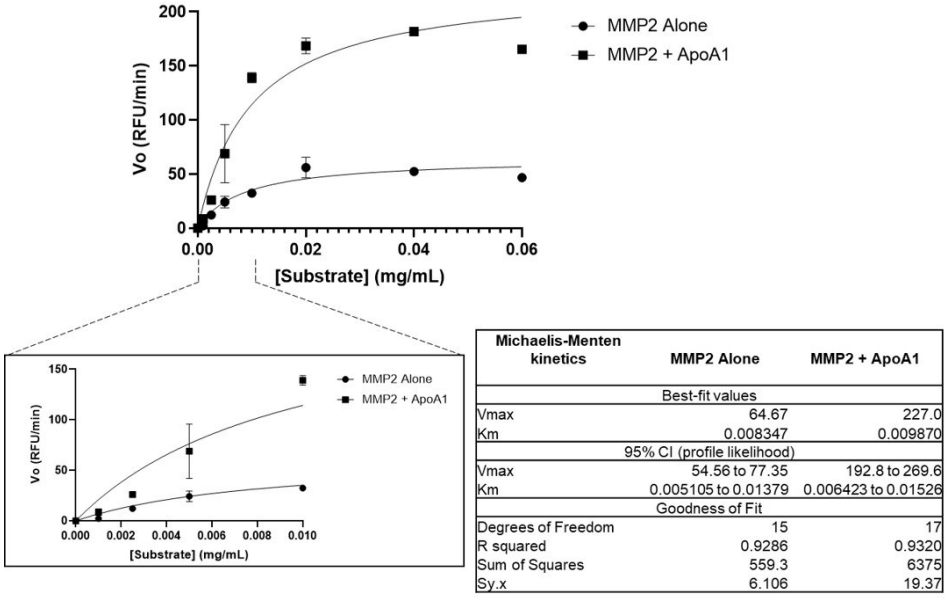

Michaelis-Menten kinetics	MMP2 Alone	MMP2 + ApoA1
Best-fit values		
Vmax	64.67	227.0
Km	0.008347	0.009870
95% CI (profile likelihood)		
Vmax	54.56 to 77.35	192.8 to 269.6
Km	0.005105 to 0.01379	0.006423 to 0.01526
Goodness of Fit		
Degrees of Freedom	15	17
R squared	0.9286	0.9320
Sum of Squares	559.3	6375
Sy.x	6.106	19.37

Figure 4.17: Kinetic analyses (Michaelis-Menten model) of the effect of ApoA1 on MMP2 activity.
MMP2 proteolytic activity was measured in the presence of vehicle or ApoA1 (at 1:10 molar ratio) with increasing concentration of substrate (fluorescein-conjugated gelatin). The data was fit into Michaelis-Menten model and presented as line/scatter plots. Measurements were taken at least in triplicates. Data presented as mean ± standard error.

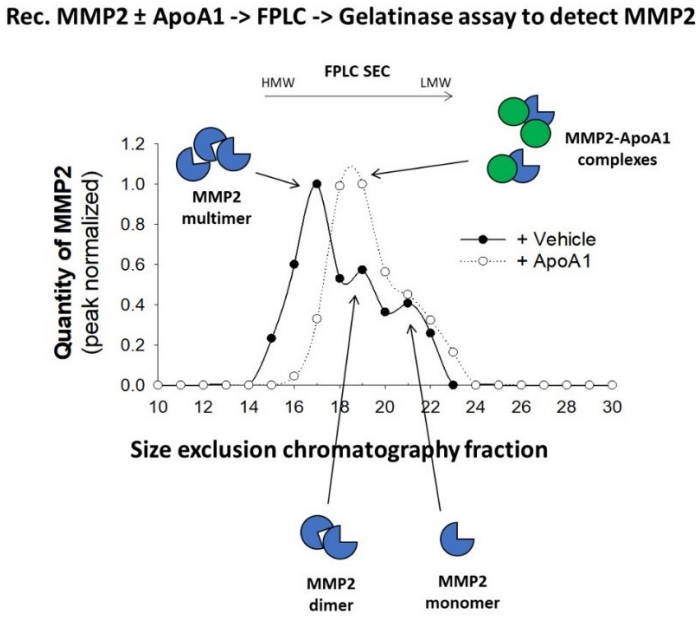

Figure 4.18: Size exclusion chromatography trace of MMP2 with vehicle or ApoA1.

The protein mixtures were applied on a Superdex 200 increase 5/150 GL column operated by an AKTA purifier. The column was pre-equilibrated with a buffer containing Tris pH7.5, 100 mM NaCl, 3 mM CaCl2.

4.3.5 ApoA1 interacts with the catalytic and hemopexin-like domains of MMP2

To determine which MMP2 domains are involved in the interaction with ApoA1/HDL, we used truncated constructs of the MMP2 catalytic and PEX domains. The proteolytic activity of the MMP2 catalytic domain (which excludes PEX) was increased both by HDL and by ApoA1 (**Figure 4.19A**). We compared the effect of ApoA1 on the activity of either the catalytic domain or intact MMP2 (a construct containing both the catalytic and PEX domains). ApoA1 increased the activity of intact MMP2 (by >120%) and that of the catalytic domain (by ~50%) (**Figure 4.19B**). MST analysis revealed that the interaction of ApoA1 with the Fib-PEX_6His construct (the PEX domain along with the partial fibronectin-like domain) has a dissociation constant K_d of 134 nM (**Figure 4.19C**), which is greater than that of ApoA1 for intact MMP2 (K_d of 58.3 nM) (**Figure 4.19A**). Complementary visual interference color binding assays confirmed that ApoA1 (a ligand) can bind to the PEX domain (which is immobilized on the surface) (**Figure 4.19A**). We concluded that both the catalytic domain and the PEX domain may be involved in the direct binding of MMP2 to ApoA1, but ApoA1 has a greater affinity for the catalytic domain of MMP2.

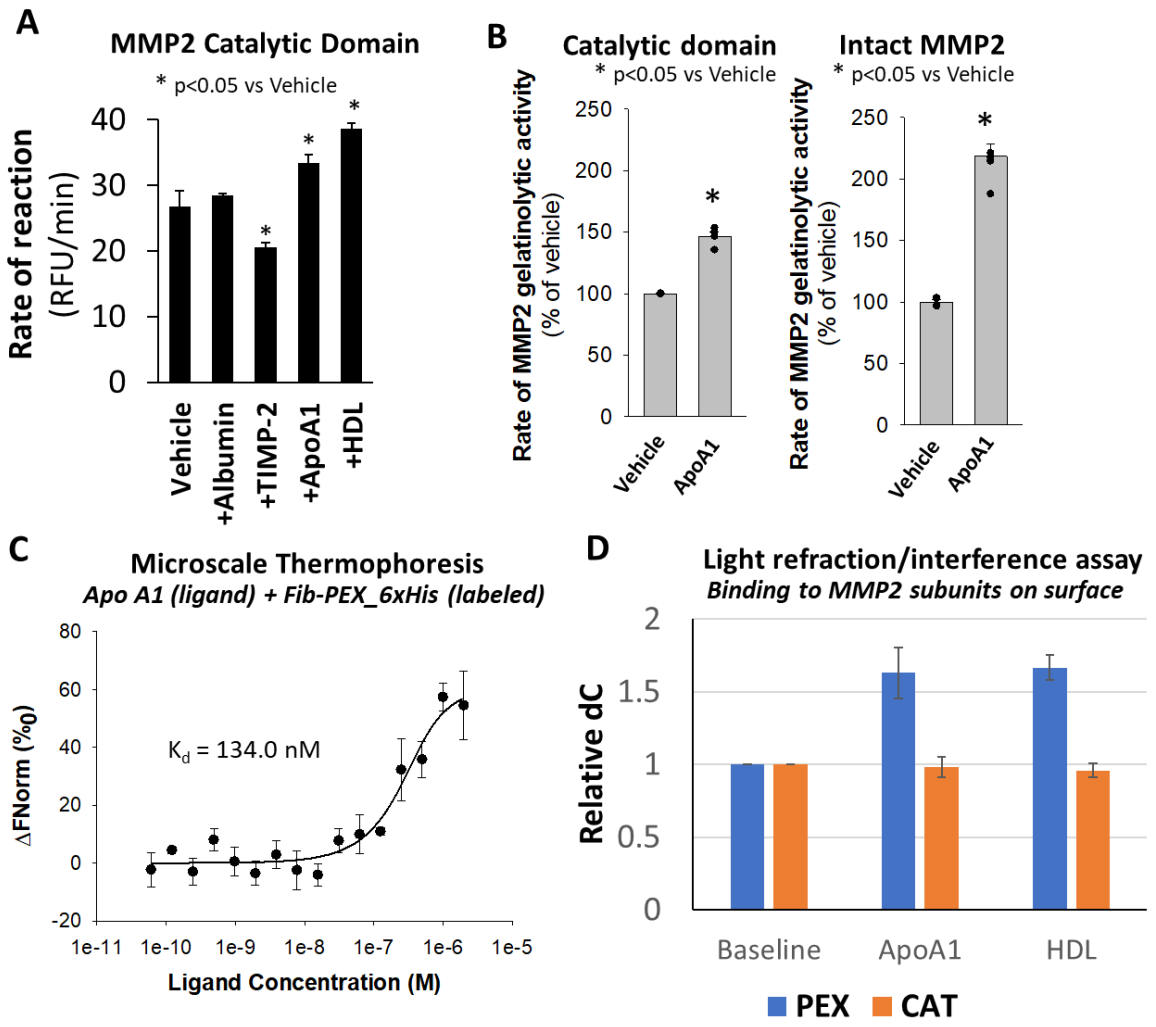

Figure 4.19: Analyses to determine the roles of PEX and the catalytic domain of MMP2 in its interaction with ApoA1.

(**A**) The proteolytic activity of a truncated construct of MMP2 containing the catalytic domain (with the PEX domain deleted) was measured in the presence of vehicle, albumin, TIMP2, ApoA1 or HDL at a 1:10 molar ratio. Measurements were taken in triplicate. The data are presented as the mean ± standard error. *p<0.05 vs vehicle (1-way ANOVA). (**B**) Comparison of the effect of ApoA1 on the proteolytic activity of the catalytic domain construct and intact MMP2. Measurements were taken in triplicate. The data are presented as the mean ± standard error. *p<0.05 vs vehicle (1-way ANOVA). (**C**) MST analyses of cells incubated with increasing concentrations of ApoA1 (0.9 nM to 30 µM) and 0.6 µM Fib-PEX_6xHis labeled with RED-tris-NTA dye. The experiments were performed in triplicate. (**D**) Light refraction/interference assay to test the binding of ApoA1 to two different constructs of truncated MMP2, the catalytic domain or the PEX domain. ApoA1 or HDL (ligands) at 100 µg/mL was added to each MMP2 construct (75 µg/mL) immobilized on the film and incubated for 30 minutes at 25°C, followed by color detection (see "Supplementary Methods"). The experiments were performed in triplicate.

4.3.6 AlphaFold models predict that active MMP2 dimerization partially occludes the active site

ProMMP2 and active MMP2 form homodimers. The crystal structure of the proMMP2 homodimer (PDB 1EAK, unpublished) without the PEX domain in the presence of an 8-mer inhibitor peptide showed that dimerization occurs via one of the fibronectin-like repeats. One of the three fibronectin-like repeats of one proMMP2 protomer forms contact with one fibronectin-like repeat and a part of the catalytic domain of the second protomer (**Figure 4.20**). The superimposition of the structure of the proMMP2 monomer (PDB 1CK7) on the protomer of the proMMP2 dimer (without the PEX domain) indicated that there was no conformational change in the catalytic domain or fibronectin-like repeats. The absence of the PEX domain did not affect the overall structure of each protomer (**Figure 4.20A**). The propeptide did not affect dimerization but occluded the catalytic zinc ion. The interaction interface consisted of hydrogen bonds and salt bridges contributed by residues from one fibronectin-like repeat and a few residues lining the active site (**Figure 4.20B).**

We found that active MMP2 forms complexes with itself, suggesting that these complexes could mediate MMP2 autolysis. In the absence of an experimental structure of the active MMP2 dimeric complex, we used AlphaFold2(*215-218*) to generate a dimer model (**Figure 4.20C-E**). In this MMP2 homodimer, the catalytic domain of one protomer interacts with the third fibronectin-like repeat, which precedes the PEX domain (**Figure 4.20C-D**). The interaction interface for the homodimer (**Figure 4.20E**) is maintained via hydrogen bonding networks between the following residues in the fibronectin-like repeat and the catalytic domain: Glu^{177}, Asp^{180}, Gly^{181}, Tyr^{182}, Gln^{298}, Asn^{343}, Gly^{367}, Tyr^{381} and Arg^{385}. This active MMP2 homodimer adopts a conformation similar to the crystal structure of the proMMP2 dimer without PEX (PDB: 1EAK), where the

active site is occluded, thus limiting substrate accessibility to the catalytic zinc ion (**Figure 4.20, Figure 4.21**).

4.3.7 Alphafold modeling of the ApoA1-MMP2 complex

Human ApoA1 is a 243-amino-acid amphipathic α-helical protein that serves as a scaffold that can pack lipids (primarily cholesterol and phospholipids), resulting in the formation of HDL particles. Currently, there is no high-resolution experimental structure for ApoA1 bound to lipids. The AlphaFold-generated ApoA1 model, when in complex with active MMP2, was primarily helical (**Figure 4.20F**). The neural network training algorithm PSSpred predicted a secondary structure of ApoA1 consisting of a long helix connected by loops (**Figure 4.22**)(*219*). The ApoA1 residues Met^{1}-Gly^{15} were predicted to form a helix followed by a coil that extends up to Trp^{32}. Upon binding to active MMP2, the N-terminal residues of ApoA1 adopt a loop followed by a beta sheet conformation that sits in the catalytic groove followed by a loop that is recognized by the fibronectin repeat (**Figure 4.20H**). At the interaction interface, the N-terminal region of ApoA1 is involved in hydrogen bond interactions with the catalytic domain of MMP2 and one fibronectin-like repeat (**Figure 4.20G**). The ApoA1 residue stretch Phe^{12} – Gln^{17} adopts an antiparallel beta sheet conformation with interchain hydrogen bonding interactions with the partner strand from the MMP2 catalytic domain (**Figure 4.20G**). Unlike Cys^{102} in proMMP2, which coordinates with the catalytic Zn, the interactors from ApoA1 (Leu^{11}-Ala^{18}) do not hinder the nucleophilic properties of this metal. Furthermore, the ApoA1 residues stretch Asp^{25} – Arg^{34} interacts with residues in the fibronectin-like repeats of MMP2. ApoA1 is released from cells after the cleavage of its signal peptide (Met^{1}-Ala^{18}) followed by subsequent cleavage of its propeptide (Arg^{19}-Gln^{24}), giving rise to mature ApoA1, which comprises 95% of all ApoA1 in the blood(*220*).

To investigate the specificity of the interaction of ApoA1 residues with MMP2, we performed *in silico* truncation studies in which two truncated ApoA1 constructs were generated via deletion of the first twenty or thirty residues (ApoA1Δ20 and ApoA1Δ30). ApoA1Δ20 did not contain the residue stretch Phe^{12} – Gln^{17}, which adopts an antiparallel beta sheet conformation in full-length ApoA1 while traversing through the catalytic groove of active MMP2 (**Figure 4.20H**). As expected, ApoA1Δ20 did not enter the same groove as the wild-type ApoA1, suggesting that the catalytic cavity of MMP2 interacts with ApoA1. The region at which ApoA1 interacts with the fibronectin-like repeat of MMP2 was intact in ApoA1Δ20, as observed in the full-length ApoA1 (**Figure 4.20I**). ApoA1Δ30 interacted neither with the catalytic groove nor with the fibronectin repeat of MMP2 (**Figure 4.20J**). ApoA1Δ30 may interact with MMP2 via the groove between the PEX domain and the catalytic domain. In this interaction, the helical structure of ApoA1Δ30 is retained, and no change in conformation from helix to loop is observed (**Figure 4.20J**).

Interestingly, ApoA1 interacts at a completely different site when modeled with proMMP2, where the active site is occluded by the propeptide (**Supplementary Figure 4.23**). The interaction interface is composed of fewer hydrogen bonds than the interaction interface of the ApoA1-active MMP2 complex, suggesting that the latter may be more energetically favorable than the ApoA1-proMMP2 complex. Direct binding MST and AI-based AlphaFold prediction interactions were performed in the absence of lipids. Thus, these findings may explain our *in vitro* data. ApoA1 adopts various conformations in the presence of lipids(*221*). Experimental cryo-EM structures are necessary to decipher the ApoA1–MMP2 interaction in the presence of lipids from a cellular perspective.

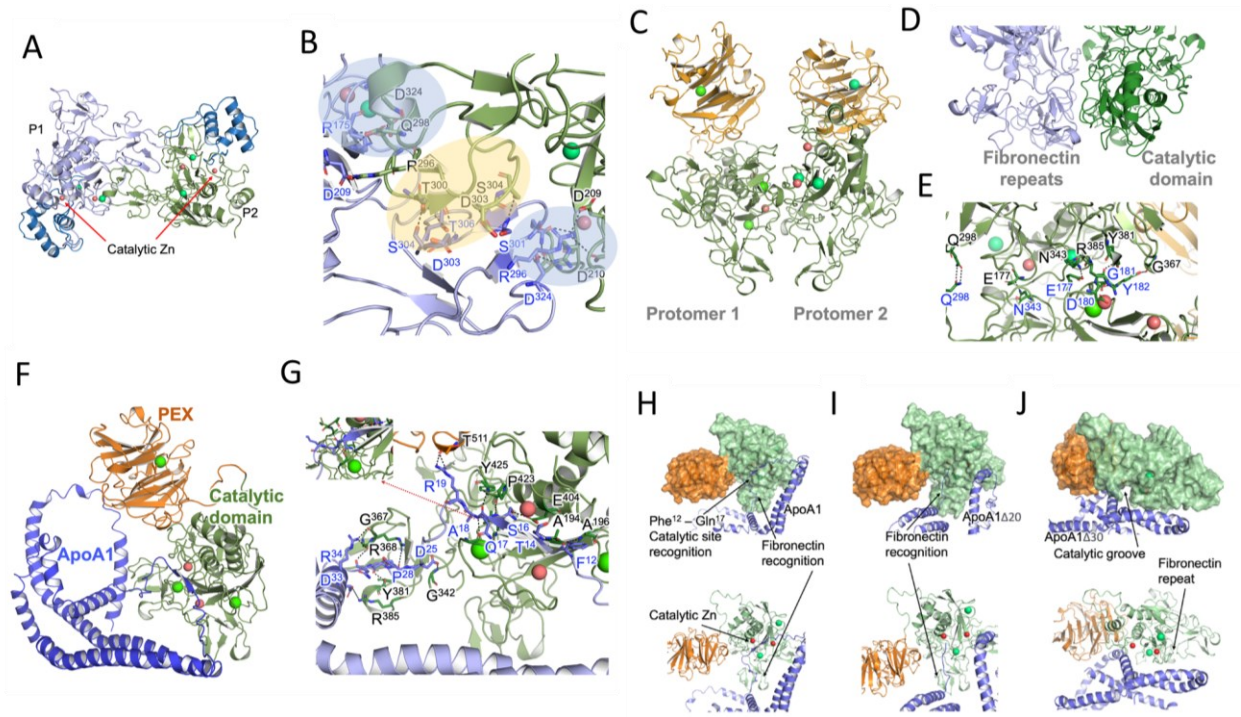

Figure 4.20: **The structure of the MMP2–ApoA1 complex modeled using AlphaFold**.

(**A**) ProMMP2 homodimerizes via its fibronectin repeat. Catalytic zinc is shown as a reference. The zinc ions (salmon red), calcium ions (lime green), the propeptide (blue) and the catalytic domain (smudge green) are shown. The two protomers (P1 and P2) are shown in light blue and green, respectively. (**B**) Interaction interface when proMMP2 molecules dimerize. Some of the interactions are presented. The interaction between fibronectin-like repeats is demarcated with yellow shading, and the interaction between fibronectin-like repeats and the catalytic domain is marked with light blue shading. (**C**) The active MMP2 homodimer model predicted by AlphaFold. (**D**) The fibronectin-like repeats of one protomer (light blue) contact the catalytic domain of the second protomer (white, green). (**E**) Some of the interface residues that form contacts between the two protomers are shown. Interacting residues from one protomer are shown in green, and those from the other are shown in blue font. The bonding atoms are connected by black dashed lines. (**F**) Overall structure of the MMP2–ApoA1 complex. (**G**) Interaction interface showing the residues of ApoA1 (blue font) interacting with active MMP2 (black font). Interacting residues are shown in stick representation. The bonding atoms are connected by black dashed lines. The inset shows a zoomed view of the N-terminus of ApoA1, which stabilizes the calcium coordinating loop. (**H-J**) The truncated ApoA1 proteins revealed the specificity of these proteins for interacting with active MMP2. The surface (top panel) and cartoon (bottom panel) representations of wild-type (WT) ApoA1, active MMP2 (**H**); ApoA1Δ20, active MMP2 (**I**); and ApoA1Δ30, active MMP2 (**J**) are shown. ApoA1Δ30 does not interact with the catalytic cavity of MMP2, which is otherwise observed in full-length ApoA1.

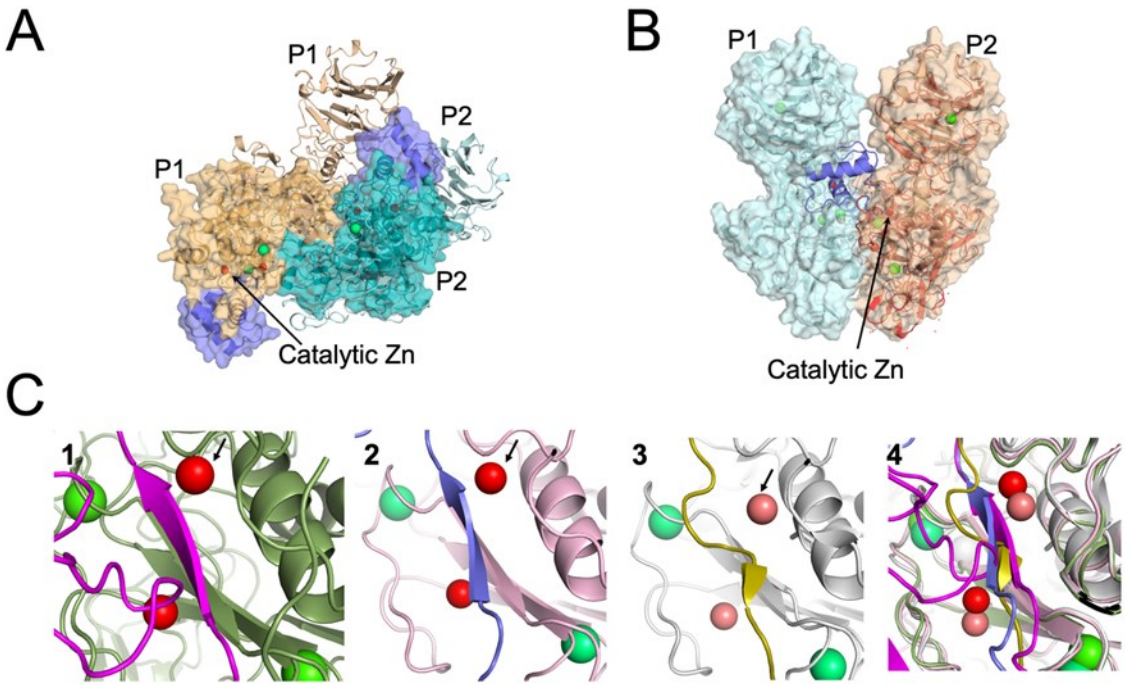

Figure 4.21: Overall structural analysis of Alphafold models.

(**A**) Overlay of crystal structure of proMMP2 dimer (PDB: 1EAK) without PEX domain (surface representation) on Alphafold-generated active MMP2 dimer with PEX domain (cartoon representation). Propetide is shown in slate blue. Protomer (P) from both complexes are marked. Zinc and calcium ions are shown in red and lime green respectively.
(**B**) AlphaFold generated model of active homodimer can partially accommodate propeptide. Active MMP2 homodimer are shown in surface representation. The crystal structure of proMMP2 (PDB: 1CK7) in red was overlayed on the P2 protomer of the dimer to verify the positioning of the propeptide (blue).
(**C**) Interaction interface of catalytic site of MMP2 for TIMP2 (pink), ApoA1 (blue), APPIP inhibitor peptide (yellow) shown in insets 1, 2 and 3 respectively. Overlay of all structures of MMP2 Position of catalytic zinc is pointed with black arrow. Calcium ions are shown in lime green.
Our analysis suggests that MMP2 homodimer in the presence of PEX domain may adopt similar conformation in the presence or absence of the propeptide occluding the active site and limiting the substrate accessibility which could lead to reduced activity.

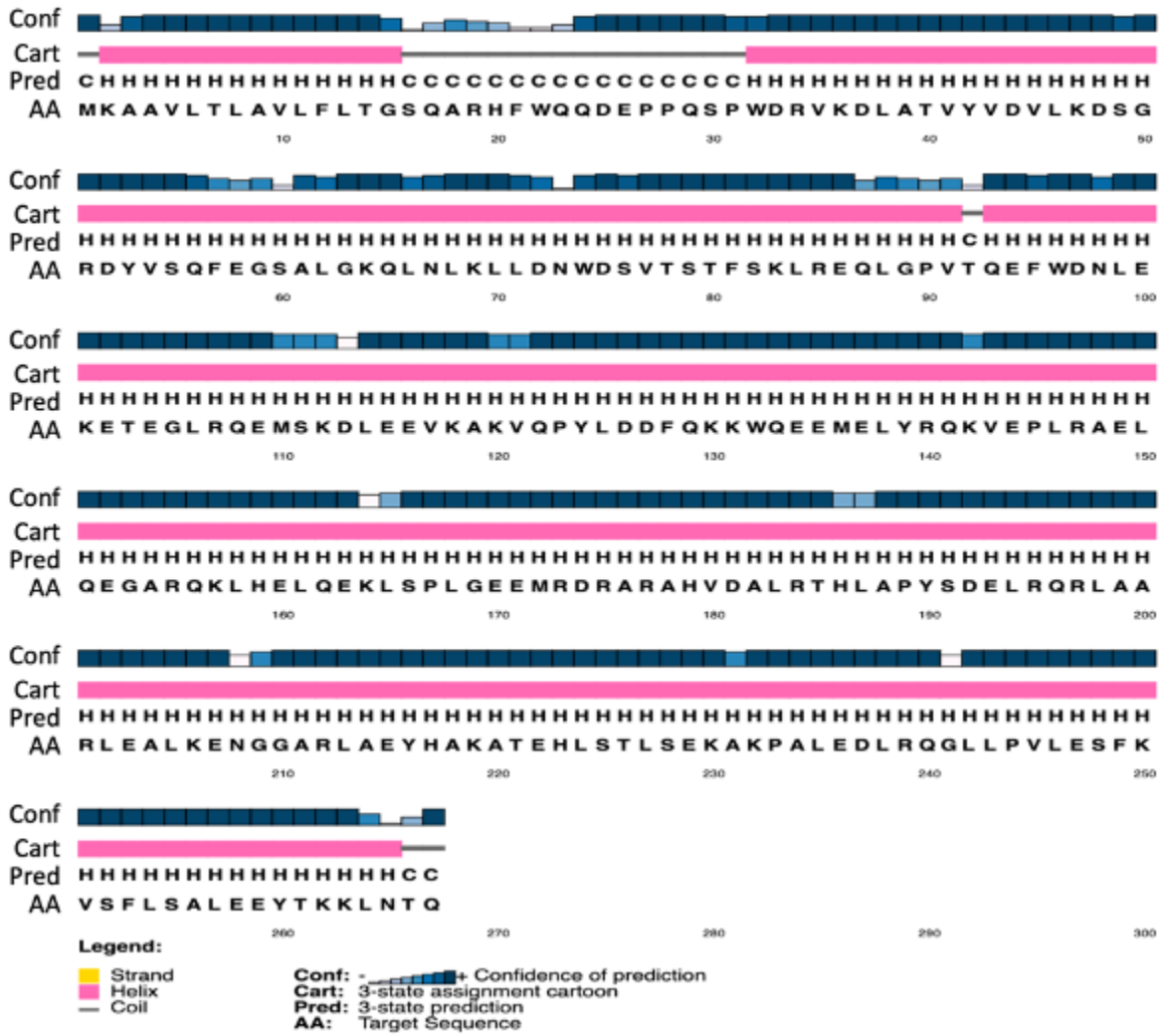

Figure 4.22: Secondary structure prediction of human ApoA1 as an output of PSSpred.

The amino acid sequence (AA), confidence score (conf) and prediction of helix (H) and coil (C) are shown.

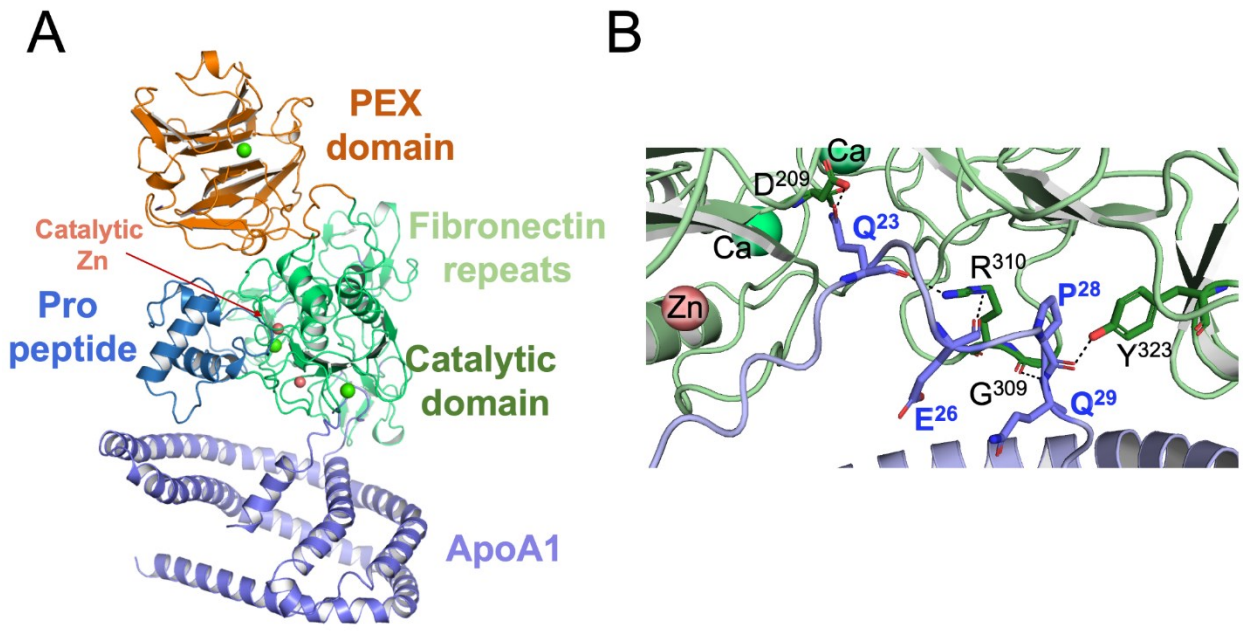

Figure 4.23: Interaction of proMMP2 with ApoA1.

A. Structure of the complex modeled using AlphaFold; **B.** Interaction interface of the two partners. Catalytic zinc and all domains are color coded. ApoA1 interacts with proMMP2 at a distinctly different site compared to that observed with active MMP2.

4.4 Discussion

The molecular interactome of matrix metalloproteinases (MMPs) in the blood circulation has not been elucidated. Consequently, it remains unclear whether MMPs circulate free or bound to endogenous inhibitors or proteins found in the blood whose large abundance makes them putative interactors that may influence the activity potential of MMPs in the blood. We report a hitherto unknown function of ApoA1: it can enable the transport, regulation and redistribution of MMP2—the most abundant MMP in the human blood circulation—from MMP2 synthesis sites to distal target organs. Through curiosity-driven studies, we discovered that ApoA1 has high affinity for the catalytic groove and fibronectin-like repeats of matrix metalloproteinase 2 (MMP2), the most abundant MMP in human blood. In healthy humans and ApoA1-expressing mice, we observed that MMP2 is associated with ApoA1 in HDL. We confirmed the

ApoA1/MMP2 interactions using multiple orthogonal interaction proteomics assays. Strikingly, we found that Apoa1 can allosterically increase the proteolytic activity of MMP2—an effect not observed in ApoA1-deficient plasma from ApoA1 KO mice. This finding was not predictable, as MMP2 was not previously known to be an allosteric enzyme. Using a high-confidence artificial intelligence (AlfaFold)-based structural model of the ApoA1/MMP2 complex, we propose a mechanism that can explain how ApoA1 binds and allosterically regulates MMP2 in the blood. Importantly, MMP2 circulates in the blood at nanomolar concentrations, as determined and utilized in the present study. ApoA1 is present in a large molar excess (>5000-fold) compared to that of MMP2. The *in vitro* studies presented here were all conducted at concentrations of apolipoproteins below physiological levels; the physiological concentration of ApoA1 is 40-70-fold greater than the highest concentration tested here. Thus, our reported interactions between MMP2 and ApoA1 are likely favorable *in vivo*, as evidenced by our studies with two different (mice and humans).

By combining AlphaFold structural modeling with studies of MMP2–ApoA1 interaction kinetics and biochemical fractionation of MMP2–ApoA1 complexes, we further revealed that MMP2 can form previously unknown homomultimeric complexes, which can increase susceptibility to autolysis. Our data suggest a theoretical model of allosteric MMP2 regulation by ApoA1. Accordingly, interaction with ApoA1 inhibits MMP2 autolysis through masking autolysis sites and allosterically increases MMP2 proteolytic activity through disrupting MMP2 homomultimers and exposing masked active sites. Notably, MMP2 circulates in the plasma mostly as proMMP2 at nanomolar concentrations(*1, 18*). Our structural modeling predicts that the affinity of ApoA1 for proMMP2 is weaker than that for active MMP2 (itself a minor component in the blood circulation). Therefore, lipid-free ApoA1 may be linked to MMP2 at

sites with high MMP2 concentrations, such as sites of high MMP2 synthesis and secretion. The high affinity interaction between ApoA1 and MMP2 is reversible in nature, suggesting that ApoA1/HDL scavenges MMP2 away from its sites of synthesis, transports it in the blood and unloads it at distal target organs; i.e., ApoA1 may serve as a vehicle for inter-organ communication via MMP2.

4.5 Materials and Methods

4.5.1 Study cohort

Human plasma: Plasma samples of six healthy adult males aged 25-35 were acquired from the Canadian BioSample Repository (CBSR), University of Alberta, Edmonton, AB, Canada. An additional plasma sample was collected from a healthy adult male aged 29 with informed consent.

Mouse plasma: Plasma from a total of fifteen different WT male mice aged 7-15 weeks (CBL57/B6) and six ApoA1 KO male mice aged 7-8 weeks were used in this study. The plasma samples were purchased from The Jackson Laboratory (Maine, US).

4.5.2 Materials:

1. Human ApoA1 6x_His Tag (Cat# AP1-H5225, Acrobiosystems, USA)
2. Apolipoprotein A1 (Cat# 178452-500UG, Sigma-Aldrich, USA)
3. Recombinant Human MMP2 6x_His Tag (Cat# NBP2-53037-50ug, Novus Biologicals, USA)
4. DQ Gelatin Fluorescein Conjugate (Cat# D12054, Thermofisher Scientific, USA)
5. High Density Lipoproteins, Human Plasma (Cat# 437641-10MG, Sigma-Aldrich, USA)
6. BS3 (bis(sulfosuccinimidyl)suberate) (Cat# A39266, Thermofisher Scientific, USA)
7. TIMP2 (Cat# SRP3174-10UG, Sigma-Aldrich, USA)

8. MMP2 active (Cat# SRP3118-10UG, Sigma-Aldrich, USA)
9. Apolipoprotein A2 (Cat# SRP6300-500UG, Sigma-Aldrich, USA)
10. Apolipoprotein E (Cat# ab280330, Abcam, UK)
11. MMP2 (catalytic domain) (Cat# BML-SE237-0010, Enzo life sciences, USA)
12. α-2-macroglobulin (Cat# SRP6314-1MG, Sigma-Aldrich, USA)
13. MMP2 Polyclonal Antibody (Cat# 10373-2-AP, Thermofisher Scientific, USA)
14. Fib-PEX Lys 359-Cys 660 (Cat# PDEH100254, ElabScience, USA)
15. MMP2 PEX domain (Cat# G04MP02H, GiottoBiotech, Italy)
16. ApoA1 antibody (Cat# Ab7614, Abcam, UK)
17. ApoE antibody (Cat# ab183597, Abcam, UK)
18. Cholesterol-SL assay (Cat# 234-60, Sekisui, Japan)
19. Bovine Serum Albumin (Cat# A2153, Sigma-Aldrich, USA)
20. Human Serum Albumin (Cat# A8763, Sigma-Aldrich, USA)
21. 1X Phospohate saline buffer (PBS) (Cat# 10010023, Thermofisher Scientific, USA)
22. Thin film for visual interference colour assay (Cat# STA-0023, Pavonis Diagnostics, Canada)

4.5.3 Fractionation of plasma by fast protein liquid chromatography (FPLC)

Fractionations were performed at the University of Alberta Faculty of Medicine & Dentistry Lipidomics Core (RRID: SCR_019176). 100 μL of EDTA-treated plasma was injected by autosampler into an Agilent 1200 high performance liquid chromatography instrument equipped with a Superose 6 Increase 10/300 gel-filtration FPLC column (Cytiva Life Sciences), which separates the intact lipoproteins by size. Separation was performed isocratically at 400 μL/min

using 150 mM NaCl with 3 mM NaN 3 as the mobile phase. To maintain the same flow rate as cholesterol or triglyceride profiling, pure deionized water was also pumped into the post-column stream at a rate of 200 µL /min. Effluent was monitored in real-time at 280 nm and the data collected and analyzed using Agilent Chemstation software. 2-minute fractions were collected and stored at 4 °C within 20 minutes.

4.5.4 Size exclusion chromatography of MMP2 complexes with ApoA1

Active recombinant MMP2 (Cat# SRP3118-10UG, Sigma-Aldrich, USA), ApoA1 (Cat# 178452-500UG, Sigma-Aldrich, USA) or their mixture (MMP2:ApoA1 = 1:10 molar ratio) was applied on a Superdex 200 increase 5/150 GL column operated by an AKTA purifier. The column was preequilibrated with a buffer containing Tris pH 7.5, 100 mM NaCl, 3 mM $CaCl_2$. Fractions were collected at 2-minute intervals and were analyzed by gelatin zymography (to detect MMP2) or SDS-PAGE/WB to detect ApoA1.

4.5.5 Microscale thermophoresis (MST) to study MMP2-ApoA1 interaction

For the MST experiments, a concentration series of MMP2 (Cat# SRP3118-10UG, Sigma-Aldrich, USA) was prepared using a 1:1 serial dilution in buffer supplemented with 20 mM Hepes (pH 7.5), 50 mM NaCl, 3 mM $CaCl_2$, and 0.05% Tween 20. The range of MMP2 concentration was from 4 µM to a final 1.95 nM, over 11 serial diluted Monolith NT.115 premium capillaries (NanoTemper) with 10 µL samples. The ApoA1 (Cat# AP1-H5225, Acrobiosystems, USA) was labeled using His-tag labeling kit RED-tris-NTA 2nd generation. The interaction for MST experiments was initiated by the addition of 10 µL of 0.6 µM His tag – labeled ApoA1. Control experiments to identify the

role of calcium, similar experiments were carried out with dilution buffer without calcium. The MMP2 concentration range used for these control experiments was 30 μM to 0.9 nM. The measurements were performed on a Monolith NT.115 (NanoTemper) using standard capillaries at 25 °C with 90% Excitation power, high MST power. Data were analyzed by MO. Control and MO. Affinity software (NanoTemper). The experiments were performed in triplicate.

4.5.6 Visual interference colour assay to study MMP2-ApoA1 interaction

Protein deposition onto anodized alumina surface: Lyophilized MMP2, MMP2 Hemopexin-like domain or MMP2 catalytic domain were first reconstituted in deionized water and then diluted to the indicated concentrations. Typically, 18-μL drops of protein solution at varying concentrations were deposited onto 7 mm diameter circles on the surface of the thin films (Cat# STA-0023, Pavonis Diagnostics, CANADA) and incubated under 100% relative humidity at 4ºC overnight to prevent autolysis. The slide was rinsed thoroughly with deionized water. MMP2 antibody or ApoA1 were diluted in deionized water as indicated and binding to their targets was analyzed by incubation under 100% relative humidity at room temperature for 30 minutes.

Color detection: The detection of binding was photographed with the use of a polarizing film to eliminate p-polarized light off the device surface and viewed at an incidence angle of 75° to generate the strongest color contrast by matching s-polarized light reflection intensities off the alumina and underlying surfaces. The red, green, and blue (RGB) coordinate system was used to quantitatively define the visible colors. The color difference or distance (dC) was calculated according to the formula:

$\text{distance}^2=(R2-R1)^2+(G2-G1)^2+(B2-B1)^2$.

4.5.7 Detection and quantitation of MMP2 protein amounts and activity

MMP2 protein and/or activity were detected and quantitated using western immunoblotting, in-gel gelatin zymography assay, in-solution gelatinase assay (fluorescein-conjugated gelatin as substrate, Cat# D12054, Thermofisher Scientific, USA) and multiplex protein detection assays following protocols previously described by us(*18, 222*). MMP2 lysis bands in zymograms were quantitated by densitometry scanning using the ImageJ software (NIH, USA).

4.5.8 Detection and quantitation of Apolipoproteins

ApoA1 and ApoE in FPLC/SEC fractions of mouse or human plasma were detected by western immunoblotting following electrophoretic separation by SDS-PAGE using their respective antibodies: ApoA1 antibody (Cat# Ab7614, Abcam, UK) and ApoE antibody (Cat# Ab183597, Abcam, UK). Immunoblot protein bands were quantitated by densitometry scanning using the ImageJ software (NIH, USA).

4.5.9 Quantitation of cholesterol in FPLC/SEC fractions

Total cholesterol in SEC fractions were measured using a cholesterol-SL assay (Cat# 234-60, Sekisui, Japan) following the manufacturer's instructions. Fractions were mixed with the cholesterol reagent at a 1:10 ratio (v/v) and incubated at 25°C for 20 minutes before reading absorbance at 505 nm.

4.5.10 2D BN-PAGE/Gelatin zymography to separate MMP2/HDL complex

Sample preparation: Recombinant active MMP2 (Cat# SRP3118-10UG, Sigma-Aldrich, USA) at a final concentration of 0.4 µM was added to increasing concentrations (0 µM, 0.4 µM, 4 µM, and 8 µM) of HDL (Cat# 437641-10MG, Sigma-Aldrich, USA) in separate tubes. The final volume was brought up to 20 µL with 1x enzyme buffer (0.05 M Tris-HCl (pH 7.4), 0.15 M NaCl, 0.013 M CaCl2, 0.003 NaN3). The samples were incubated at 25°C for 30 minutes. The loading buffer (75 mM 6-aminocaproic acid, 15 mM BisTris, 0.3% Coomassie blue G-250 (Cat# 35050, Serva, USA)) was then added to the samples before loading onto the gel.

Blue-Native PAGE: Our Blue-Native PAGE protocol was adapted from standard BN-PAGE protocols previously described by Wittig et al.(*223*) and Thangthaeng et al.(*224*). Gels were prepared with 4.7 mL gel buffer solution (500 mM 6-aminocaproic acid, 50 mM BisTris (pH 7.1)), 1.2 mL of 40% Acrylamide/bisacrylamide (crosslinking ratio: 29:1) (Cat# 161-0146, Bio-rad, USA), 45 µL 10% (w/v) ammonium persulfate, 3 µL TEMED (Cat# T9281-25ML, Sigma-Aldrich, USA). The anode buffer was composed of 50 mM BisTris (pH 7.1), and the cathode buffer was composed of 50 mM tricine, 15 mM BisTris (pH 7.1), 0.025% Coomassie blue G-250. Then the electrophoretic separation of the proteins/complexes was performed. The individual lanes were excised and placed on a 10% acrylamide gelatin zymography gel for a second dimensional separation and detection of MMP2 or on a 10% acrylamide SDS-PAGE followed by western immunoblot to detect HDL (by immunodetection of ApoA1).

4.5.11 Chemical cross-linking of MMP2 and its interactors

Active recombinant MMP2 (Cat# SRP3118-10UG, Sigma-Aldrich, USA) was pre-incubated with vehicle (1x PBS with 500 µM O-phenanthroline) or interactor proteins including ApoA1

(Cat# 178452-500UG, Sigma-Aldrich, USA), ApoA2 (Cat# SRP6300-500UG, Sigma-Aldrich, USA), ApoE (Cat# ab280330, Abcam, UK), Albumin (Cat# A8763, Sigma-Aldrich, USA), α-2-macroglobulin (Cat# SRP6314-1MG, Sigma-Aldrich, USA) or TIMP2 (Cat# SRP3174-10UG, Sigma-Aldrich, USA) at a 1:5 molar ratio (MMP2:interactor) for 60 minutes on ice followed by addition of freshly prepared 5 mM BS3 (bis(sulfosuccinimidyl)suberate) solution (in 1x PBS) and incubation at 25°C for 30 minutes. After the incubation, the reaction was quenched by adding 50 mM Tris-HCl (pH 7.4). The reaction mixtures were analyzed by gelatin zymography to detect MMP2 and MMP2 complexes.

4.5.12 *In silico* Structural Modeling

The Artificial Intelligence (AI) system, AlphaFold, developed by DeepMind, was used to model the structures of active MMP2 homodimer, proMMP2-Timp2 heterodimer, active MMP2-Timp2 heterodimer, MMP2-ApoA1 heterodimer and FibPEX-ApoA1 heterodimer. AlphaFold incorporates both physical and biological understandings of protein structure by integrating multi-sequence alignments into the framework of its deep learning algorithm. AlphaFold, has been ranked as more accurate than competing methods by the Critical Assessment of protein Structure Prediction (CASP) experiments(*215*). CASP is a biennially held gold standard assessment for the accuracy of structure prediction(*216*). AlphaFold2-multimer(*217*) was executed within a Colab notebook v1.5.3(*215, 218*), leveraging Amber99sb force fields(*225*), to meticulously ensure the peptide bond geometry's accuracy after prediction. This resulted in the complex adopting a more relaxed structural configuration. Each run used the multimer_V2 weights, 48 cycles and yielded 5 models. The AlphaFold2 used MMseq2 algorithm. The plots showing the sequence coverage information used in modeling can be found in the supplemental section. The structures were analyzed using PyMOL v.2.5.4 (Schrödinger, LLC.).

Alphafold assessed the intra-domain confidence or the quality of protein as a per residue pLDDT score. Models with scores > 90 are high confidence. Models with scores < 70 are low confidence. The predicted template modeling score (pTM) represent the global confidence score and depends on the quality of template used for modeling. The pTM score >0.5 is considered high enough to make inference.

4.5.13 Statistical Analyses

SigmaPlot 14.0 (Systat Software, San Jose, CA) was used to conduct statistical analysis on the results and plot graphs. We performed one way ANOVA, where appropriate (as indicated in the figure legends), to determine statistical significance in the difference when comparing two conditions. For all experiments, the n value presented in the figure legends refer to distinct and independent sample measurements. Data are presented as mean ± standard error of mean.

5 Chapter 5: Conclusions

5.1 New findings and their implications

In the research presented in chapter 2, we advanced the phenotypic characterization of MMP2 deficiency by identifying molecular traits that are similarly dysregulated in MMP2 deficient patients and *Mmp2*$^{-/-}$ mice which are the standard study model for the rare multisystem pediatric syndrome elicited by MMP2 deficiency in humans. Specifically, we identified cytokines and hormones previously unknown to be commonly dysregulated in MMP2-deficient mice and children; the cytokines dysregulated in MMP2 deficiency include known inducers of osteoporosis. Our data suggests that glucocorticoid-induced osteoporosis may be a specific phenotype characteristic of MMP2 deficiency.

In the research presented in chapter 3, we describe the identification of FBG as an endogenous interactor and inhibitor of MMP2 in the blood. Our data indicate that a pathological elevation of circulating FBG could limit MMP2 binding to and cleavage of important physiological substrates, which may contribute to cause a state of non-genetic MMP2 activity insufficiency with as-yet poorly understood pathophysiology. FBG expression is elevated during inflammation due to infections, arthritis, atherosclerosis, heart failure, and kidney failure, as well as being mechanistically implicated in thrombosis(*32, 226, 227*). FBG and its derivative peptides also function as chemo-attractants for leukocytes (*226, 228*). MMPs, including MMP2, are well known modulators of immune cell chemoattraction(*1, 2, 56*). However, the interplay between FBG and MMPs in the settings of the above inflammatory conditions remains poorly understood. MMP2 deficiency causes inflammation amid skeletal and cardiac disorders(*2, 57, 95*), suggesting that prolonged inhibition of MMP2 activity by FBG, and perhaps also by other acute phase

reactants (as is the case of alpha-2 macroglobulin(*165*)) or TIMPs, may be pro-inflammatory as well.

In chapter 4, we report that apolipoprotein A1 – the major protein component of HDL – binds MMP2 and allosterically increases its proteolytic activity. We also observed that, in addition to ApoA1, MMP2 may interact with albumin, ApoA2 and ApoE, and several MMPs and TIMPs appeared to form high-molecular-mass complexes in the blood. Hence, we propose the use of the new term "transporter and regulator of the activity potential" (TRAP) of MMPs to define multiprotein complexes that transport MMPs in the blood and may additionally cause MMP activity to increase, decrease or remain unchanged—*without* immediate biological effects—while simultaneously enabling secreted MMPs in the blood to reach distal target organs and participate in interorgan communication. Current knowledge supports this proposed TRAP hypothesis. In addition to affecting ApoA1/HDL, the network of blood-borne proteins that governs MMP transport and regulation currently includes at least three endogenous inhibitors: TIMPs, alpha-2 macroglobulin and fibrinogen (*18*).

In normal physiology, TRAP complexes might sequester and redistribute MMPs from sites of normal synthesis to distal target organs, effectively enabling homeostatic interorgan communication via MMPs. In disease conditions associated with high MMP synthesis foci (such as sites of atherosclerotic plaques, myocardial ischemia or cancer tumors), TRAP complexes may redistribute MMPs and hence promote the pathogenesis of MMP-mediated comorbidities. In atherosclerosis, MMPs are secreted in large quantities at atherosclerotic plaques, where the cleavage of extracellular proteins (e.g., collagens) promotes plaque rupture(*13, 58*). Future research should establish whether sequestration of MMPs (such as MMP2) by specific TRAP complexes (such as ApoA1/HDL) can prevent plaque rupture—a potentially novel mechanism of

the anti-atherogenic effects of ApoA1 unrelated to the canonical reverse cholesterol transport mediated by ApoA1/HDL(*213*). Hence, considering the TRAP hypothesis can help clarify the complex relationships between apolipoprotein levels and cholesterol levels as a marker for the risk of acute myocardial infarction(*229, 230*). A similar argument can be made for TRAP complexes in other disease conditions associated with high MMP synthesis foci (such as sites of myocardial ischemia, joint inflammation in arthritis or cancer tumors).

Meanwhile, allosteric activation of MMP2 by ApoA1 can be beneficial through increasing the cleavage and inactivation of proinflammatory MMP2 substrates, such as monocyte chemoattractant protein 3 (MCP3/CCL7), to dampen inflammation or to decrease vascular smooth muscle cell proliferation(*231-233*). Allosteric activation of MMP2 by ApoA1 can be detrimental through promoting proinflammatory processes and vascular damage mediated by extracellular matrix-derived proinflammatory neoepitopes/peptides(*53, 232, 234*). The TRAPs of MMPs may serve to remove excess MMPs from the circulation. In the liver, HDL interacts with the scavenger receptor class B, type I (SR-B1, HDL receptor) on hepatocytes. SR-B1 selectively enables the uptake of cholesterol from HDL(*235*). Future research should determine whether the ApoA1/HDL/MMP2 complex interaction with SR-B1 can result in the release of Apoa1-bound MMP2, and if this release of MMP2 affects the extracellular matrix remodeling or inflammatory status in the liver. Alternatively, endocytosis into hepatic cells and subsequent lysosomal processing could serve to remove MMP2 that is delivered to the liver via ApoA1/HDL TRAP complexes.

Historically, MMP activity potential has been measured using metrics including MMP gene expression (quantitation of mRNA), MMP protein levels, ratios of MMPs to TIMPs (endogenous inhibitor) and ratios of quantity of active MMP to proMMP (zymogen). Our findings suggest that

these metrics do not accurately estimate the activity potential of MMPs. In the case of MMP2, we find that there are endogenous inhibitors besides TIMPs (i.e., fibrinogen) as well as allosteric activators (ApoA1/HDL) that affect MMP2 activity. Therefore, at least in the case of MMP2, the use of these metrics to suggest elevation or downregulation of MMP2 in disease conditions should be made with caution.

We speculate that ApoA1 sequesters MMP2 in the blood circulation and redistributes it to organs, such as the liver or kidneys where MMP2 may be cleared from the circulation. In addition to ApoA1/HDL, a network of bloodborne proteins and complexes thereof may contribute to interorgan communication via MMPs (proposed "TRAP of MMPs" hypothesis). Disease-specific TRAPs of MMPs may govern MMP activity in the circulation and interorgan communication via MMPs and could serve as therapeutic targets or biomarkers in pathologies associated with alterations in the blood levels of either apolipoproteins or MMPs.

In conclusion, the findings presented in this thesis indicate that a network of blood-borne proteins, including fibrinogen and ApoA1/HDL, may regulate the activity potential of MMP2 in the circulation. Blood-borne proteins and complexes, including fibrinogen and ApoA1/HDL, act as a TRAP of MMP2 and may cause MMP2 activity to increase, decrease or remain unchanged while enabling secreted MMP2 in the blood to reach distal target organs.

5.2 Limitations

Chapter 2 described new molecular phenotypic characteristics of MMP2 deficiency. The rarity of genetic MMP2 deficiency resulted in limited access to patient samples which made it impossible to have a large number of different patient samples with controlled parameters (age, sex, etc) to allow for more rigorous statistical analyses. Additionally, MONA patients received treatment

with pharmacological drugs (such as bisphosphonates to reduce skeletal pain and increase bone mineral density which may have unpredictable side effects and affect the upregulation or downregulation of the serum factors analyzed. Hence, we adopted a limited approach where we selected an eight-year-old male MMP2 deficient MONA patient as a representative case for human MMP2 deficiency / MONA in the initial serum screening analyses.

In chapter 3, while we observed clear inhibition of MMP2 activity by fibrinogen at physiological concentrations *in vitro*, a demonstration of similar inhibition *in vivo* is required to reinforce our findings. The complexity of different factors (such as the presence of endogenous inhibitors and allosteric activators) that influence MMP2 activity *in vivo* makes it difficult to test the isolated effects of fibrinogen on MMP2 *in vivo*.

In chapter 4, the data demonstrates the allosteric effects of ApoA1 in increasing MMP2 activity and their association in human and mouse plasma. A limitation of the work is the composition of the ApoA1/HDL-MMP2 complex in vivo has not been characterized to say whether other proteins that influence MMP2 (such as TIMPs) are part of these complexes. There is also no demonstration of inter-organ communication via MMP/ApoA1 complex- though it is a plausible consequence of the research. Structural basis of ApoA1-MMP2 interaction and activation as predicted by the alphafold data lacks experimental verification (e.g., cryo-EM).

5.3 Future Directions

Ultimately, our findings present new prospects for future research to advance our understanding of the role of MMP2 in pathophysiology, potentially leading to identification of effective therapeutic interventions.

Chapter 2: While our observations associate increased circulating bioactive cortisol with MMP2 deficiency, further studies are necessary to elucidate the molecular mechanisms of this association and the specific consequences of elevated cortisol in the pathogenesis of MONA. The novel phenotypic traits of MMP2 deficiency identified in our research which are common to humans and mice merit being targeted in future fundamental research to explore their potential use as biomarkers or therapeutic targets.

Chapter 3: Fibrinogen, while stabilizing platelet aggregates, might also play an anti-aggregatory role in MMP2 mediated platelet activation by inhibiting MMP2 activity – a hypothesis worth investigating in future studies. Structural studies are necessary to elucidate the molecular basis of MMP2 inhibition which may help the development of specific synthetic inhibitors of MMP2 based on the inhibition mechanism of fibrinogen.

Chapter 4: In atherosclerosis, MMP2 is secreted in large quantities at atherosclerotic plaques, where the cleavage of extracellular proteins (e.g., collagens) promotes plaque rupture(*13, 58*). Future research should establish whether sequestration of MMPs (such as MMP2) by specific TRAP complexes (such as ApoA1/HDL) can prevent plaque rupture—a potentially novel mechanism of the anti-atherogenic effects of ApoA1 unrelated to the canonical reverse cholesterol transport mediated by ApoA1/HDL(*213*). Hence, considering the TRAP hypothesis can help clarify the complex relationships between apolipoprotein levels and cholesterol levels as a marker for the risk of acute myocardial infarction(*229, 230*).

Experimental cryo-EM structures are necessary to decipher the ApoA1–MMP2 interaction in the presence of lipids to reveal the observed allosteric activation mechanism which may lead to the development of synthetic MMP2 activator – potentially useful in the treatment of MMP2 deficiency.

6 Bibliography

1. W. C. Parks, C. L. Wilson, Y. S. Lopez-Boado, Matrix metalloproteinases as modulators of inflammation and innate immunity. *Nat Rev Immunol* **4**, 617-629 (2004).
2. C. Fernandez-Patron, Z. Kassiri, D. Leung, Modulation of Systemic Metabolism by MMP-2: From MMP-2 Deficiency in Mice to MMP-2 Deficiency in Patients. *Compr Physiol* **6**, 1935-1949 (2016).
3. K. Kessenbrock, V. Plaks, Z. Werb, Matrix metalloproteinases: regulators of the tumor microenvironment. *Cell* **141**, 52-67 (2010).
4. H. Nagase, R. Visse, G. Murphy, Structure and function of matrix metalloproteinases and TIMPs. *Cardiovasc Res* **69**, 562-573 (2006).
5. H. E. Van Wart, H. Birkedal-Hansen, The cysteine switch: a principle of regulation of metalloproteinase activity with potential applicability to the entire matrix metalloproteinase gene family. *Proc Natl Acad Sci U S A* **87**, 5578-5582 (1990).
6. N. Cui, M. Hu, R. A. Khalil, Biochemical and Biological Attributes of Matrix Metalloproteinases. *Prog Mol Biol Transl Sci* **147**, 1-73 (2017).
7. J. Liu, R. A. Khalil, Matrix Metalloproteinase Inhibitors as Investigational and Therapeutic Tools in Unrestrained Tissue Remodeling and Pathological Disorders. *Prog Mol Biol Transl Sci* **148**, 355-420 (2017).
8. H. Piccard, P. E. Van den Steen, G. Opdenakker, Hemopexin domains as multifunctional liganding modules in matrix metalloproteinases and other proteins. *J Leukoc Biol* **81**, 870-892 (2007).
9. R. Visse, H. Nagase, Matrix metalloproteinases and tissue inhibitors of metalloproteinases: structure, function, and biochemistry. *Circ Res* **92**, 827-839 (2003).
10. D. H. Lovett *et al.*, A novel intracellular isoform of matrix metalloproteinase-2 induced by oxidative stress activates innate immunity. *PLoS One* **7**, e34177 (2012).
11. E. Morgunova *et al.*, Structure of human pro-matrix metalloproteinase-2: activation mechanism revealed. *Science* **284**, 1667-1670 (1999).
12. L. Nissinen, V. M. Kahari, Matrix metalloproteinases in inflammation. *Biochim Biophys Acta* **1840**, 2571-2580 (2014).
13. A. C. Newby, Metalloproteinases and vulnerable atherosclerotic plaques. *Trends Cardiovasc Med* **17**, 253-258 (2007).
14. E. Hardy, C. Fernandez-Patron, Destroy to Rebuild: The Connection Between Bone Tissue Remodeling and Matrix Metalloproteinases. *Front Physiol* **11**, 47 (2020).

15. E. B. Springman, E. L. Angleton, H. Birkedal-Hansen, H. E. Van Wart, Multiple modes of activation of latent human fibroblast collagenase: evidence for the role of a Cys73 active-site zinc complex in latency and a "cysteine switch" mechanism for activation. *Proc Natl Acad Sci U S A* **87**, 364-368 (1990).
16. A. Y. Strongin *et al.*, Mechanism of cell surface activation of 72-kDa type IV collagenase. Isolation of the activated form of the membrane metalloprotease. *J Biol Chem* **270**, 5331-5338 (1995).
17. C. J. Morrison *et al.*, Cellular activation of MMP-2 (gelatinase A) by MT2-MMP occurs via a TIMP-2-independent pathway. *J Biol Chem* **276**, 47402-47410 (2001).
18. H. Sarker *et al.*, Identification of fibrinogen as a natural inhibitor of MMP-2. *Sci Rep* **9**, 4340 (2019).
19. K. Brew, D. Dinakarpandian, H. Nagase, Tissue inhibitors of metalloproteinases: evolution, structure and function. *Biochim Biophys Acta* **1477**, 267-283 (2000).
20. R. Khokha, A. Murthy, A. Weiss, Metalloproteinases and their natural inhibitors in inflammation and immunity. *Nat Rev Immunol* **13**, 649-665 (2013).
21. G. Murphy, Tissue inhibitors of metalloproteinases. *Genome Biol* **12**, 233 (2011).
22. A. A. Rehman, H. Ahsan, F. H. Khan, alpha-2-Macroglobulin: a physiological guardian. *J Cell Physiol* **228**, 1665-1675 (2013).
23. I. Tchetverikov *et al.*, Active MMPs captured by alpha 2 macroglobulin as a marker of disease activity in rheumatoid arthritis. *Clin Exp Rheumatol* **21**, 711-718 (2003).
24. L. Sottrup-Jensen, Alpha-macroglobulins: structure, shape, and mechanism of proteinase complex formation. *J Biol Chem* **264**, 11539-11542 (1989).
25. X. Serifova, E. Ugarte-Berzal, G. Opdenakker, J. Vandooren, Homotrimeric MMP-9 is an active hitchhiker on alpha-2-macroglobulin partially escaping protease inhibition and internalization through LRP-1. *Cell Mol Life Sci* **77**, 3013-3026 (2020).
26. D. K. Strickland *et al.*, Sequence identity between the alpha 2-macroglobulin receptor and low density lipoprotein receptor-related protein suggests that this molecule is a multifunctional receptor. *J Biol Chem* **265**, 17401-17404 (1990).
27. S. Higashi, K. Miyazaki, Identification of a region of beta-amyloid precursor protein essential for its gelatinase A inhibitory activity. *J Biol Chem* **278**, 14020-14028 (2003).
28. J. D. Mott *et al.*, Post-translational proteolytic processing of procollagen C-terminal proteinase enhancer releases a metalloproteinase inhibitor. *J Biol Chem* **275**, 1384-1390 (2000).
29. J. Oh *et al.*, The membrane-anchored MMP inhibitor RECK is a key regulator of extracellular matrix integrity and angiogenesis. *Cell* **107**, 789-800 (2001).

30. M. W. Mosesson, K. R. Siebenlist, D. A. Meh, The structure and biological features of fibrinogen and fibrin. *Ann N Y Acad Sci* **936**, 11-30 (2001).
31. P. Comeglio *et al.*, Blood clotting activation during normal pregnancy. *Thromb Res* **84**, 199-202 (1996).
32. J. L. Ebersole, D. Cappelli, Acute-phase reactants in infections and inflammatory diseases. *Periodontol 2000* **23**, 19-49 (2000).
33. G. Felsenfeld, A brief history of epigenetics. *Cold Spring Harb Perspect Biol* **6**, (2014).
34. J. Bednar *et al.*, Nucleosomes, linker DNA, and linker histone form a unique structural motif that directs the higher-order folding and compaction of chromatin. *Proc Natl Acad Sci U S A* **95**, 14173-14178 (1998).
35. L. Marino-Ramirez, M. G. Kann, B. A. Shoemaker, D. Landsman, Histone structure and nucleosome stability. *Expert Rev Proteomics* **2**, 719-729 (2005).
36. G. Egger, G. Liang, A. Aparicio, P. A. Jones, Epigenetics in human disease and prospects for epigenetic therapy. *Nature* **429**, 457-463 (2004).
37. K. D. Robertson, DNA methylation and chromatin - unraveling the tangled web. *Oncogene* **21**, 5361-5379 (2002).
38. T. Jenuwein, C. D. Allis, Translating the histone code. *Science* **293**, 1074-1080 (2001).
39. S. M. Kooistra, K. Helin, Molecular mechanisms and potential functions of histone demethylases. *Nat Rev Mol Cell Biol* **13**, 297-311 (2012).
40. R. C. Trievel, Structure and function of histone methyltransferases. *Crit Rev Eukaryot Gene Expr* **14**, 147-169 (2004).
41. J. K. Lam, M. Y. Chow, Y. Zhang, S. W. Leung, siRNA Versus miRNA as Therapeutics for Gene Silencing. *Mol Ther Nucleic Acids* **4**, e252 (2015).
42. J. Vandooren, P. E. Van den Steen, G. Opdenakker, Biochemistry and molecular biology of gelatinase B or matrix metalloproteinase-9 (MMP-9): the next decade. *Crit Rev Biochem Mol Biol* **48**, 222-272 (2013).
43. C. Yan, D. D. Boyd, Regulation of matrix metalloproteinase gene expression. *J Cell Physiol* **211**, 19-26 (2007).
44. A. V. Chernov, A. Y. Strongin, Epigenetic regulation of matrix metalloproteinases and their collagen substrates in cancer. *Biomol Concepts* **2**, 135-147 (2011).
45. H. Wang *et al.*, Genetic and epigenetic mechanisms combine to control MMP1 expression and its association with preterm premature rupture of membranes. *Hum Mol Genet* **17**, 1087-1096 (2008).

46. E. Chicoine *et al.*, Evidence for the role of promoter methylation in the regulation of MMP-9 gene expression. *Biochem Biophys Res Commun* **297**, 765-772 (2002).
47. J. Couillard, M. Demers, G. Lavoie, Y. St-Pierre, The role of DNA hypomethylation in the control of stromelysin gene expression. *Biochem Biophys Res Commun* **342**, 1233-1239 (2006).
48. S. L. Berger, Histone modifications in transcriptional regulation. *Curr Opin Genet Dev* **12**, 142-148 (2002).
49. P. Sudarsanam, F. Winston, The Swi/Snf family nucleosome-remodeling complexes and transcriptional control. *Trends Genet* **16**, 345-351 (2000).
50. C. Yan, H. Wang, Y. Toh, D. D. Boyd, Repression of 92-kDa type IV collagenase expression by MTA1 is mediated through direct interactions with the promoter via a mechanism, which is both dependent on and independent of histone deacetylation. *J Biol Chem* **278**, 2309-2316 (2003).
51. S. Chang *et al.*, Histone deacetylase 7 maintains vascular integrity by repressing matrix metalloproteinase 10. *Cell* **126**, 321-334 (2006).
52. D. A. Young *et al.*, Histone deacetylase inhibitors modulate metalloproteinase gene expression in chondrocytes and block cartilage resorption. *Arthritis Res Ther* **7**, R503-512 (2005).
53. S. C. A. de Jager, I. E. Hoefer, Beyond the matrix: MMP2 as critical regulator of inflammation-mediated vascular dysfunction. *Cardiovasc Res* **113**, 1705-1707 (2017).
54. X. Feng, J. M. McDonald, Disorders of bone remodeling. *Annu Rev Pathol* **6**, 121-145 (2011).
55. R. Hardy, M. S. Cooper, Bone loss in inflammatory disorders. *J Endocrinol* **201**, 309-320 (2009).
56. T. Klein, R. Bischoff, Physiology and pathophysiology of matrix metalloproteases. *Amino Acids* **41**, 271-290 (2011).
57. R. A. Mosig *et al.*, Loss of MMP-2 disrupts skeletal and craniofacial development and results in decreased bone mineralization, joint erosion and defects in osteoblast and osteoclast growth. *Hum Mol Genet* **16**, 1113-1123 (2007).
58. W. Olejarz, D. Lacheta, G. Kubiak-Tomaszewska, Matrix Metalloproteinases as Biomarkers of Atherosclerotic Plaque Instability. *Int J Mol Sci* **21**, (2020).
59. Q. Yu, I. Stamenkovic, Cell surface-localized matrix metalloproteinase-9 proteolytically activates TGF-beta and promotes tumor invasion and angiogenesis. *Genes Dev* **14**, 163-176 (2000).
60. N. Mitsiades, W. H. Yu, V. Poulaki, M. Tsokos, I. Stamenkovic, Matrix metalloproteinase-7-mediated cleavage of Fas ligand protects tumor cells from chemotherapeutic drug cytotoxicity. *Cancer Res* **61**, 577-581 (2001).
61. G. Bergers *et al.*, Matrix metalloproteinase-9 triggers the angiogenic switch during carcinogenesis. *Nat Cell Biol* **2**, 737-744 (2000).

62. A. Boire *et al.*, PAR1 is a matrix metalloprotease-1 receptor that promotes invasion and tumorigenesis of breast cancer cells. *Cell* **120**, 303-313 (2005).
63. A. V. Chernov, N. E. Sounni, A. G. Remacle, A. Y. Strongin, Epigenetic control of the invasion-promoting MT1-MMP/MMP-2/TIMP-2 axis in cancer cells. *J Biol Chem* **284**, 12727-12734 (2009).
64. N. Sato, N. Maehara, G. H. Su, M. Goggins, Effects of 5-aza-2'-deoxycytidine on matrix metalloproteinase expression and pancreatic cancer cell invasiveness. *J Natl Cancer Inst* **95**, 327-330 (2003).
65. L. M. B. Klassen *et al.*, MMP9 gene expression regulation by intragenic epigenetic modifications in breast cancer. *Gene* **642**, 461-466 (2018).
66. P. Brockmeyer, B. Hemmerlein, Epigenetic modification suppresses proliferation, migration and invasion of urothelial cancer cell lines. *Oncol Lett* **12**, 1693-1700 (2016).
67. S. Wang, W. Wu, F. X. Claret, Mutual regulation of microRNAs and DNA methylation in human cancers. *Epigenetics* **12**, 187-197 (2017).
68. S. K. Raghuwanshi *et al.*, G protein-coupled receptor kinase 6 deficiency promotes angiogenesis, tumor progression, and metastasis. *J Immunol* **190**, 5329-5336 (2013).
69. S. Yao *et al.*, Hypermethylation of the G protein-coupled receptor kinase 6 (GRK6) promoter inhibits binding of C/EBPalpha, and GRK6 knockdown promotes cell migration and invasion in lung adenocarcinoma cells. *FEBS Open Bio* **9**, 605-617 (2019).
70. A. M. Cock-Rada *et al.*, SMYD3 promotes cancer invasion by epigenetic upregulation of the metalloproteinase MMP-9. *Cancer Res* **72**, 810-820 (2012).
71. S. Asuthkar, K. K. Velpula, C. Chetty, B. Gorantla, J. S. Rao, Epigenetic regulation of miRNA-211 by MMP-9 governs glioma cell apoptosis, chemosensitivity and radiosensitivity. *Oncotarget* **3**, 1439-1454 (2012).
72. P. Liu, M. Sun, S. Sader, Matrix metalloproteinases in cardiovascular disease. *Can J Cardiol* **22 Suppl B**, 25B-30B (2006).
73. K. C. Chen *et al.*, OxLDL up-regulates microRNA-29b, leading to epigenetic modifications of MMP-2/MMP-9 genes: a novel mechanism for cardiovascular diseases. *FASEB J* **25**, 1718-1728 (2011).
74. A. C. Newby, Matrix metalloproteinases regulate migration, proliferation, and death of vascular smooth muscle cells by degrading matrix and non-matrix substrates. *Cardiovasc Res* **69**, 614-624 (2006).
75. H. C. Kuo, S. C. Li, L. H. Huang, Y. H. Huang, Epigenetic hypomethylation and upregulation of matrix metalloproteinase 9 in Kawasaki disease. *Oncotarget* **8**, 60875-60891 (2017).

76. J. Fernandez-Tajes *et al.*, Genome-wide DNA methylation analysis of articular chondrocytes reveals a cluster of osteoarthritic patients. *Ann Rheum Dis* **73**, 668-677 (2014).
77. H. I. Roach *et al.*, Association between the abnormal expression of matrix-degrading enzymes by human osteoarthritic chondrocytes and demethylation of specific CpG sites in the promoter regions. *Arthritis Rheum* **52**, 3110-3124 (2005).
78. J. Song *et al.*, MicroRNA-222 regulates MMP-13 via targeting HDAC-4 during osteoarthritis pathogenesis. *BBA Clin* **3**, 79-89 (2015).
79. N. Akhtar *et al.*, MicroRNA-27b regulates the expression of matrix metalloproteinase 13 in human osteoarthritis chondrocytes. *Arthritis Rheum* **62**, 1361-1371 (2010).
80. Y. Araki, T. Mimura, Matrix Metalloproteinase Gene Activation Resulting from Disordred Epigenetic Mechanisms in Rheumatoid Arthritis. *Int J Mol Sci* **18**, (2017).
81. E. Karouzakis, R. E. Gay, B. A. Michel, S. Gay, M. Neidhart, DNA hypomethylation in rheumatoid arthritis synovial fibroblasts. *Arthritis Rheum* **60**, 3613-3622 (2009).
82. Y. Araki *et al.*, Histone Methylation and STAT-3 Differentially Regulate Interleukin-6-Induced Matrix Metalloproteinase Gene Activation in Rheumatoid Arthritis Synovial Fibroblasts. *Arthritis Rheumatol* **68**, 1111-1123 (2016).
83. X. Wang *et al.*, Elevated microRNA1455p increases matrix metalloproteinase9 by activating the nuclear factorkappaB pathway in rheumatoid arthritis. *Mol Med Rep* **20**, 2703-2711 (2019).
84. M. L. Lindsey, Assigning matrix metalloproteinase roles in ischaemic cardiac remodelling. *Nat Rev Cardiol* **15**, 471-479 (2018).
85. D. Rodriguez, C. J. Morrison, C. M. Overall, Matrix metalloproteinases: what do they not do? New substrates and biological roles identified by murine models and proteomics. *Biochim Biophys Acta* **1803**, 39-54 (2010).
86. S. H. Ahmed *et al.*, Matrix metalloproteinases/tissue inhibitors of metalloproteinases: relationship between changes in proteolytic determinants of matrix composition and structural, functional, and clinical manifestations of hypertensive heart disease. *Circulation* **113**, 2089-2096 (2006).
87. W. S. Bradham *et al.*, Release of matrix metalloproteinases following alcohol septal ablation in hypertrophic obstructive cardiomyopathy. *J Am Coll Cardiol* **40**, 2165-2173 (2002).
88. A. T. Yan *et al.*, Plasma matrix metalloproteinase-9 level is correlated with left ventricular volumes and ejection fraction in patients with heart failure. *J Card Fail* **12**, 514-519 (2006).
89. G. A. McQuibban *et al.*, Matrix metalloproteinase activity inactivates the CXC chemokine stromal cell-derived factor-1. *J Biol Chem* **276**, 43503-43508 (2001).

90. G. A. McQuibban *et al.*, Matrix metalloproteinase processing of monocyte chemoattractant proteins generates CC chemokine receptor antagonists with anti-inflammatory properties in vivo. *Blood* **100**, 1160-1167 (2002).
91. C. J. Morrison, G. S. Butler, D. Rodriguez, C. M. Overall, Matrix metalloproteinase proteomics: substrates, targets, and therapy. *Curr Opin Cell Biol* **21**, 645-653 (2009).
92. S. A. Peeters *et al.*, Plasma matrix metalloproteinases are associated with incident cardiovascular disease and all-cause mortality in patients with type 1 diabetes: a 12-year follow-up study. *Cardiovasc Diabetol* **16**, 55 (2017).
93. M. T. Nurmohamed, M. Heslinga, G. D. Kitas, Cardiovascular comorbidity in rheumatic diseases. *Nat Rev Rheumatol* **11**, 693-704 (2015).
94. B. Tuysuz *et al.*, A novel matrix metalloproteinase 2 (MMP2) terminal hemopexin domain mutation in a family with multicentric osteolysis with nodulosis and arthritis with cardiac defects. *Eur J Hum Genet* **17**, 565-572 (2009).
95. J. A. Martignetti *et al.*, Mutation of the matrix metalloproteinase 2 gene (MMP2) causes a multicentric osteolysis and arthritis syndrome. *Nat Genet* **28**, 261-265 (2001).
96. R. A. Mosig, J. A. Martignetti, Loss of MMP-2 in murine osteoblasts upregulates osteopontin and bone sialoprotein expression in a circuit regulating bone homeostasis. *Dis Model Mech* **6**, 397-403 (2013).
97. F. C. Castberg *et al.*, Multicentric osteolysis with nodulosis and arthropathy (MONA) with cardiac malformation, mimicking polyarticular juvenile idiopathic arthritis: case report and literature review. *Eur J Pediatr* **172**, 1657-1663 (2013).
98. G. S. Bhavani *et al.*, Clinical and mutation profile of multicentric osteolysis nodulosis and arthropathy. *Am J Med Genet A* **170A**, 410-417 (2016).
99. K. Inoue *et al.*, A crucial role for matrix metalloproteinase 2 in osteocytic canalicular formation and bone metabolism. *J Biol Chem* **281**, 33814-33824 (2006).
100. J. M. Zhang, J. An, Cytokines, inflammation, and pain. *Int Anesthesiol Clin* **45**, 27-37 (2007).
101. M. N. Weitzmann, C. Roggia, G. Toraldo, L. Weitzmann, R. Pacifici, Increased production of IL-7 uncouples bone formation from bone resorption during estrogen deficiency. *J Clin Invest* **110**, 1643-1650 (2002).
102. G. Toraldo, C. Roggia, W. P. Qian, R. Pacifici, M. N. Weitzmann, IL-7 induces bone loss in vivo by induction of receptor activator of nuclear factor kappa B ligand and tumor necrosis factor alpha from T cells. *Proc Natl Acad Sci U S A* **100**, 125-130 (2003).
103. M. S. Lee *et al.*, GM-CSF regulates fusion of mononuclear osteoclasts into bone-resorbing osteoclasts by activating the Ras/ERK pathway. *J Immunol* **183**, 3390-3399 (2009).

104. E. Canalis, A. M. Delany, Mechanisms of glucocorticoid action in bone. *Ann N Y Acad Sci* **966**, 73-81 (2002).
105. C. Fernandez-Patron, M. W. Radomski, S. T. Davidge, Vascular matrix metalloproteinase-2 cleaves big endothelin-1 yielding a novel vasoconstrictor. *Circ Res* **85**, 906-911 (1999).
106. G. D. Kitas, M. Salmon, M. Farr, J. S. Gaston, P. A. Bacon, Deficient interleukin 2 production in rheumatoid arthritis: association with active disease and systemic complications. *Clin Exp Immunol* **73**, 242-249 (1988).
107. E. Canalis, Clinical review 83: Mechanisms of glucocorticoid action in bone: implications to glucocorticoid-induced osteoporosis. *J Clin Endocrinol Metab* **81**, 3441-3447 (1996).
108. T. Suda *et al.*, Modulation of osteoclast differentiation and function by the new members of the tumor necrosis factor receptor and ligand families. *Endocr Rev* **20**, 345-357 (1999).
109. H. Takayanagi, Osteoimmunology: shared mechanisms and crosstalk between the immune and bone systems. *Nat Rev Immunol* **7**, 292-304 (2007).
110. S. Rauber *et al.*, Resolution of inflammation by interleukin-9-producing type 2 innate lymphoid cells. *Nat Med* **23**, 938-944 (2017).
111. E. Kindstedt *et al.*, CCL11, a novel mediator of inflammatory bone resorption. *Sci Rep* **7**, 5334 (2017).
112. X. Zhang *et al.*, Epidermal growth factor receptor plays an anabolic role in bone metabolism in vivo. *J Bone Miner Res* **26**, 1022-1034 (2011).
113. K. Tamama, V. H. Fan, L. G. Griffith, H. C. Blair, A. Wells, Epidermal growth factor as a candidate for ex vivo expansion of bone marrow-derived mesenchymal stem cells. *Stem Cells* **24**, 686-695 (2006).
114. J. H. Kim *et al.*, The mechanism of osteoclast differentiation induced by IL-1. *J Immunol* **183**, 1862-1870 (2009).
115. P. Ruscitti *et al.*, The role of IL-1beta in the bone loss during rheumatic diseases. *Mediators Inflamm* **2015**, 782382 (2015).
116. J. Jules *et al.*, Molecular basis of requirement of receptor activator of nuclear factor kappaB signaling for interleukin 1-mediated osteoclastogenesis. *J Biol Chem* **287**, 15728-15738 (2012).
117. M. N. Weitzmann, S. Cenci, L. Rifas, C. Brown, R. Pacifici, Interleukin-7 stimulates osteoclast formation by up-regulating the T-cell production of soluble osteoclastogenic cytokines. *Blood* **96**, 1873-1878 (2000).
118. J. H. Kim *et al.*, Interleukin-7 Induces Osteoclast Formation via STAT5, Independent of Receptor Activator of NF-kappaB Ligand. *Front Immunol* **8**, 1376 (2017).

119. Y. K. Kang, M. C. Zhang, IL-23 promotes osteoclastogenesis in osteoblast-osteoclast co-culture system. *Genet Mol Res* **13**, 4673-4679 (2014).
120. L. Chen, X. Q. Wei, B. Evans, W. Jiang, D. Aeschlimann, IL-23 promotes osteoclast formation by up-regulation of receptor activator of NF-kappaB (RANK) expression in myeloid precursor cells. *Eur J Immunol* **38**, 2845-2854 (2008).
121. A. C. Hirbe *et al.*, Granulocyte colony-stimulating factor enhances bone tumor growth in mice in an osteoclast-dependent manner. *Blood* **109**, 3424-3431 (2007).
122. N. Ruef *et al.*, Granulocyte-macrophage colony-stimulating factor-dependent CD11c-positive cells differentiate into active osteoclasts. *Bone* **97**, 267-277 (2017).
123. T. Watanabe *et al.*, Direct stimulation of osteoclastogenesis by MIP-1alpha: evidence obtained from studies using RAW264 cell clone highly responsive to RANKL. *J Endocrinol* **180**, 193-201 (2004).
124. S. Yano *et al.*, Functional expression of beta-chemokine receptors in osteoblasts: role of regulated upon activation, normal T cell expressed and secreted (RANTES) in osteoblasts and regulation of its secretion by osteoblasts and osteoclasts. *Endocrinology* **146**, 2324-2335 (2005).
125. H. B. Kwak *et al.*, Monokine induced by interferon-gamma is induced by receptor activator of nuclear factor kappa B ligand and is involved in osteoclast adhesion and migration. *Blood* **105**, 2963-2969 (2005).
126. G. Mori, P. D'Amelio, R. Faccio, G. Brunetti, The Interplay between the bone and the immune system. *Clin Dev Immunol* **2013**, 720504 (2013).
127. N. Bucay *et al.*, osteoprotegerin-deficient mice develop early onset osteoporosis and arterial calcification. *Genes Dev* **12**, 1260-1268 (1998).
128. E. Berry *et al.*, Matrix metalloproteinase-2 negatively regulates cardiac secreted phospholipase A2 to modulate inflammation and fever. *J Am Heart Assoc* **4**, (2015).
129. P. K. Siiteri *et al.*, The serum transport of steroid hormones. *Recent Prog Horm Res* **38**, 457-510 (1982).
130. K. Pichler *et al.*, Bisphosphonates in multicentric osteolysis, nodulosis and arthropathy (MONA) spectrum disorder - an alternative therapeutic approach. *Sci Rep* **6**, 34017 (2016).
131. H. C. Blair *et al.*, Osteoblast Differentiation and Bone Matrix Formation In Vivo and In Vitro. *Tissue Eng Part B Rev* **23**, 268-280 (2017).
132. Y. C. Guo, Q. Yuan, Fibroblast growth factor 23 and bone mineralisation. *Int J Oral Sci* **7**, 8-13 (2015).
133. H. Wang *et al.*, Overexpression of fibroblast growth factor 23 suppresses osteoblast differentiation and matrix mineralization in vitro. *J Bone Miner Res* **23**, 939-948 (2008).

134. K. Yokota *et al.*, Combination of tumor necrosis factor alpha and interleukin-6 induces mouse osteoclast-like cells with bone resorption activity both in vitro and in vivo. *Arthritis Rheumatol* **66**, 121-129 (2014).
135. J. Xu *et al.*, IL-23, but not IL-12, plays a critical role in inflammation-mediated bone disorders. *Theranostics* **10**, 3925-3938 (2020).
136. S. R. Goldring, E. M. Gravallese, Mechanisms of bone loss in inflammatory arthritis: diagnosis and therapeutic implications. *Arthritis Res* **2**, 33-37 (2000).
137. A. B. Avci, E. Feist, G. R. Burmester, Targeting GM-CSF in rheumatoid arthritis. *Clin Exp Rheumatol* **34**, 39-44 (2016).
138. X. Guo *et al.*, Pharmacodynamic biomarkers and differential effects of TNF- and GM-CSF-targeting biologics in rheumatoid arthritis. *Int J Rheum Dis* **22**, 646-653 (2019).
139. G. R. Burmester *et al.*, A randomised phase IIb study of mavrilimumab, a novel GM-CSF receptor alpha monoclonal antibody, in the treatment of rheumatoid arthritis. *Ann Rheum Dis* **76**, 1020-1030 (2017).
140. G. R. Burmester *et al.*, Mavrilimumab, a Fully Human Granulocyte-Macrophage Colony-Stimulating Factor Receptor alpha Monoclonal Antibody: Long-Term Safety and Efficacy in Patients With Rheumatoid Arthritis. *Arthritis Rheumatol* **70**, 679-689 (2018).
141. C. Crotti, M. Biggioggero, A. Becciolini, E. Agape, E. G. Favalli, Mavrilimumab: a unique insight and update on the current status in the treatment of rheumatoid arthritis. *Expert Opin Investig Drugs* **28**, 573-581 (2019).
142. J. K. Gjerstad, S. L. Lightman, F. Spiga, Role of glucocorticoid negative feedback in the regulation of HPA axis pulsatility. *Stress* **21**, 403-416 (2018).
143. F. Roelfsema *et al.*, Impact of age, sex and body mass index on cortisol secretion in 143 healthy adults. *Endocr Connect* **6**, 500-509 (2017).
144. N. Ljubijankic *et al.*, Daily fluctuation of cortisol in the saliva and serum of healthy persons. *Bosn J Basic Med Sci* **8**, 110-115 (2008).
145. D. T. Krieger, W. Allen, F. Rizzo, H. P. Krieger, Characterization of the normal temporal pattern of plasma corticosteroid levels. *J Clin Endocrinol Metab* **32**, 266-284 (1971).
146. E. D. Weitzman *et al.*, Twenty-four hour pattern of the episodic secretion of cortisol in normal subjects. *J Clin Endocrinol Metab* **33**, 14-22 (1971).
147. T. T. Chung, K. Gunganah, J. P. Monson, W. M. Drake, Circadian variation in serum cortisol during hydrocortisone replacement is not attributable to changes in cortisol-binding globulin concentrations. *Clin Endocrinol (Oxf)* **84**, 496-500 (2016).

148. S. Gong *et al.*, Dynamics and correlation of serum cortisol and corticosterone under different physiological or stressful conditions in mice. *PLoS One* **10**, e0117503 (2015).
149. E. V. Yang *et al.*, Stress-related modulation of matrix metalloproteinase expression. *J Neuroimmunol* **133**, 144-150 (2002).
150. K. E. Hannibal, M. D. Bishop, Chronic stress, cortisol dysfunction, and pain: a psychoneuroendocrine rationale for stress management in pain rehabilitation. *Phys Ther* **94**, 1816-1825 (2014).
151. F. Ebrahimi *et al.*, Effects of interleukin-1 antagonism on cortisol levels in individuals with obesity: a randomized clinical trial. *Endocr Connect* **8**, 701-708 (2019).
152. H. O. Besedovsky, A. del Rey, Immune-neuro-endocrine interactions: facts and hypotheses. *Endocr Rev* **17**, 64-102 (1996).
153. T. J. Hahn, L. R. Halstead, S. L. Teitelbaum, B. H. Hahn, Altered mineral metabolism in glucocorticoid-induced osteopenia. Effect of 25-hydroxyvitamin D administration. *J Clin Invest* **64**, 655-665 (1979).
154. L. Dalle Carbonare *et al.*, Comparison of trabecular bone microarchitecture and remodeling in glucocorticoid-induced and postmenopausal osteoporosis. *J Bone Miner Res* **16**, 97-103 (2001).
155. J. Rubin *et al.*, Dexamethasone promotes expression of membrane-bound macrophage colony-stimulating factor in murine osteoblast-like cells. *Endocrinology* **139**, 1006-1012 (1998).
156. L. C. Hofbauer *et al.*, Stimulation of osteoprotegerin ligand and inhibition of osteoprotegerin production by glucocorticoids in human osteoblastic lineage cells: potential paracrine mechanisms of glucocorticoid-induced osteoporosis. *Endocrinology* **140**, 4382-4389 (1999).
157. R. M. Pereira, A. M. Delany, E. Canalis, Cortisol inhibits the differentiation and apoptosis of osteoblasts in culture. *Bone* **28**, 484-490 (2001).
158. M. Tzaphlidou, Bone architecture: collagen structure and calcium/phosphorus maps. *J Biol Phys* **34**, 39-49 (2008).
159. A. M. Delany, B. Y. Gabbitas, E. Canalis, Cortisol downregulates osteoblast alpha 1 (I) procollagen mRNA by transcriptional and posttranscriptional mechanisms. *J Cell Biochem* **57**, 488-494 (1995).
160. A. M. Delany, J. J. Jeffrey, S. Rydziel, E. Canalis, Cortisol increases interstitial collagenase expression in osteoblasts by post-transcriptional mechanisms. *J Biol Chem* **270**, 26607-26612 (1995).
161. B. Bauvois, New facets of matrix metalloproteinases MMP-2 and MMP-9 as cell surface transducers: outside-in signaling and relationship to tumor progression. *Biochim Biophys Acta* **1825**, 29-36 (2012).

162. E. M. Wilson *et al.*, Plasma matrix metalloproteinase and inhibitor profiles in patients with heart failure. *J Card Fail* **8**, 390-398 (2002).
163. H. W. Jackson, V. Defamie, P. Waterhouse, R. Khokha, TIMPs: versatile extracellular regulators in cancer. *Nat Rev Cancer* **17**, 38-53 (2017).
164. H. S. Alameddine, J. E. Morgan, Matrix Metalloproteinases and Tissue Inhibitor of Metalloproteinases in Inflammation and Fibrosis of Skeletal Muscles. *J Neuromuscul Dis* **3**, 455-473 (2016).
165. R. Rodriguez-Calvo *et al.*, NR4A receptors up-regulate the antiproteinase alpha-2 macroglobulin (A2M) and modulate MMP-2 and MMP-9 in vascular smooth muscle cells. *Thromb Haemost* **113**, 1323-1334 (2015).
166. B. Schmidt, L. Mitchell, F. A. Ofosu, M. Andrew, Alpha-2-macroglobulin is an important progressive inhibitor of thrombin in neonatal and infant plasma. *Thromb Haemost* **62**, 1074-1077 (1989).
167. J. Schaller, S. S. Gerber, The plasmin-antiplasmin system: structural and functional aspects. *Cell Mol Life Sci* **68**, 785-801 (2011).
168. J. Kurzepa *et al.*, Role of MMP-2 and MMP-9 and their natural inhibitors in liver fibrosis, chronic pancreatitis and non-specific inflammatory bowel diseases. *Hepatobiliary Pancreat Dis Int* **13**, 570-579 (2014).
169. L. L. Shen, R. P. McDonagh, J. McDonagh, J. Hermans, Early events in the plasmin digestion of fibrinogen and fibrin. Effects of plasmin on fibrin polymerization. *J Biol Chem* **252**, 6184-6189 (1977).
170. S. Monaco *et al.*, Modulation of the proteolytic activity of matrix metalloproteinase-2 (gelatinase A) on fibrinogen. *Biochem J* **402**, 503-513 (2007).
171. K. M. Thrailkill *et al.*, Physiological matrix metalloproteinase concentrations in serum during childhood and adolescence, using Luminex Multiplex technology. *Clin Chem Lab Med* **43**, 1392-1399 (2005).
172. M. Fountoulakis *et al.*, Depletion of the high-abundance plasma proteins. *Amino Acids* **27**, 249-259 (2004).
173. G. Sawicki, E. Salas, J. Murat, H. Miszta-Lane, M. W. Radomski, Release of gelatinase A during platelet activation mediates aggregation. *Nature* **386**, 616-619 (1997).
174. W. S. Choi, O. H. Jeon, H. H. Kim, D. S. Kim, MMP-2 regulates human platelet activation by interacting with integrin alphaIIbbeta3. *J Thromb Haemost* **6**, 517-523 (2008).

175. E. Falcinelli, S. Giannini, E. Boschetti, P. Gresele, Platelets release active matrix metalloproteinase-2 in vivo in humans at a site of vascular injury: lack of inhibition by aspirin. *Br J Haematol* **138**, 221-230 (2007).
176. E. Falcinelli, G. Guglielmini, M. Torti, P. Gresele, Intraplatelet signaling mechanisms of the priming effect of matrix metalloproteinase-2 on platelet aggregation. *J Thromb Haemost* **3**, 2526-2535 (2005).
177. S. P. Jackson, The growing complexity of platelet aggregation. *Blood* **109**, 5087-5095 (2007).
178. M. J. Santos-Martinez, C. Medina, J. F. Gilmer, M. W. Radomski, Matrix metalloproteinases in platelet function: coming of age. *J Thromb Haemost* **6**, 514-516 (2008).
179. C. Fernandez-Patron *et al.*, Differential regulation of platelet aggregation by matrix metalloproteinases-9 and -2. *Thromb Haemost* **82**, 1730-1735 (1999).
180. V. Costantini *et al.*, Fibrinogen deposition without thrombin generation in primary human breast cancer tissue. *Cancer Res* **51**, 349-353 (1991).
181. P. J. Simpson-Haidaris, B. Rybarczyk, Tumors and fibrinogen. The role of fibrinogen as an extracellular matrix protein. *Ann N Y Acad Sci* **936**, 406-425 (2001).
182. M. Pereira *et al.*, The incorporation of fibrinogen into extracellular matrix is dependent on active assembly of a fibronectin matrix. *J Cell Sci* **115**, 609-617 (2002).
183. M. Giannandrea, W. C. Parks, Diverse functions of matrix metalloproteinases during fibrosis. *Dis Model Mech* **7**, 193-203 (2014).
184. F. L. Craciun *et al.*, Pharmacological and genetic depletion of fibrinogen protects from kidney fibrosis. *Am J Physiol Renal Physiol* **307**, F471-484 (2014).
185. B. Vidal *et al.*, Fibrinogen drives dystrophic muscle fibrosis via a TGFbeta/alternative macrophage activation pathway. *Genes Dev* **22**, 1747-1752 (2008).
186. S. Kim, J. A. Nadel, Fibrinogen binding to ICAM-1 promotes EGFR-dependent mucin production in human airway epithelial cells. *Am J Physiol Lung Cell Mol Physiol* **297**, L174-183 (2009).
187. C. Fernandez-Patron, L. Castellanos-Serra, P. Rodriguez, Reverse staining of sodium dodecyl sulfate polyacrylamide gels by imidazole-zinc salts: sensitive detection of unmodified proteins. *Biotechniques* **12**, 564-573 (1992).
188. C. Fernandez-Patron *et al.*, Understanding the mechanism of the zinc-ion stains of biomacromolecules in electrophoresis gels: generalization of the reverse-staining technique. *Electrophoresis* **19**, 2398-2406 (1998).
189. J. M. Kollman, L. Pandi, M. R. Sawaya, M. Riley, R. F. Doolittle, Crystal structure of human fibrinogen. *Biochemistry* **48**, 3877-3886 (2009).

190. R. Z. Kramer, J. Bella, P. Mayville, B. Brodsky, H. M. Berman, Sequence dependent conformational variations of collagen triple-helical structure. *Nat Struct Biol* **6**, 454-457 (1999).
191. H. S. Rasmussen, P. P. McCann, Matrix metalloproteinase inhibition as a novel anticancer strategy: a review with special focus on batimastat and marimastat. *Pharmacol Ther* **75**, 69-75 (1997).
192. D. Bhattacharya, J. Cheng, 3Drefine: consistent protein structure refinement by optimizing hydrogen bonding network and atomic-level energy minimization. *Proteins* **81**, 119-131 (2013).
193. D. Bhattacharya, J. Nowotny, R. Cao, J. Cheng, 3Drefine: an interactive web server for efficient protein structure refinement. *Nucleic Acids Res* **44**, W406-409 (2016).
194. S. R. Comeau, D. W. Gatchell, S. Vajda, C. J. Camacho, ClusPro: a fully automated algorithm for protein-protein docking. *Nucleic Acids Res* **32**, W96-99 (2004).
195. S. R. Comeau, D. W. Gatchell, S. Vajda, C. J. Camacho, ClusPro: an automated docking and discrimination method for the prediction of protein complexes. *Bioinformatics* **20**, 45-50 (2004).
196. D. Kozakov, R. Brenke, S. R. Comeau, S. Vajda, PIPER: an FFT-based protein docking program with pairwise potentials. *Proteins* **65**, 392-406 (2006).
197. D. Kozakov *et al.*, How good is automated protein docking? *Proteins* **81**, 2159-2166 (2013).
198. D. Kozakov *et al.*, The ClusPro web server for protein-protein docking. *Nat Protoc* **12**, 255-278 (2017).
199. S. Jha, S. P. Kanaujia, A. M. Limaye, Direct inhibition of matrix metalloproteinase-2 (MMP-2) by (-)-epigallocatechin-3-gallate: A possible role for the fibronectin type II repeats. *Gene* **593**, 126-130 (2016).
200. E. F. Pettersen *et al.*, UCSF Chimera--a visualization system for exploratory research and analysis. *J Comput Chem* **25**, 1605-1612 (2004).
201. O. Trott, A. J. Olson, AutoDock Vina: improving the speed and accuracy of docking with a new scoring function, efficient optimization, and multithreading. *J Comput Chem* **31**, 455-461 (2010).
202. M. D. Winn *et al.*, Overview of the CCP4 suite and current developments. *Acta Crystallogr D Biol Crystallogr* **67**, 235-242 (2011).
203. L. F. Judit Castillo-Armengol, and Isabel C Lopez-Mejia, Inter-organ communication: a gatekeeper for metabolic health. *EMBO reports* **20: e47903**, (2019).
204. G. E. Billman, Homeostasis: The Underappreciated and Far Too Often Ignored Central Organizing Principle of Physiology. *Front Physiol* **11**, 200 (2020).
205. E. A. Richter, M. Hargreaves, Exercise, GLUT4, and skeletal muscle glucose uptake. *Physiol Rev* **93**, 993-1017 (2013).
206. C. F. Cori, G. T. Cori, Carbohydrate metabolism. *Annu Rev Biochem* **15**, 193-218 (1946).

207. C. Fernandez-Patron *et al.*, Vascular matrix metalloproteinase-2-dependent cleavage of calcitonin gene-related peptide promotes vasoconstriction. *Circ Res* **87**, 670-676 (2000).
208. I. Tchetverikov *et al.*, Leflunomide and methotrexate reduce levels of activated matrix metalloproteinases in complexes with alpha2 macroglobulin in serum of rheumatoid arthritis patients. *Ann Rheum Dis* **67**, 128-130 (2008).
209. X. Wang *et al.*, MMP-2 inhibits PCSK9-induced degradation of the LDL receptor in Hepa1-c1c7 cells. *FEBS Lett* **589**, 490-496 (2015).
210. W. G. Stetler-Stevenson, P. D. Brown, M. Onisto, A. T. Levy, L. A. Liotta, Tissue inhibitor of metalloproteinases-2 (TIMP-2) mRNA expression in tumor cell lines and human tumor tissues. *J Biol Chem* **265**, 13933-13938 (1990).
211. Q. Meng *et al.*, Residue 2 of TIMP-1 is a major determinant of affinity and specificity for matrix metalloproteinases but effects of substitutions do not correlate with those of the corresponding P1' residue of substrate. *J Biol Chem* **274**, 10184-10189 (1999).
212. H. F. Bigg, Y. E. Shi, Y. E. Liu, B. Steffensen, C. M. Overall, Specific, high affinity binding of tissue inhibitor of metalloproteinases-4 (TIMP-4) to the COOH-terminal hemopexin-like domain of human gelatinase A. TIMP-4 binds progelatinase A and the COOH-terminal domain in a similar manner to TIMP-2. *J Biol Chem* **272**, 15496-15500 (1997).
213. M. Ouimet, T. J. Barrett, E. A. Fisher, HDL and Reverse Cholesterol Transport. *Circ Res* **124**, 1505-1518 (2019).
214. S. Filou *et al.*, Distinct Roles of Apolipoproteins A1 and E in the Modulation of High-Density Lipoprotein Composition and Function. *Biochemistry* **55**, 3752-3762 (2016).
215. J. Jumper *et al.*, Highly accurate protein structure prediction with AlphaFold. *Nature* **596**, 583-589 (2021).
216. A. Kryshtafovych, T. Schwede, M. Topf, K. Fidelis, J. Moult, Critical assessment of methods of protein structure prediction (CASP)-Round XIII. *Proteins* **87**, 1011-1020 (2019).
217. M. O. N. Richard Evans, Alexander Pritzel, Natasha Antropova, Andrew Senior, Tim Green, Augustin Žídek, Russ Bates, Sam Blackwell, Jason Yim, ProfileOlaf Ronneberger, Sebastian Bodenstein, Michal Zielinski, Alex Bridgland, Anna Potapenko, Andrew Cowie, Kathryn Tunyasuvunakool, Rishub Jain, Ellen Clancy, Pushmeet Kohli, John Jumper, Demis Hassabis, Protein complex prediction with AlphaFold-Multimer. *bioRxiv*, (2022).
218. E. Bisong, *Building Machine Learning and Deep Learning Models on Google Cloud Platform: A Comprehensive Guide for Beginners.*, (2019).

219. R. Yan, D. Xu, J. Yang, S. Walker, Y. Zhang, A comparative assessment and analysis of 20 representative sequence alignment methods for protein structure prediction. *Sci Rep* **3**, 2619 (2013).
220. C. Jacobs-Cacha *et al.*, A misprocessed form of Apolipoprotein A-I is specifically associated with recurrent Focal Segmental Glomerulosclerosis. *Sci Rep* **10**, 1159 (2020).
221. V. Gogonea, Structural Insights into High Density Lipoprotein: Old Models and New Facts. *Front Pharmacol* **6**, 318 (2015).
222. H. Sarker *et al.*, Comparative Serum Analyses Identify Cytokines and Hormones Commonly Dysregulated as Well as Implicated in Promoting Osteolysis in MMP-2-Deficient Mice and Children. *Front Physiol* **11**, 568718 (2020).
223. I. Wittig, H. P. Braun, H. Schagger, Blue native PAGE. *Nat Protoc* **1**, 418-428 (2006).
224. N. Thangthaeng, N. Sumien, M. J. Forster, R. A. Shah, L. J. Yan, Nongradient blue native gel analysis of serum proteins and in-gel detection of serum esterase activities. *J Chromatogr B Analyt Technol Biomed Life Sci* **879**, 386-394 (2011).
225. V. Hornak *et al.*, Comparison of multiple Amber force fields and development of improved protein backbone parameters. *Proteins* **65**, 712-725 (2006).
226. D. Davalos, K. Akassoglou, Fibrinogen as a key regulator of inflammation in disease. *Semin Immunopathol* **34**, 43-62 (2012).
227. G. D. Lowe, Circulating inflammatory markers and risks of cardiovascular and non-cardiovascular disease. *J Thromb Haemost* **3**, 1618-1627 (2005).
228. W. F. Skogen, R. M. Senior, G. L. Griffin, G. D. Wilner, Fibrinogen-derived peptide B beta 1-42 is a multidomained neutrophil chemoattractant. *Blood* **71**, 1475-1479 (1988).
229. G. Florvall, S. Basu, A. Larsson, Apolipoprotein A1 is a stronger prognostic marker than are HDL and LDL cholesterol for cardiovascular disease and mortality in elderly men. *J Gerontol A Biol Sci Med Sci* **61**, 1262-1266 (2006).
230. M. J. McQueen *et al.*, Lipids, lipoproteins, and apolipoproteins as risk markers of myocardial infarction in 52 countries (the INTERHEART study): a case-control study. *Lancet* **372**, 224-233 (2008).
231. M. Maddaluno *et al.*, Monocyte chemotactic protein-3 induces human coronary smooth muscle cell proliferation. *Atherosclerosis* **217**, 113-119 (2011).
232. A. M. Manicone, J. K. McGuire, Matrix metalloproteinases as modulators of inflammation. *Semin Cell Dev Biol* **19**, 34-41 (2008).
233. G. A. McQuibban *et al.*, Inflammation dampened by gelatinase A cleavage of monocyte chemoattractant protein-3. *Science* **289**, 1202-1206 (2000).

234. R. P. Iyer, N. L. Patterson, G. B. Fields, M. L. Lindsey, The history of matrix metalloproteinases: milestones, myths, and misperceptions. *Am J Physiol Heart Circ Physiol* **303**, H919-930 (2012).

235. D. L. Silver, N. Wang, X. Xiao, A. R. Tall, High density lipoprotein (HDL) particle uptake mediated by scavenger receptor class B type 1 results in selective sorting of HDL cholesterol from protein and polarized cholesterol secretion. *J Biol Chem* **276**, 25287-25293 (2001).